UNIVERSITÀ DEGLI STUDI DI PADOVA

DIPARTIMENTO DI INGEGNERIA INDUSTRIALE

CORSO DI LAUREA MAGISTRALE IN
INGEGNERIA CHIMICA E DEI PROCESSI INDUSTRIALI

Tesi di Laurea Magistrale in
Ingegneria Chimica e dei Processi Industriali

Modelling of natural gas sweetening and dehydration processes

Relatore: Prof. Fabrizio Bezzo
Correlatori: Dr. Mayank Patel
Dr. Luis Domingues

Laureando: FEDERICO PANIZZOLO TERRIN

Anno accademico 2016/2017

"Essentially, all models are wrong,
but some are useful"
George E.P. Box

Abstract

The raw natural gas extracted from production wells contains many impurities that must be removed in order to achieve the specifications of the liquified natural gas (LNG) and/or the pipeline gas. In order to achieve such specifications, the raw gas must pass through a series of purification steps, which compose the so-called "natural gas chain".

Two key passages are the "sweetening" (removal of H_2S and CO_2) and the "dehydration" processes. In the case of sweetening, the most common process technique involves an aqueous solution of alkanolamines as absorbing solvent. For dehydration, there are two possible options: the absorption process involving triethylene glycol and the adsorption process with solid dessicants.

In this thesis, the sweetening process as well as the two dehydration technical possibilities are modelled using the gPROMS® ProcessBuilder process simulator.

The two absorption processes are represented, separately, at steady state conditions, using the thermodynamic model SAFT-γ Mie (gSAFT®), an equation of state which exploits the group contributions approach.

After the thermodynamic model validation against experimental data, the two processes are modelled and then used to simulate some case studies from the scientific literature. The accuracy of the simulation results is verified by comparison with data available from the literature. Eventually, the two absorption processes are joint together in series, building an unique flowsheet.

In the second part of the work, the dynamic process of pressure-temperature swing adsorption has been modelled using Peng - Robinson EoS as thermodynamic model.

This work contributes to show the advantages that the use of SAFT-γ Mie (and gPROMS® ProcessBuilder) can bring on modelling the absorption processes involved in the natural gas chain. Furthermore, the work on the adsorption process higlights the flexibility of custom modelling in gPROMS® ProcessBuilder, where the intrisic mathematical framework can be easily adapted to a specific features of a unit operation.

Riassunto

La produzione e consumo mondiale di gas naturale hanno mostrato un rapido aumento negli ultimi 25 anni. Le previsioni future dicono, inoltre, che intorno all'anno 2025 il consumo di gas naturale supererà quello di carbone, diventando quindi il secondo combustibile più usato, dopo il petrolio. Il gas naturale offre numerosi vantaggi ambientali se comparato con altri combustibili fossili. Esso infatti ha emissioni trascurabili di anidride solforsa e ossidi di azono, ma soprattutto l'emissione di anidride carbonica può arrivare ad essere fino al 60 % inferiore rispetto al carbone. Al giorno d'oggi esso è impiegato in svariati settori, dal domestico dove trova largo consumo, all'industria, nel settore dei trasporti e nella generazione di elettricità.

Il gas naturale deriva dalla degradazione di materia organica accumulatasi nel sottosuolo in milioni di anni. I suoi principali costituenti sono alcani con un basso numero di atomi di carbonio, tra i quali il metano costituisce l'elemento principale, seguito da etano, propano e quantità inferiori di butano e alcani con un maggior numero di atomi di carbonio. Tuttavia, il gas naturale quando viene estratto dalle riserve del sottosuolo, per mezzo di pozzi di estrazione, presenta una serie di componenti "indesiderati" che devono essere rimossi prima di rendere il combustibile disponibile al mercato.

In questo contesto di rapida ascesa della produzione di gas naturale, appare quindi chiaro come l'ottimizzazione di tutti i processi che vanno dall'estrazione iniziale dal sottosuolo al trasporto verso l'utente finale, passando per la depurazione intermedia, sia una necessità per le compagnie di produzione. E' pertanto chiaro che l'utilizzo di software per la simulazione di questi processi diventi un elemento chiave in questo crescente mercato, dove anche la minima miglioria può portare ad un notevole vantaggio economico.

L'obiettivo del lavoro di tesi è quello di modellare due dei principali processi di purificazione del gas naturale, attraverso l'uso del simulatore di processo gPROMS® ProcessBuilder, sviluppato da PSE (Process Systems Enterprise, Ltd.). Questo software sfrutta la tecnologia *equation oriented*, la quale permette la risoluzione simultanea di grandi sistemi di equazioni algebriche e differenziali. In particolare può essere applicato sia per sistemi a stato stazionario che per sistemi dinamici.

I due processi studiati sono l'addolcimento (ossia la rimozione di anidride carbonica e acido solfidrico) e la disidratazione (ossia la rimozione d'acqua). In particolare, per quanto riguarda l'addolcimento si è considerato il processo di assorbimento chimico con uso di dietanol-ammina (DEA), mentre nel caso della disidratazione sono stati presi in considerazione il processo di assobimento fisico, con l'uso di trietilen-glicole (TEG) come solvente, ed il processo di adsorbimento su setacci molecolari.

Nella prima parte del lavoro i due processi di assorbimento sono stati implementati, separatamente, a stato stazionario, con l'utilizzo del modello termodinamico SAFT-γ Mie, un'equazione di stato fondata sul metodo a gruppi. Questo modello presenta i classici vantaggi dei metodi "a gruppi", dove le molecole sono viste come costituite da un insieme di più gruppi, presentando una grande flessibilità e predittività, unita ai vantaggi delle equazioni di stato di non essere, in linea di principio, limitate nel campo di applicabilità. Prima di procedere alla costruzione dei *flowsheets*, il modello termodinamico è validato rispetto a dati sperimentali presenti in letteratura. Successivamente, partendo da precedenti studi di letteratura, i due impianti sono stati modellati e simulati. I risultati ottenuti possono considerarsi affidabili anche se si discostano leggermente da quelli presenti in letteratura per via delle differenti metodologie e strumenti di simulazione. Alla fine i due processi sono stati uniti, "in serie", a formare un unico *flowsheet*. Questo unico processo è stato poi ottimizzato permettendo una parziale riduzione dei costi operativi. Il più importante risultato è tuttavia la dimostrazione del fatto che il modello termodinamico riesca a predirre correttamente le interazioni del gas con due solventi di natura completamente diversa all'interno dello stesso modello di processo.

Nella seconda parte del lavoro di tesi è invece affrontato il modello dinamico di adsorbimento di acqua su un letto di setacci molecolari (zeolite 5A). Inizialmente, partendo da uno studio di letteratura, un singolo letto adsorbente è stato implementato all'interno dell'ambiente gPROMS®. In questa fase è stata di fondamentale importanza la scelta dell'isoterma di equilibrio (modello Langmuir a due siti) ed il settaggio dei bilanci di materia, attraverso il coefficiente di dispersione assiale, il coefficiente di diffusione molecolare nel microporo ed il numero dei punti della griglia di integrazione numerica. Una volta trovato il tempo di saturazione del letto e studiato l'influenza dei parametri sopra citati attraverso studi di sensitività, è stato implementato un processo a due letti, operanti in parallelo. Questo è stato fatto in modo tale da rendere il processo continuo: mentre un letto sta adsorbendo, l'altro viene rigenerato e viceversa così da non dover interrompere le operazioni ogni qual volta il letto raggiunge saturazione. Se il processo di adsorbimento di acqua è favorito da "basse" temperature ed "alte pressione" appare evidente che per rigenerare il letto sia necessario il contratio ossia l'innalzamento di temperatura e l'abbassamento di pressione. Ciò è possibile attraverso specifici step di riscaldamento-raffreddamento e pressurizzazione-depressurizzazione, dove parte del gas disidratato proveniente da un letto è convogliato verso l'altro letto fungendo da gas di stripping. I risultati lasciano tuttavia suggerire che il processo possa venir migliorato ottimizzando i tempi e le caratteristiche dei vari steps che costituiscono ciascun ciclo.

Contents

List of Figures

List of Tables

Introduction

The production of natural gas has grown a lot over the past 25 years due to its large availability and its lower enviromental impact when compared to other fossil fuels. The CO_2 emissions can be 60 % lower than in the case of coal. That is why future predictions say that by year 2025 natural gas will overtake coal, becoming the second most used fuel in the world after oil.

In this growing consumption-production contest, it is clear that the optimization of all the processes required to bring the gas from the producing wells to the final users can provide huge advantages in terms of profits for gas suppliers.

The easiest way to optimize a certain process is to exploit a validated process model which can be used to study the influence of different parameters so as to find the optimum operating conditions and to explore different process configurations.

In this thesis, three of the typical processes present in the natural gas chain are modelled: the sweetening process via chemical absorbtion (with diethanol amine as absorbing solvent), the dehydration process either via physical absorption (with triethylene glycol as absorbing solvent) or via adsorption with molecular sieves.

The tool used to model and simulate such plants is the gPROMS® ProcessBuilder, developed by PSE (Process Systems Enterprise, Ltd.), leading supplier of advance process modelling software. It is an equation-oriented modelling system, which allows the simultaneous resolution of large systems of algeabric and differential equations. In particular, it can be applied to a wide variety of problems, from steady state simulations to dynamic simulations (in this work the two absorption processes are modelled as steady state, whereas the adsorption one is a dynamic one).

The thesis begins with a chapter dedicated to the literature review. Starting from a general description of the natural gas chain, the focus is headed to the description of the most important processes of the chain, i.e. sweetening and dehydration. The main technologies considered are the reactive/chemical absorption and the adsorption. The chapter eventually discusses the most recent literature studies on the modelling pf these processes by means of commercial process simulators.

The second chapter introduces SAFT-γ Mie, the thermodynamic model used to model the two absorption processes. After a brief description of the theory behind the model, a validation is provided against literature data. It is also described Mutiflash™, the thermodynamic package used to simulate the adsorption process (with the Peng - Robinson equation of state).

In the third chapter the sweetening process model is presented. Firstly, the flowsheet is introduced, describing the main units and the process specifications. Then, the model results are presented and compared with the literature source, through which the model has been implemented. In the last section a sensitivity analysis is

carried out on the tray efficiencies of the contactor and regenerator columns. This is done in order to find the minimum tray efficiency that allows to stay within the specifications in terms of H_2S concentration in the sweet gas.

The fourth chapter, describes the dehydration process via chemical absorption. After a first section, where the contactor model is validated against experimental data, the flowsheet main units are described and the product specifications are defined. Finally, the results are presented and compared with literature data.

The fifth chapter presents the whole flowsheet, built by joining the two flowsheet of sweetening and dehydration in series. The process is then optimized in terms of energy consumption.

In the sixth chapter, the dehydration via adsorption process is described. The chapter starts with a description of the single bed model, with a particular focus on its most important mathematical equations. After that, the single bed model results are described together with three sensitivity analyses on key model parameters. In the last part of the chapter the two beds pressure - temperature swing adsorption process (PTSA) is described. This configuration allows to achieve a continuous operation by alternating adsorption-regeneration steps among the two beds.

In the conclusions, the results are summarized and suggestions for future work are provided.

Chapter 1

Literature review

This introductory chapter presents the literature review carried out at the beginning of the work. The purpose of this initial study is to present the main processes that bring the natural gas from the drilling wells to the final users. After that, the processes available for acid gases and water removal (respectively called sweetening and dehydration) are described, with a particular focus on absorption and adsorption methods. In the end, the most recent studies on modelling these processes by means of process simulators, are summarized.

1.1 Natural gas

The demand of natural gas has increased quite a lot over the recent years and is expected to play an increasingly important role in world economy growth in the coming decades.

Natural gas offers important benefits when compared to other fossil fuels: for example, its combustion emits less CO_2 than petroleum derivative fuels. The CO_2 emissions from natural gas can be 60 % less than coal when used for electricity generation. Figure 1.1 shows the fast growing world's production - consumption of natural gas over the past 25 years.

It is one of the most widely used forms of energy nowadays. Commonly used in the residential sector (cooking stoves, home furnaces and water heaters), it can be used in the industrial, commercial, electicity generation and transportation sectors as well (Demirbas, 2010).

Due to difficulty in storing, natural gas needs to be transported from the producer to the consumer as quickly as possible. Over short and medium distances, up to about 3 000 km, natural gas is transported as gas through pipelines. In case the laying of pipelines is not possible because the distance between the source and the consumer exceeds 3 000 km or because of geographical or political reasons, the gas is cooled down to, approximately, $-162°C$ near the source, becoming liquified natural gas (LNG). LNG is transported by ship and converted into gas in the proximity of the consumer (Heinz-Wolfgang, 2008). In figure 1.2, major trade movements across the world during 2015, are presented. The trade movements are also distinguished between pipeline gas and LNG.

Pipelines are a very convenient method of transport but not as flexible as shipping. If the pipelines have to be shut down, then also the receveing facilities have

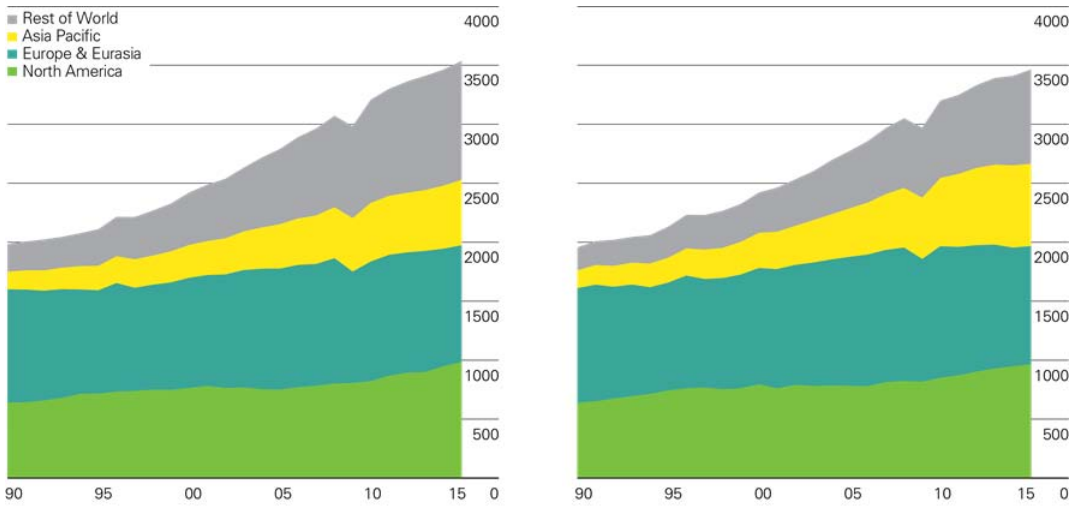

Figure 1.1: Gas production (on the left) and gas consumption (on the right) by region in billion of cubic meters (©BP Statistical review of energy, 2016).

to be shut down because of the difficulties in storing, with a consequent stop of production. There are also minor methodologies to transport natural gas, such as gas trasported as solid (gas hydrate) or converted to a liquid with the use of methanol or ammonia (Marques, 2014), but they have little or none commercial application.

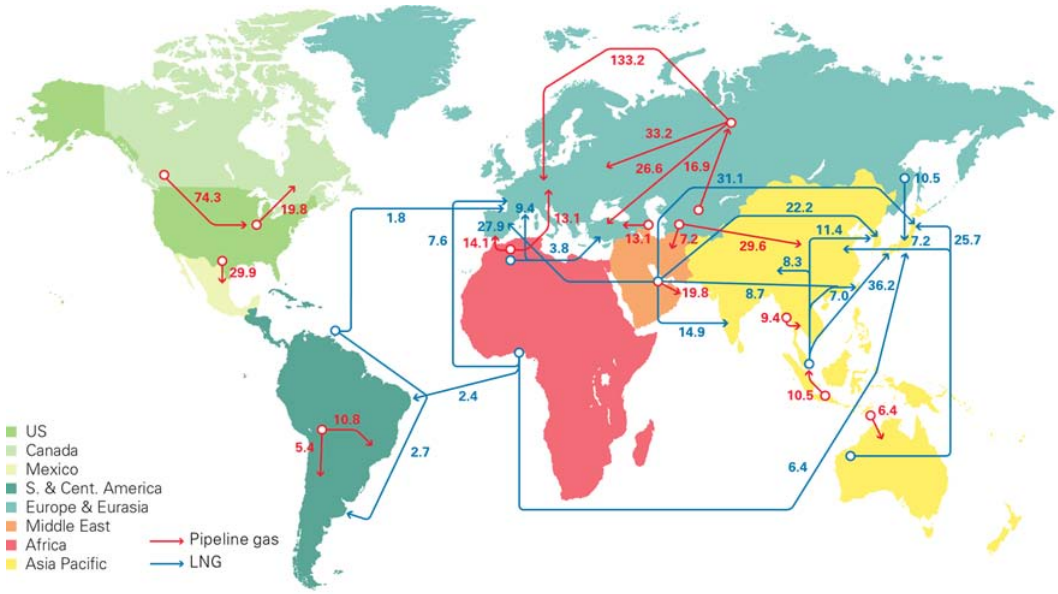

Figure 1.2: Major pipeline gas and LNG trade movements in 2015. Trade flows are reported in billion of cubic meters (©BP Statistical review of energy, 2016).

The composition of raw natural gas extracted from producing wells depends on the type, depth and location of the underground deposit as well as on the geology of the area. Oil and gas are often found together in the same reservoir. The gas coming from oil wells is commonly called "associated" (meaning that it is dissolved in crude oil), whereas the gas without any association with crude oil is called "non-associated". Most natural gas production contains, to varying degrees, small hydrocarbons (from two to height carbons) and impurities, in addition to the main element: methane (Tobin *et al.*, 2006). Table 3.1 shows the typical composition

of natural gas. Water is almost always present, but it is not presented in this list because it is common practice, unless the gas has not been previously dehydrated, to assume the entering gas satured in water at the nominal conditions of pressure and temperature.

Table 1.1: Typical composition of natural gas (Heinz-Wolfgang, 2008).

Component	**Chemical formula**	**Molar composition range** [%]
Methane	CH_4	50 - 95
Ethane	C_2H_6	2 - 20
Propane	C_3H_8	1 - 12
Butane	C_4H_{10}	0 - 4
Higher alkanes	$C_5H_{12}+$	0 - 1
Hydrogen sulfide	H_2S	0 - 6
Carbon dioxide	CO_2	0 - 99
Nitrogen	N_2	0 - 70
Oxigen	O_2	0 - 0.02
Helium	He	0 - 1
Other inert gases	-	traces

1.2 The gas chain

As already anticipated in the previous section, there are many impurities present in the raw natural gas coming from the production wells. Table 1.2 shows the composition specifications for pipeline gas and LNG with respect to the main impurities.

Table 1.2: Composition specifications for pipeline gas and LNG (Kidnay and Parrish, 2006).

Impurity	**Pipeline gas**	**LNG** [%]
H_2O	150 ppmv	< 0.1 ppmv
H_2S	5.7 - 22.9 $mgSm^{-3}$	< 4 ppmv
CO_2	3 - 4 mol %	< 50 ppmv
Total sulphur	115 - 459 $mgSm^{-3}$	< 20 ppmv
N_2	3 mol %	< 1 mol %
Hg	-	< 0.01 μgNm^{-3}
C_4H_{10}	-	< 2 mol %
C_5+	-	< 0.1 mol%
Aromatics	-	< 2 ppmv

As one may notice, the impurities amount allowed in LNG are way tighter than in the pipelines gas due to the extreme low temperatures required during the liquefaction process.

In order to achieve such sales specifications, the raw gas must pass through a series of processes which are commonly called "natural gas chain". A typical natural gas chain is represented in figure 1.3.

The number of steps and the type of techiniques used in the process of creating pipeline/LNG quality natural gas most often depends upon the source of the

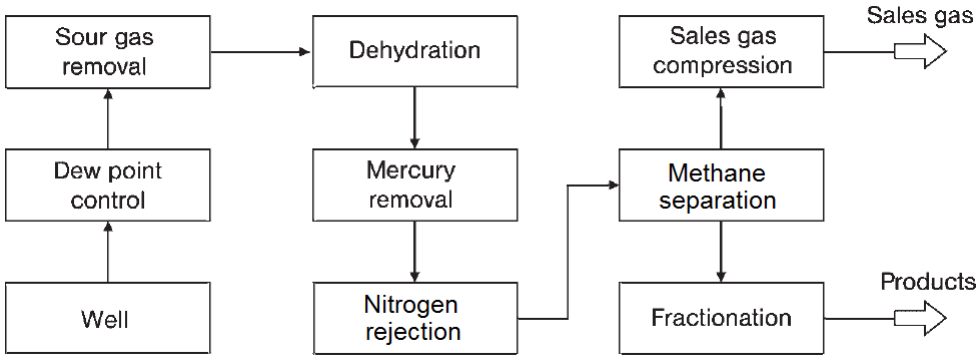

Figure 1.3: Typical process block diagram showing the classical stages involved in the production of pipeline-quality natural gas an LNG.

wellhead production stream. In some cases, in fact, some steps may not be present, they may be integrated into one unit or operation, performed in different order or not required at all (Tobin *et al.*, 2006). The main stages are described below:

Dew point control: In many cases pressure relief at the wellhead will cause a separation of gas from oil. Raw natural gas is commonly collected from a group of adjacent wells and is first processed at that collection point for removal of free liquid, water and condensate. The gas may be separated by the use of a simple closed tank, where the gas is separated by gravity, whereas in some cases a multi-stage oil separation process is needed to separate the crude oil from the gas stream, with intermediate heating and cooling units. After the transportation through pipelines, a separator to remove the condensate is needed. The condensate is usually then transported to an oil refinery and the water is disposed as wastewater. The gas stream enters the processing following plant at high pressure (Tobin *et al.*, 2006).

Sour gas removal: The initial purification of raw natural gas is usually the removal of acid gases, CO_2 and H_2S which cause corrosion and pose a major safety risk. There are many processes available, deeply described in §1.3. Carbon dioxide removed from gas can be used for re-injection in support of tertiary enhanced oil recovery efforts in the local production area or can be vented to the atmosphere if it satisfies environmental regulation. If the offgas contains more than about 10 tons per day of sulfur (as hydrogen sulfide), it is usually routed into a sulphur recovery unit which converts hydrogen sulphide into either elemental sulphur or sulphuric acid (almost all of the elemental sulphur is recovered for gas and oil treating). The Claus process is, by far, the most well known for recovering elemental sulphur. For cases that involve smaller quantities of sulfur, because of either a very low concentration in the feed gas or a small quantity of feed gas, direct oxidation may be the preferred route.

Dehydration: After the acid gas removal unit, the gas is sent to the water removal unit. The gas stream, at this point is usually water saturated (especially if the alkanolamines absorption process is used as acid gas removal method), therefore it cannot enter the following cryogenic units (due to the formation of hydrates and other technical issues). Dehydration of natural gas is accomplished by several methods. Among these, the processes of physical absorption (with glycol as solvent) or, alternatively, the temperature swing adsorption are the most common techniques exploited in the gas industry (see section §1.4 for a detailed description).

Mercury removal: Mercury must be removed for its toxic nature and also

because it corrodes alluminium in the heat exchangers as it amalgamates with it, weakening the material. Mercury can be removed using chemisorption, a sulphur impregnated carbon adsorbent or molecular sieves (Marques, 2014).

Nitrogen rejection: Nitrogen must be removed because of its impact on the gas combustion (NO_x are formed) and also in order to reduce the size and cost of next processing facilities. It is typically removed by a criogenic process, even though membrane or other absorbent technologies might be used (Kidnay and Parrish, 2006).

Methane separation: The process of demethanizing the gas stream can occur as a separate operation in the gas plant or as a part of the nitrogen rejection unit. There are different processes available for this purpose, such as cryogenic separation and absorption. Essentialy, cryogenic processing consists of lowering the temperature of the gas stream at around $-84°C$ where all the hydrocarbons condensate, exept methane which stays in gas phase. The absorption process, instead, uses a "lean" absorbing oil to separate the methane from the rest of hydrocarbons. An absorption tower is involved, where the absorption oil soaks up a large amount of the havier hydrocarbons. The enriched oil is then distilled in an another tower and recycled back (Tobin *et al.*, 2006).

Fractionation: During the fractionation the different gases present in the remaining gas stream are separated exploiting the different boiling points.

1.3 Sweetening

One of the main step in the natural gas chain is the removal of CO_2 and H_2S to obtain a gas available for the market. CO_2 must be removed for two main reasons: first of all it is a not-flammable components, second of all it can condensate in the cryogenic units. On the other hand H_2S is a corrosive molecule (in presence of water can lead the formation of sulphuric acid) as well as highly toxic. For these reasons, tipically, the concentration of CO_2 in the sweet gas should be around 2-3 mol% whereas H_2S must be below 4ppmv.

There are several available processes in the market for the removal of acid gases and the selection of a specific one depends on several discriminant factors. First of all, the selection depends on the quality and quantity of acid gas contaminants to be removed:

- CO_2 is the only contaminant;
- H_2S is the only contaminant,
- CO_2 and H_2S are present simultaneously;
- H_2S must be removed selectively when also CO_2 is present.

The selection also depends on other key factors such as the conditions of temperature and pressure at which the sour gas is avalilable, the volume of gas to be processed, the hydrocarbon composition of the gas and the capital and operating costs. Table 1.3 shows the selection factors to consider for the choice of sweetening process, in terms of partial pressure in the sour gas and plant size.

Table 1.3: Guidelines for acid gas removal. The dividing line between "high" and "low" is roughly 20 MMscfd for plant size and 100 psia for partial pressure. Table adapted from Kohl and Nielsen (2007).

Type of process	Partial pressure	Plant size
Chemical absorption	Low	Big
Physical absorption	High	Big
Adsorption	Low	Small
Membrane	High	Small

Both absorption in amine solution and absorption in a physical solvent are suitable process technique for treating high volume gas streams containing acid gases.

However, physical absorption processes are not economically competitive when the acid gas content is low because the capacity of physical solvents is a strong function of partial pressure.

Membrane permeation is particularly applicable to the removal of carbon dioxide from high-pressure gas. The process becomes less competitive with absorption processes as the plant size is increased.

Adsorption is a viable option for hydrogen sulfide removal when the amount of sulfur is very small and the gas contains heavier sulfur compounds (such as mercaptans and carbon disulfide) that must also be removed. For adsorption to be the preferred process for carbon dioxide removal, there must be a high carbon dioxide partial pressure in the feed, the need for a very low concentration of carbon dioxide in the product, and the presence of other gaseous impurities that can also be removed by the adsorbent (Kohl and Nielsen, 1997).

Nevertheless the most important process for natural gas sweetening is, by far, the chemical absortion. In the next section the attention is pointed toward this specific process. To study in deep the other available technique see literature books such as Kohl and Nielsen (1997) or GPSA (2004).

1.3.1 Alkanolamines absorption

Chemical absorption with aqueous solutions of alkanolamines is the most widely used technique in gas sweetening industry. Each amine has at least one hydroxyl group and one amino group. In general, it can be considered that the hydroxyl group serves to reduce the vapour pressure and increase the water solubility, while the amino group provides the necessary alkalinity in water solutions to cause the absorption of acid gases. At this point it is possible to recognize three types of amines. Primary amines, such as monoethanolamine (MEA), have two hydrogen atoms attached to the nitrogen and they are generally the most alkaline. Secondary amines, such as diethanolamine (DEA), have one hydrogen atom directly attached to the nitrogen atom, and tertiary amines, such as methyldietranolamnie (MDEA), represent completely substituted ammonia molecules with no hydrogen atoms attached to the nitrogen. Figure 1.4 shows their chemical formula.

The acid gas absorption in the alkanolamines solution is achieved in two steps. In the first step the acid gas dissolves into the solution and then the dissolved gas reacts with the amine. Because of their alkaline nature, amines are able to react

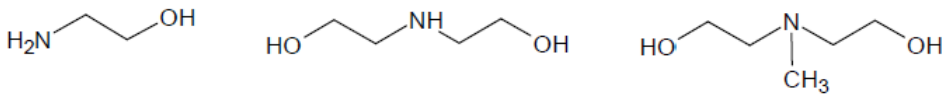

Figure 1.4: Molecular structure of MEA, DEA and MDEA.

with the acid species and forming an acid-base complex, reaction that is highly exothermic.

The principle reactions that occurs, when for example a secondary amine is used to absorb H_2S and CO_2, are listed below.

In the case of H_2S there are two steps that lead the reaction between the amine and the acid molecules: the amine protonation (from water ionization) and the ionization of the dissolved H_2S.

$$H_2O \rightleftharpoons H^+ + OH^- \tag{1.1}$$

$$R_1R_2NH + H^+ \rightleftharpoons R_1R_2NH_2^+ \tag{1.2}$$

$$H_2S \rightleftharpoons H^+ + HS^- \tag{1.3}$$

Therefore the formation of the amine hydrosulphide is possible.

$$R_1R_2NH_2^+ + HS^- \rightleftharpoons R_1R_2NH_2^+HS^- \tag{1.4}$$

In the case of CO_2 there are two possible mechanisms that may occur during the absorption. In the first mechanism CO_2 hydrolyses forming bicarbonate ions that react with the protonized amine.

$$CO_2 + H_2O \rightleftharpoons H^+ + HCO_3^- \tag{1.5}$$

$$R_1R_2NH_2^+ + HCO_3^- \rightleftharpoons R_1R_2NH_2^+HCO_3^- \tag{1.6}$$

The second mechanism is possible only if a reactive hydrogen is present in the amine structure (therefore this mechanism is not possible where tertiary amines are used). CO_2 reacts with the amine forming the carbamate.

$$R_1R_2NH + CO_2 \rightleftharpoons R_1R_2NCOO^- + H^+ \tag{1.7}$$

The carbarmate further reacts with another amine molecule forming the amine salt.

Altough other reactions may occur producing different species, these are not considered influencial in the analysis and design of sweetening units.

All the above reactions are reversible, in particulat the left to the right direction of the reactions represents the absorption phase favoured by low temperature and high pressure (exothermic). The right to the left direction of the reactions, instead, represents the regeneration phase: they are endothermic and favoured by high temperature and low pressure (Kohl and Nielsen, 1997). The equilibrium concentrations of molecular H_2S and CO_2 in solution are proportional to their partial pressures in the gas phase (i.e. Henry law) so these reaction are driven to the right by increased acid gas partial pressure (Kohl and Nielsen, 1997).

1.3.1.1 Process description

Figure 1.5 describes a general process flow for an alkanolamine trating plant.

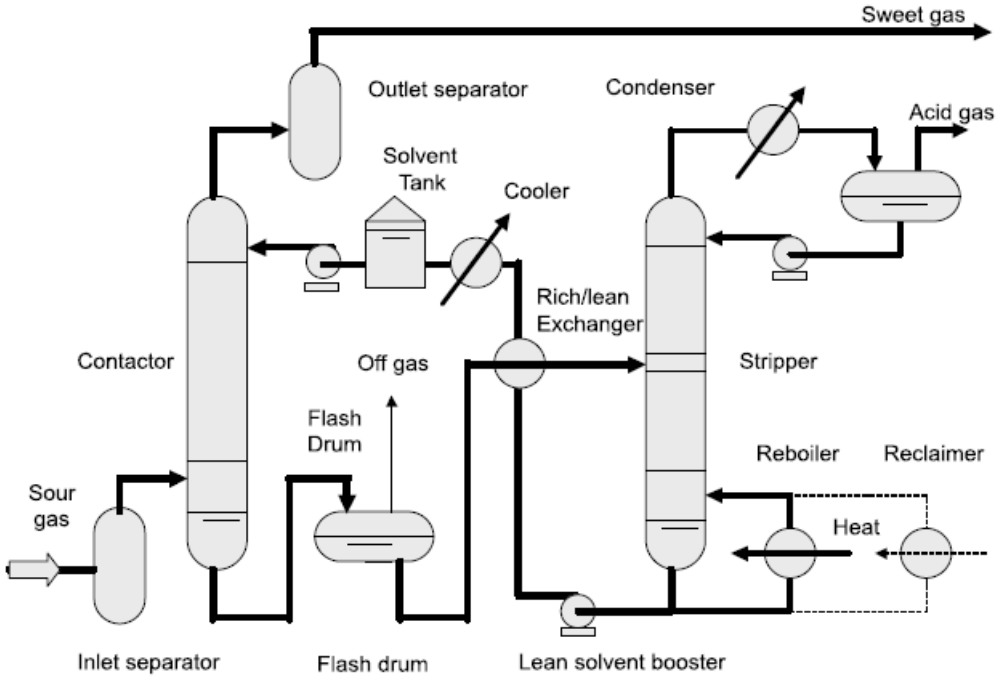

Figure 1.5: Typical gas sweetening process flow diagram by chemical absorption (GPSA, 2004).

The sour natural gas enters the plant through an inlet separator (or feed knock – out drum) to remove free liquids, such as water and hydrocarbons, and/or entrained solids. From the separator the gas enters the bottom of the contactor column and flows upward through the column in counter current contact with the aqueous amine solution (lean solution).

The lean solution inlet temperature should be, at least, 5°C higher than the feed gas to avoid hydrocarbon condensation. But, at the same time, an higher solution inlet temperature can lead to a lower acid gas absorption capacity and a higher water loss. Therefore, it is important to control the acid gas inlet temperature, and if necessary a dedicated equipment must be installed, such as an inlet cooler or a heat exchanger.

In the contactor column the acid gases present in the natural gas react with the solution forming the renegerable salts; the reaction is exothermic, therefore it will raise the temperature of the gas. The sweetened gas leaves the top of the contactor and passes through an outlet separator to remove any liquid carried over. This gas is water saturated, therefore a dehydration treatment is required downstream. Instead,

the amine solution, loaded with acid gases (rich solution), leaves the bottom of the column. The absorber column can be equipped with trays (around 20) or packing beds (generally 2 or 3). The column must be equipped with pressure differential instruments to monitor any abnormalities in the pressure drops. For example if the pressure drops arise very quickly, it means that there is a presence of foam, whereas a slow increase in the pressure drops indicates a tray or bed fouling.

The rich amine solution leaving the contactor is routed to a flash drum. This drum, whose operating pressure is between 7 and 15 bar allows to remove the absorbed hydrocarbons.

The rich solution from the amine flash drum, then passes through the rich/lean heat exchanger where heat is absorbed from the lean solution. Normally, lean solution inlet temperature is between 110°C and 130°C, whereas the rich solution inlet temperature is between 90°C and 110°C.

Then, the pressure could be further reduced to 1-2 bar. Now the rich solution is ready to be fed at the top of the regenerator (stripper) column. Generally, the regenerator is equipped following the same rules of the absorber, with the same issues related to the pressure drops.

In the reboiler the solution is heated up to produce steam so as to reverse the chemical reactions, therefore stripping out the absorbed acid gases. The reboiler duty is controlled by heating medium rate (steam or oil) and the regenerated solution outlet temperature is only a function of operating pressure and amine strength, usually it is around 110°C and 130°C. Clearly, the regenerated solution is routed back to the absorber, passing through the amine/amine exchanger to heat up the rich solution coming from the absorber. The temperature of the lean solution leaving the amine/amine heat exchanger is still high, therefore a cooler is required to provide the right temperature to enter the absorption column. After that, a mechanical filter might be present to remove impurities in order to prevent erosion and foaming.

The water vapour and acid gases mixture enters the condenser, that uses available cooling medium such as water or air, to condense the water vapour (generating the column reflux). The acid gas can be either vented, incinerated or sent to sulfur recovery facilities (Kohl and Nielsen, 1997 and GPSA, 2004).

A certain amount of water is continuously lost throughout the process, therefore a continuous water make up is required.

1.3.1.2 Solvent selection

One important factor to consider during the design of a sweetening unit is the selection of the amine which optimizes the equipment size and minimizes the plant operating costs. Following the work of Kohl and Nielsen (1997), some of the factors to be considered in the selection of the proper amine are: the selection of an amine which may be used at an higher concentration and/or gas loading (reducing at the same time the regenerator reboiler/condenser size and duty, also selecting amines with lower heat of reaction) so as to minimize the solution circulation rate, the selection of an amine (or mixture) that selectively absorbs H_2S rejecting CO_2 (if allowed by the sales gas specifications) and the selection of an amine solution resistant to degradation (reducing solution losses). In table 1.4 the main properties of MEA, DEA and MDEA are reported.

The most significant development in formulated solvents is the advent of tailored

Table 1.4: MEA, DEA and MDEA main features.

Features	**MEA**	**DEA**	**MDEA**
MW	61.09	105.14	119.17
Concentration	15-25 wt%	30-40 wt%	40-50 wt%
Selective H_2S removal	No	No	Yes
Degradation (by)	Yes (COS, CO_2, CS_2)	Some (COS, CO_2, CS_2)	No
Advantages	High alkalinity and low MW.	Low vapour pressure.	Highly resistant to thermal and chemical degradation, non corrosive, low heat of reaction.
Disadvantages	Irreversible reactions with COS, CO_2, CS_2, corrosive, high heat of reaction and high vapor pressure.	Not suitable for high CO_2 content.	Unable to form carbamate, very slow absorption of CO_2 (depending on the situations this may also be an advantage).

amine mixtures. These are usually based on MDEA, but contain other amines as well as corrosion inhibitors, foam depressants and others, blended for specific applications. These mixtures can be designed to provide selective H_2S removal, partial or complete CO_2 removal, high acid gas loading, COS removal, and other special features (Kohl and Nielsen, 1997).

Screening the available solvents to reach the optimum configuration passes through several steps. Based on a case study approach, each sweetening unit should test solvents to figure out whether any of them can meet the required specifications or not. All the tests rely first on theoretical modelling and simulation studies for a preliminary screening to reduce the experimental costs. If the specifications are not met, a possible solution to overtake the problem would be blending two types of amines, usually a tertiary amine with a primary or a secondary amine.

The thermodynamics, kinetics and physical properties of the promising solvents need to be studied experimentally and to be modelled to the appropriate theoretical models. When such data are available these solvents can be simulated and compared to the utilization of common amines. Several types of atoms and functional groups can be attached to the organic chain of the alkanolamine to tailor their properties. This would determine hundreds and may be thousands of chemical structures that may be possible candidates for further investigation (Muhammad and GadelHak, 2014).

1.4 Dehydration

Water vapour is, probably, the most common undesirable component in gas streams. If the temperature of the pipeline decreases below the dew temperature T_{dew} of the water vapour present in the gas, the water starts condensing. Many problems can appear such as the hydrates formation in combination with methahe (which may plug the valves); if the gas contains CO_2 or H_2S it becomes corrosive;

water increases the volume and decreases the heating value of the gas; and a gas with water vapour cannot be processed in cryogenic plants (Netusil and Ditl, 2012).

Two processes predominate for water vapour removal: absorption in glycol solution and adsorption on solid dessicants. Comparisons are made based on the dew point requirement, energy consumptions and costs. Figure 1.6 shows the selection of the dehydration methods based on the dew point requirement.

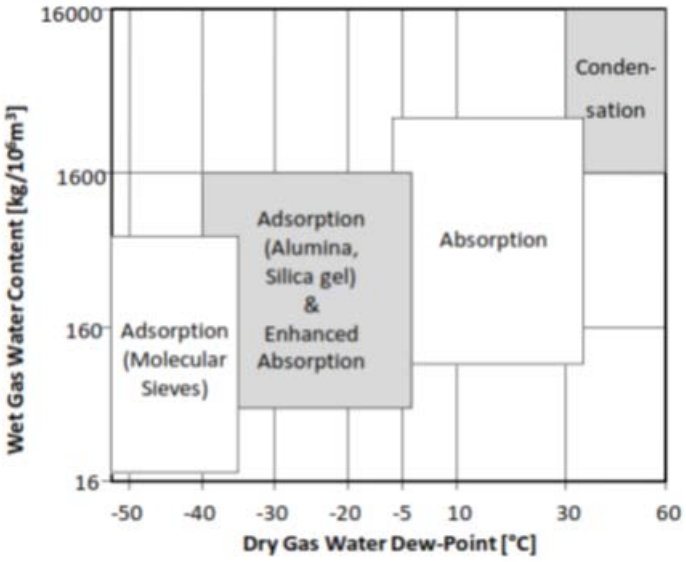

Figure 1.6: Selection of dehydration method (Netusil and Dit, 2012).

Absorption by TEG is the most widely used method in the petroleum industry to dehydrate the natural gas for pipeline transportation. $T_{dew} = -10°\text{C}$ is reached and this water content is sufficient for pipeline distribution of natural gas. By improving the reboiler design T_{dew} can be 2 or 3 times lower (Netušil and Ditl, 2012). Adsorption dehydration can achieve very low water content $T_{dew} = -50°\text{C}$, therefore this method is applied where a very low dew point are required, for instance in LNG plants. Condensation methods are suitable only in cases where a high-pressure difference is available.

The disadvantage of adsorption is that it requires high capital investment and has high space requirements (Netušil and Ditl, 2012). Solid desiccant processes are also preferred for very small installations where operating simplicity is a critical factor (Kohl and Nielsen, 1997). In addition, adsorption process consumes more power compared to absorption process as showed in figure 1.7.

1.4.1 Dehydration via absorption

For commercial dehydration purposes, the dehydration methods should have high absorption efficiency, flexibility during operation and should be economically suitable. These reasons have led to the widespread use of glycols for gas dehydration. They are chosen for their high hygroscopicity, low affinity for hydrocarbons and acid gases, excellent stability with regard to thermal and chemical decomposition, low vapour pressures, easy regeneration, low tendency to foam, and ready availability at moderate cost (Kohl and Nielsen, 1997).

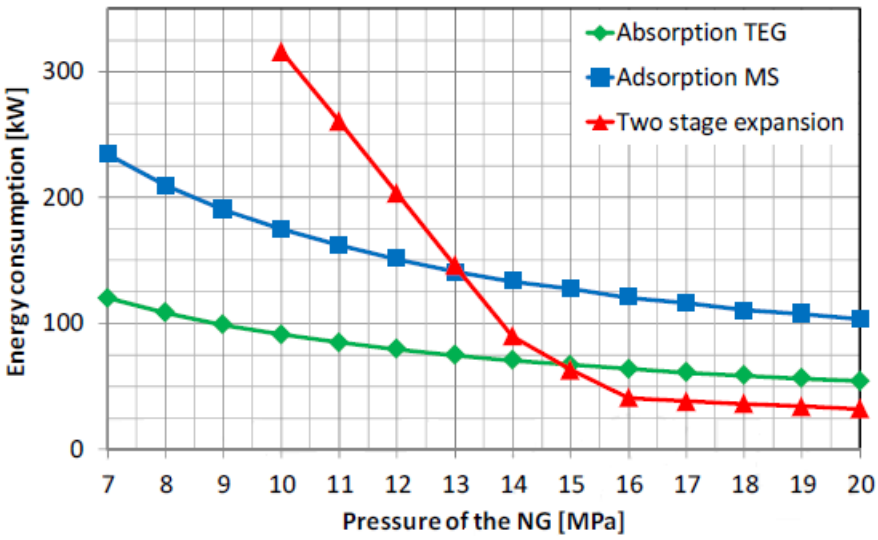

Figure 1.7: Energy results consumption for different dehydration methods (Netusil and Dit, 2012).

In particular, triethylene glycol (TEG) has become the industry standard for natural gas, even though other glycols are employed where they are able to meet the same performance at lower cost such as diethylene glycol (DEG).

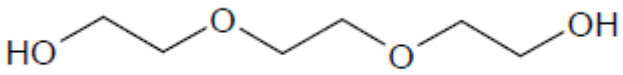

Figure 1.8: Molecular structure of TEG.

DEG is preferred for applications below 10°C because of the high viscosity of TEG in this temperature range. TEG is recommended for contact temperatures above about 50°C to minimize vapour losses.

1.4.1.1 Process description

Figure 1.9 shows a simplified flow diagram of a typical glycol dehydration unit. The process scheme is quite similar to the sweetening one previously described.

The wet gas is fed through an inlet scrubber to remove any free liquids that may be present. Removing liquids in the scrubber also decreases the amount of water that has to be removed in the absorption column, decreasing the size of the contactor and the TEG needed in the process. Liquid hydrocarbons are also removed in the inlet scrubber, which may increase the glycol tendency to foaming, therefore decreasing the process efficiency.

Then the gas flows up to the contactor column (absorber), which typically contains 3 up to 10 trays. The lean glycol is fed to the top of the contactor and absorbs water from the gas while flowing downward through the column; the dried gas leaves the top of the contactor. The dry gas may also pass through a scrubber, which removes any entrained glycol droplets before the product gas enters the pipeline.

After the contactor column, the rich glycol, which contains 3 up to 7 % of water is depressurized by a flash valve (not shown in figure 1.9). Then, the rich glycol is

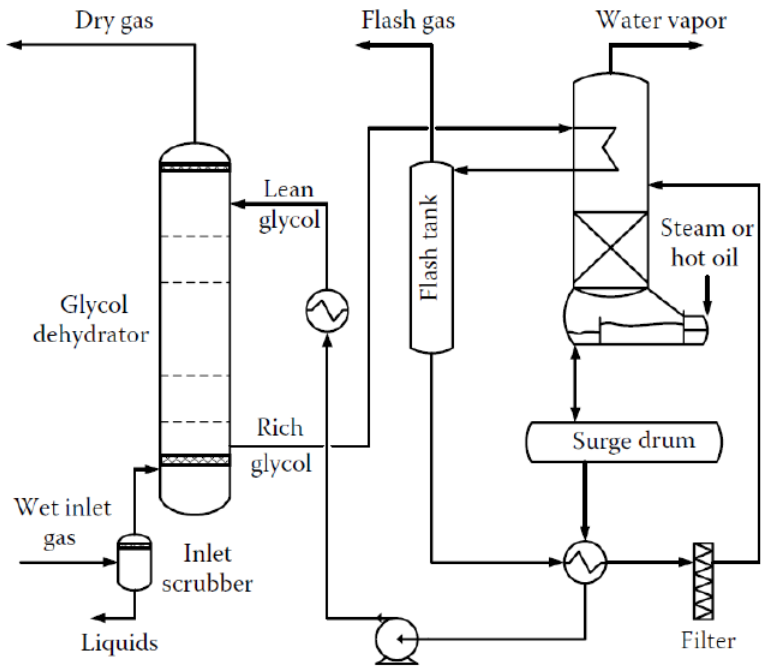

Figure 1.9: Process flow diagram for glycol dehydration unit (Adapted from GPSA Engineering Data Book, 2012).

often used to provide cooling to condense water vapour at the top of the stripper column. This raises the temperature of the rich glycol, which then may be further heated by an heat exchanger with hot lean glycol (not present in figure 1.9).

Then the rich glycol enters a reduced pressure flash tank where dissolved hydrocarbon gases are released. The released gases are recovered and used for fuel or other purposes. After flashing, the rich glycol passes through another glycol glycol heat exchanger, where it is further heated and a filtration system. Finally it enters the regenerator column (stripper).

Because of the extreme difference in the boiling points of glycol and water, a very sharp separation can be achieved with a relatively short column. Water reflux must be provided at the top of the column by condensing part of the overhead product so as to minimize glycol losses in the overhead vapour stream.

The pressure of the regeneration system is just above atmospheric pressure and the reboiler temperature can be at maximum 204°C, being limited by the glycol degradation. At this conditions the maximum glycol purity achievable is 98.6 wt%. The hot lean glycol is finally pumped back through the glycol glycol heat exchanger and back to the contactor (Kidnay and Parrish, 2006).

There exist different methods to achieve higher purities of the lean glycol flowing from the regenerator. This methods go under the name of "enhanced glycol concentration processes". The most common method is the use of a stripping gas or by means of vaccum reboiler. To deeply understand these methods and other enhanced processes see GPSA (2004).

1.4.2 Dehydration via adsorption

In this method water is adsorbed on solid dessicants such as molecular sieves, silica gel or alumina. However, the most efficient adsorbents are molecular sieves

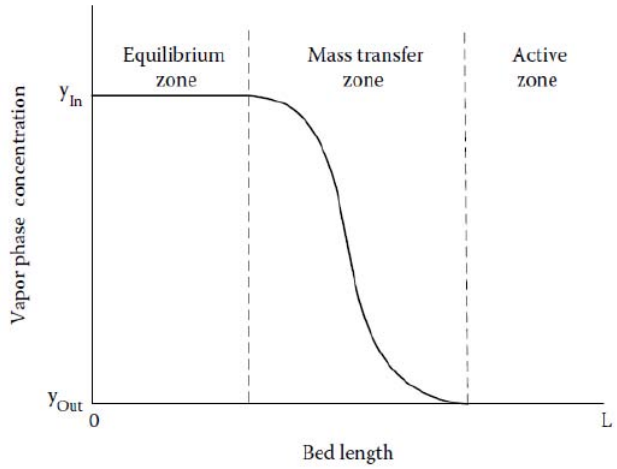

Figure 1.10: Water concentration profile along the adsorption bed divided between the equilibrium, the mass transfer and the active zone (Kidnay and Parrish, 2006).

(zeolites), able to achieve a water content below 0.1 ppmv (Dan Laudal, 2009).

Molecules are attracted to the bed surface due to two type of forces: dispersion repulsion and electrostatic. These mechanisms lead to an overall equilibrium, therefore for a given partial pressure and temperature an equilibrium concentration on the solid exists, for each species present in the gas mixture. Molecules with an high polarity are more strongly adsorbed than weakly polar or non polar components, such as methane (Marques, 2004).

When a wet gas passes through a solid bed, water is firstly adsorbed in the inlet zone of the bed, leaving the rest of the bed still active (active zone). As the adsorbent near the inlet becomes saturated (equilibrium zone) the zone of adsorption moves through the entire bed. This concentration wave is called mass transfer zone (MTZ) as shown in figure 1.10.

When the adsorption "wave" reaches the outlet the water content of the product gas rapidly increases, meaning that the bed is saturated and it is not able to remove water anymore. Usually, in the industry, the adsorption step can last from 8 to 24 hours (GPSA, 2004).

Regeneration of the bed can be performed by heating the bed or by decreasing its pressure. Processes that involved this regeneration methods are respectively called temperature swing adsorption (TSA) and pressure swing adsorption (PSA). A combination of these two method (PTSA) tough, seems to be a promising future option (Netusil and Ditl, 2012).

Since the dynamic nature of this process, to get a continuous process it is necessary to involve two ore more beds working in parallel. Figure 1.11 shows a typical TSA process with two adsorption beds.

The gas is fed to one of the beds where water is removed. Meanwhile the other bed is being regenerated by means of a hot dry gas, that can come from external source or be part of the dehydrated natural gas (as in this case). The hot gas (heated by an external heater) flows into the saturated bed where water is desorbed. Then the gas flows into a cooler where water is condensed and removed in a separator. Finally the remaining gas is compressed and recycled back to the inlet wet gas feed.

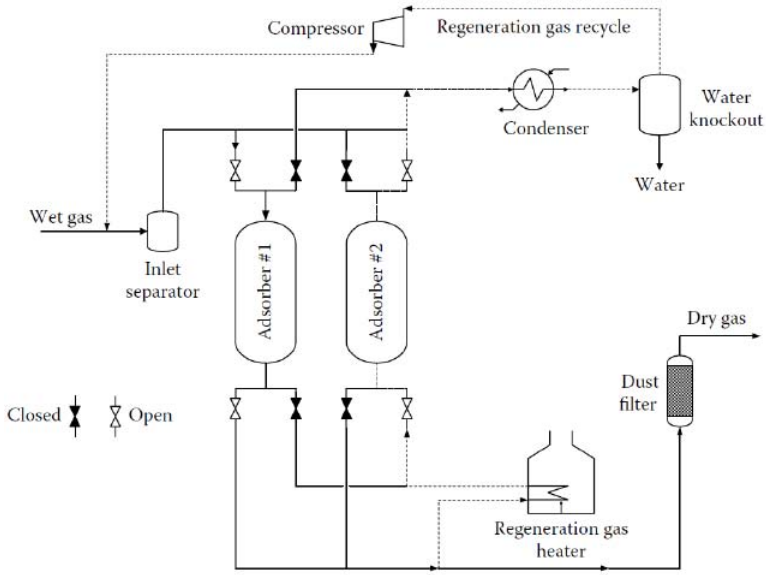

Figure 1.11: Solid dessicant dehydrator twin towers system (Adapted from GPSA Engineering Data Book, 2012).

1.5 Modelling

The aim of this last section has been collecting the main studies present in literature concerning the modelling of the processes described before. The main points have been finding the principle topics of interest, the tools involved to achieve good simulations results (i.e. the most common process simulators and the thermodynamic models) and, lastly, finding reliable data that could be reproduced.

Table 1.5 (and 1.6) reports some of the most recent studies, present in literature, on modelling the natural gas sweetening process; the study description and the simulation tools used are also reported.

First of all, from the studies description it is possible to see that DEA and MDEA (and their blends) are the main solvents of interest. Secondly, most of the studies look for an optimization of the process by playing with design parameters such as the amine concentration, flowrate as well as trying different process configurations.

Finally, from the analysis of the simulation tools, it is possible to state that the sequential modular [1] process simulator Aspen HYSYS® is the most used process simulator tools involved on modelling and optimizing the sweetening process. One of the main point of strength of Aspen HYSYS® is probably the thermodynamic package available, the DRB Amine Package (as described in Aspen Technology, Inc., 2006), which contains specific thermodynamic models, tailored for the sweetening process: Kent Einsenberg (Kent and Eisenberg, 1976; based on regression to experimental data) and Li Mather (Li and Mather, 1996; based on stronger thermodynamic foundation). In particular, these thermodynamic models correctly predict the solubility of CO_2 and H_2S in the different amines.

In Muhammad and GadelHak (2015), among the various suggestions to design and improve the modelling of the main columns (i.e. the absorber and the stripper),

[1] Sequential modular approach solves each unit operation sequentially and individually, according to the flow direction. Individual modules are developed for each unit operation.

Table 1.5: Summary of research works on modelling the sweetening (via absorption) process.

Reference	Study description	Simulation tools
Aliabad and Mirzaei (2009)	Theoretical investigation of the simultaneous absorption of CO_2 and H_2S into acqueous solutions of MDEA and DEA, comparing the results of two different process simulators.	The use of amine solvents have been investigated using Aspen HYSYS® and ASPEN. Electrolyte NRTL and the Amine Package have been used as thermodynamic models.
Nazir *et al.* (2010)	Study of the effect of declining pressure on the sweetening process involving MEA, DEA and MDEA as absorbing solvent.	Aspen HYSYS® using the Amine Package with Kent Eisenberg thermodynamic model for acqueous amine solutions and non ideal vapour phase.
Pellegrini *et al.* (2011)	Design of a purification unit in a large size NG plant of the Emirates with MDEA. The results are compared among three different process simulators.	Aspen HYSYS® (stage efficiency approach taking into account mass transfer and chemical reactions for all species), ProMax® (stage efficiency taking into account mass transfer only for non reactive species), Aspen Plus® (rate based model, prediction of mass transfer based on the film theory by Lewis and Whitman (1924).
Abdulrahman *et al.* (2013)	Simulation and optimization of a sweetening plant for Khurmala (Kurdistan region) natural gas. The simulation work is achieved examining DEA, MEA, MDEA and their blends as absorbing solvent.	Aspen HYSYS® v.7.3 is used to simulate the plant with the Kent Eisenberg (in the Amine Package) as thermodynamic model.
Berrouk and Ochieng (2014)	Discussion of the major optimization techniques based on the Benfield HiPure process. The acid gas first comes into contact with a 30 %wt solution of K_2CO_3 promoted with 3 % of DEA and is then contacted with a 20 %wt solution of DEA.	ProMax® simulator is used to perform a parametric study to improve process performance. The Electolytic ELR-PR (model that improves the NRTL acid gas model in the previous version TSWEET). Kinetic models allows to model the rate-based reactions taking place in the absorber.
Al-Lagtah *et al.* (2015)	Reviews the current operation of an existing plant (Lekhwair, Oman), which uses MDEA as solvent and pruposes some modifications to the existing plant to increase its profitability and sustainability. The results have been also validated against plant data.	Aspen HYSYS® v7.3 is used to study, simulate and optimize the plant. The DBR amine package is used rather than the traditional amine package because it better handles the reaction between CO_2 and MDEA. The modified Kent Einsenberg thermodynamic model is used to predict the vapour pressures and loading of CO_2 and H_2S.

Table 1.6: Summary of reasearch works on modelling the sweetening (via absorption) process (continue of table 1.5).

Reference	**Study description**	**Simulation tools**
Qeshta *et al.* (2015)	Study the LPG sweetening process using MDEA as solvent. The effects of design parameters such as amine flowrate, concentration and temperature are explored in order to find the optimum combination.	The flowsheet used has been developed within Aspen HYSYS® v.8.0 using the Amine Package. The model results have been compared with DOW Chemical company's results.
Tavan *et al.* (2016)	Techniques such as supersonic gas separation, mixed amines, and multi lean amine streams processes are simulated to adress common issues in the sweetening plants like equipment corrosion and high energy demand. In particular different blends of MDEA and DEA have been studied.	Aspen HYSYS® v.3.1 has been used to simulate the process with the Amine Package (Kent Eisenberg as thermodynamic model).

there is particular focus on the distiction between equilibrium-based and rate-based approaches. In the equilibrium-based approach the vapour and the liquid are assumed to leave each tray at equilibrim conditions and factor such as the Murphee efficiency are employed to correct the performance of the theoretical tray. But, in the case of reactive separation where the deviations from equilibrium are very large, like in the case of sweetening, it would be necessary to model such systems with a rate-based approach. The rate-based approach avoids the approximation of equilibrium and by modelling the mass and heat transfer coefficients it calculates the concentration distribution between the liquid and vapour phases. Although the informations regarding the thermodinamic model are always present, it is, quite rarely specified whether the equilibrium-based or the rate-based approach is used to model the contactor and the regenerator columns.

Table 1.2 reports the main studies present in literature on modelling the dehydration process via glycols absorption.

Also in this case process simulators are used to optimize the plant by chaging the process scheme, whereas TEG is the only solvent of interest in this process. Therefore, changing the process configuration, rather than searching for different solvents, seems to be the main option in order to optimize the process. Also in this case Aspen HYSYS® is the most common process simulator involved to model and optimize the process. Still, its main point of strength seems to be the specific thermodynamic package design for absorption processes with glycols, the Glycol Package (Aspen Technology, Inc. 2006) and the Hydrate utility package, which is able to calculate the temperature of hydrate formation in the gas stream. In particular within the Glycol Package there is the possibility to choose between Peng - Robinson, preferred for MEG and DEG, and Twu Sim Tassone (TST), a specific advanced equation of state developed for modelling TEG - water system for glycol gas dehydration process (Twu *et al.*, 2005).

Since its nature of pure absorption process, without reactions (differently from the sweetening process), the common approach to model the two columns (contactor and regenerator) is using the equilibrium-based approach.

Table 1.7: Summary of research works on modelling the glycol (via absorption) process.

Reference	Study description	Simulation tools
Abdulrahman *et al.* (2013)	Developing a dehydration process for Khurmala (Kurdistan region), continuing the study after the simulation of the sweetening plant. The dehydration process has been simulated and optimized by using several types of solvents such as TEG, DEG and MEG.	Aspen HYSYS® v.7.3 process simulator has been involved in modelling such process with the Glycol Package.
Ghati (2013)	Design of a dehydration process with TEG as absorbing solvent for the Songo Songo (Tanzania) natural gas. Sensitivity analyses are also provided to optimize the process.	Aspen HYSYS® with Peng - Robinson fluid package.
El Mawgoud *et al.* (2014)	Modelling and simulation for revamping a dehydration gas plant named "Akik" existing in Egypt and owned by Khalda Petroleum Company. Three different alternatives have been considered and investigated to choose te optimum one with respect to the minimum equipment costs. TEG is the solvent chosen.	The plant has been simulated using Aspen HYSYS® with Peng - Robinson Eos for VLE calculations and calculation of the liquid densities for hydrocarbon systems.
Anyadiegwu *et al.* (2014)	Desing and simulation of a natural gas dehydrating plant, exploring the system response to different TEG flowrates.	Aspen HYSYS® has been used as process simulator (information on the thermodynamic model chosen are not provided). The Hydrate utility package has also been used to evaluate the temperature of hydrates formation.

Altough in literature many studies can be found regarding the basic concepts and mathematical models to describe mass transfer and isotherm behaviour on adsorption column (e.g. Shafeeyan *et al.* 2014, Xu *et al.* 2013) and there are a lot of experimental works, where the adsorption equilibrium and kinetics of water on different solid adsorbents have been studied (e.g. Wang and Douglas 2009, Ribeiro *et al.* 2008), there are just few studies on modelling natural gas dehydration beds. In Gholami *et al.* (2010) a mathematical model is developed to simulate an adsorption process for dehydration of a gas stream. The dual site Langmuir isotherm is employed in predicting adsorption equilibrium and the Peng-Robinson equation is used as thermodynamic model. The mathematical model is solved by a finite volume method and the results verified against experimental data. In Al Wahedi *et al.* (2016) a new method for the design of natural gas dryers is presented. Two process schemes of TSA, based on common industrial conditions, are considered, which differ in the source of the regeneration gas. The method formulates a mixed

integer non linear programming (MINLP) where the objective is to minimize the net present value of ensued cost (NPVC) while meeting all process constraints. In Ahn and Lee (2003), a deep description of the mathematical model that allowed to model a TSA air drying process is present.

1.6 Motivation

The first part of the work is driven by the objective to show the opportunity of modelling the natural gas chain processes using gPROMS® ProcessBuilder and gSAFT® as thermodynamic package. The main advantage deriving from this approach would be the possibility of modelling all the different processes involved in the gas chain, by using the same thermodynamic model, without the use of tailored packages. Thus, having one single flowsheet, which embeds more processes in series, would allow to better understand how, for instance, the changing of a certain parameter, would affect the whole chain. Having a whole flowsheet implemented in an equation oriented process simulator, like gPROMS®, would also allow to build rigorous optimization problems, taking into account at the same time constraints, variables and objective functions from different unit operations. Furthermore, the use of gSAFT® in absorption processes, would allow to easily test the performance of different solvents in order to find the best one who fits certain operational constraints.

In the case of the adsorption process, the aim is to build a general mathematical framework able to model the adsorption of water in zeolites. In particular, the idea is to build a multiple beds flowsheet which would allow to achieve continuous operation.

Chapter 2

Thermodynamics

The need to accurate property prediction required in the gas industry leads to a continuous developing and improvement of thermodynamic tools. In particular, the most important aspect of these thermodynamic tools is their predictive capability, which is the ability to accurate predict a wide range of process conditions without the need of experimental data for the determination of model parameters. Concerning the processes of sweetening and dehydration the future perspective looks for a thermodynamic model able to deal with a widespread range of components and impurities in order to represent the processes in the most realistic way. This aspect becomes very useful for a common problem in the sector of gas processing, which is the ability to explore a large desing space of compounds for the selection of the optimal solvent and investigate the effects of variations in the composition. For this purpose a specific class of methodologies, the so called group contribution equation of state (GC - EoS), have been developed.

In this chapter it is illustrated the thermodynamic model chosen for the simulation of the two absorption processes of sweetening and dehydration, the SAFT-γ Mie, implemented in the gSAFT® package. Starting from a general description of theory behind this GC - EoS, it is reported the procedure carried out in order to validate the thermodynamic model for those processes. In the end, it is also illustrated Multiflash™, the thermodynamic package involved in modelling the dehydration via adsorption process.

2.1 SAFT-γ Mie

Altough GC methods have been introduced for their high predictability and flexibility in the calculation of fluid properties, they present important drawbacks such as the limited T and P range of reliable applicability, the inconsistency in the description of the critical region and the fact, that they cannot provide the calculation of other important properties commonly involved in process design like density, heat capacity, etc. On the other hand, equations of state are not limited, in principle, in their range of applicability and can be used to calculate other thermodynamic properties; however, they are less predictive than GC methods, as component based parameters are needed. In an effort to use equations of state in a predictive manner, they have been combined with group contributions methods in order to take the most from both the metodologies and, at the same time, to overcome the main

drawbacks.

One of these GC EoS is the so-called Statistical Association Fluid Theory (SAFT). Different approaches are embeeded within the SAFT framework and in this work, in particular, the SAFT-γ Mie approach is involved. For an overview of the SAFT general theory and the different theories within it refer to Papaioannou (2012).

In the SAFT-γ Mie approach molecules are represented as associating heteronuclear chains of fused spherical segments. Each compound i is defined by a set of values $\nu_{i,k}$, that denote the number of functional groups of type k in the compound. A given group k is characterized by one or more identical segments ν_k^* and a shape factor S_k which translates the extent to which the segments of a given group k contribute to the overall molecular properties. Various SAFT version exist in the literature and they mainly differ in their choice of rappresenting the intermolecular potential for the "sphere-sphere" interactions (e.g. Lennard- Jones, Square-Well, Mie potential). The Mie pair potential is a generalized form of the Lennard Jones potential, with variable attractive and repulsive ranges. In the case of interactions between segments of the same group-type k, the Mie potential is written as:

$$\Phi_{kk}^{Mie}(r_{kk}) = C_{kk}\epsilon_{kk}\left[\left(\frac{\sigma_{kk}}{r_{kk}}\right)^{\lambda_{kk}^r} - \left(\frac{\sigma_k}{r_{kk}}\right)^{\lambda_{kk}^a}\right] \tag{2.1}$$

where r_{kk} is the centre – centre distance between the segments, σ_{kk} is the diameter of the segments, ϵ_{kk} is the depth of the potential, and C_{kk} is a constant function of the repulsive (λ_{kk}^r) and attractive (λ_{kk}^a) exponents of the potential and is defined as:

$$C_{kk} = \frac{\lambda_{kk}^r}{\lambda_{kk}^r - \lambda_{kk}^a}\left(\frac{\lambda_{kk}^r}{\lambda_{kk}^a}\right)^{\frac{\lambda_{kk}^a}{\lambda_{kk}^r - \lambda_{kk}^a}} \tag{2.2}$$

which ensures that the minimum of the potential is at $-\epsilon_{kk}$. The group interaction is then characterized by the diameter of each segment σ_{kk}, the potential well-depth ϵ_{kk} and the repulsive and attractive ranges of the interaction potential λ_{kk}^r and λ_{kk}^a.

The interaction between unlike groups k and l is characterized by an unlike segment diameter σ_{kl} defined as:

$$\sigma_{kl} = \frac{\sigma_{kk} + \sigma_{ll}}{2} \tag{2.3}$$

The unlike dispersion energy obtained using a modified geometric mean that takes into account the size and asymmetry of the groups as:

$$\epsilon_{kl} = \frac{\sqrt{\sigma_{kk}^3\sigma_{ll}^3}}{\sigma_{kl}^3}\sqrt{\epsilon_{kk}\epsilon_{ll}} \tag{2.4}$$

and the unlike repulsive and attractive exponents of the Mie potential as:

$$\lambda_{kl} = 3 + \sqrt{(\lambda_{kk} - 3)(\lambda_{ll} - 3)} \tag{2.5}$$

In common with other SAFT approaches, additional short-ranges sites can be used to model the association (e.g. hydrogen bonds) interactions present in some

polar compounds. The association interactions are modelled by means of square-well sites, therefore a site placed on a segment k interacts with a site b placed on a segment l as shown in (2.6):

$$\Phi^{HB}_{kl,ab}(r_{kl,ab}) = \begin{cases} -\epsilon^{HB}_{kl,ab} & r_{kl,ab} \leq r^{c}_{kl,ab} \\ 0 & r_{kl,ab} > r^{c}_{kl,ab} \end{cases} \tag{2.6}$$

where $r_{kl,ab}$ is the centre-centre distance between sites a and b, $-\epsilon^{HB}_{kl,ab}$ is the association energy, and $r^{c}_{kl,ab}$ is the cut-off range of the interaction; between sites a and b. In order to completely describe a group with association sites is therefore important to specify the number $N_{ST,k}$ of the different site types and the number of sites of each type, e.g. $n_{k,a}, n_{k,a}$,...,$n_{k,NST}$ togheter with the position $r^{d}_{kl,ab}$ of the site. These parameters and the number of segments ν^{*}_{k} are chosen a priori based on the chemical nature of each group, examining different possibilities by a trial-and-error approach. The unlike values of the association energy is calculated by a simple geometric mean:

$$\epsilon^{HB}_{kl,ab} = \sqrt{\epsilon^{HB}_{kk,aa}\epsilon^{HB}_{ll,bb}} \tag{2.7}$$

while the unlike range of the association site-site interaction is:

$$r^{c}_{kl,ab} = \left(\frac{\sqrt[3]{r^{c}_{kk,aa}} + \sqrt[3]{r^{c}_{ll,bb}}}{2} \right) \tag{2.8}$$

Figures 2.1 and 2.2 respectively show how some natural gas components and the solvents involved in the absorption section of this work, are structured within the SAFT-γ Mie approach. To notice how each molecule is represented as a ensable of different groups and association sites.

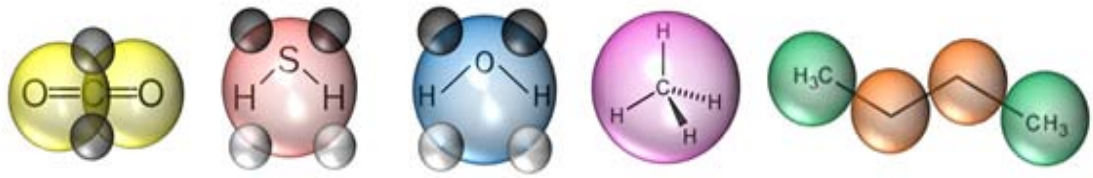

Figure 2.1: Structure of some the natural gas components (CO_2, H_2S, H_2O, CH_4 and C_4H_{10}) within the SAFT-γ Mie approach.

Figure 2.2: Structure of the solvents involved in the absorption section of this work (DEA and TEG) within the SAFT-γ Mie approach.

Generally, each SAFT equation of state is then written in terms of the Helmholtz free energy (A) as a sum of different contributions:

$$\frac{A}{Nk_bT} = \frac{A^{ideal}}{Nk_bT} + \frac{A^{monomeric}}{Nk_bT} + \frac{A^{chain}}{Nk_bT} + \frac{A^{association}}{Nk_bT} \tag{2.9}$$

where A^{ideal} corresponds to the free energy of the ideal polyatomic gas system, $A^{monomeric}$ is the residual free energy due to the interactions between the monomeric Mie segments, A^{chain} refers to the energy due to the formation of a chain of tangential or fused monomeric Mie segments, $A^{association}$ is the free energy due to the association between molecules, N K_b and T are respectively the total number of moleculs, the Boltzmann constant and the absolute temperature. Figure 2.3 helps to visualize how each term contribute to the overall energy of the system.

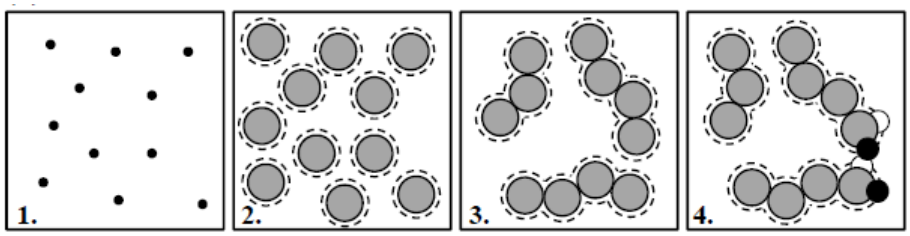

Figure 2.3: Individual contributions to the free energy of the system within the framework of SAFT-γ Mie type methods: 1) Ideal gas; 2) Monomer term; 3) Chain term; 4) Association (Papaioannou, 2012).

The complex description of how each term is calculated goes well beyond the purposes of this work. For this reason, for a better understanding of the theory behind the calculation of the Helmhotlz free energy refer to Papaioannou *et al.* (2014).

Once the functional form of the Helmholtz free energy has been specified, other properties, such as pressure P, chemical potential μ_i, internal energy U, enthalpy H, entropy S, Gibbs free energy G, second order derivative properties (c_v, c_p), the speed of sound u, isothermal compressibility k_T, thermal expansion coefficient α and Joule-Thompson coefficient μ_{JT} can be obtained algebraically from the standard thermodynamic relations (Papaioannou *et al.*, 2014) Below the expressions to derive pressure and chemical potential from the Hemoholtz free energy are shown:

$$P = \left(\frac{-\partial A}{\partial V}\right)_{T,N} \mu_i = \left(\frac{\partial A}{\partial N_i}\right)_{T,V,N_j}$$

2.2 gSAFT®

gSAFT®is a physical property package developed at Process Systems Enterprise Ltd., used in gPROMS®platform products. This property package has either the SAFT - Variable Range Square Well (SAFT - VR SW) or the SAFT-γ Mie equation of state as basis, and it is used in the platform as a call of a databank.

In the SAFT-γ Mie EoS each non associating group is described by the following set of parameters: the number of segments (ν_k^*), shape factor (S_k), segment diameter (σ_{kk}), dispersion energy (ϵ_{kk}) and the repulsive and attractive exponents of the

potential (λ^r_{kk} and λ^a_{kk}). In the case of associating groups, additional parameters are introduced, such as the number of types of associating sites of a group k (N_{STk}), the number of sites of each type ($n_{k,a}$) and the energy ($\epsilon^{HB}_{kk,ab}$) and range ($r^c_{kk,ab}$) of interaction for each pair of sites. All the parameters just mentioned are estimated by means of appropriate experimental data, except for the number of segments which is determined by a trial-and-error approach. The unlike group parameters σ_{kl} and λ_{kl} can be calculated using the mixing rules described in the previous paragraph, whereas the unlike dispersion energy ϵ_{kl}, the unlike association energy $\epsilon^{HB}_{kl,ab}$ and the unlike range of association $r^c_{kl,ab}$ are estimated by regression of experimental data. In figure 2.4 the group present in the gSAFT databank are listed, specifying wether the like - unlike parameters are present or not.

Within gPROMS enviroment, the parameters estimation via regression of experimental data is performed via gSAFT Material Modeller (gSAFTmm), an auxiliary tool which involves the Python^{TM} language.

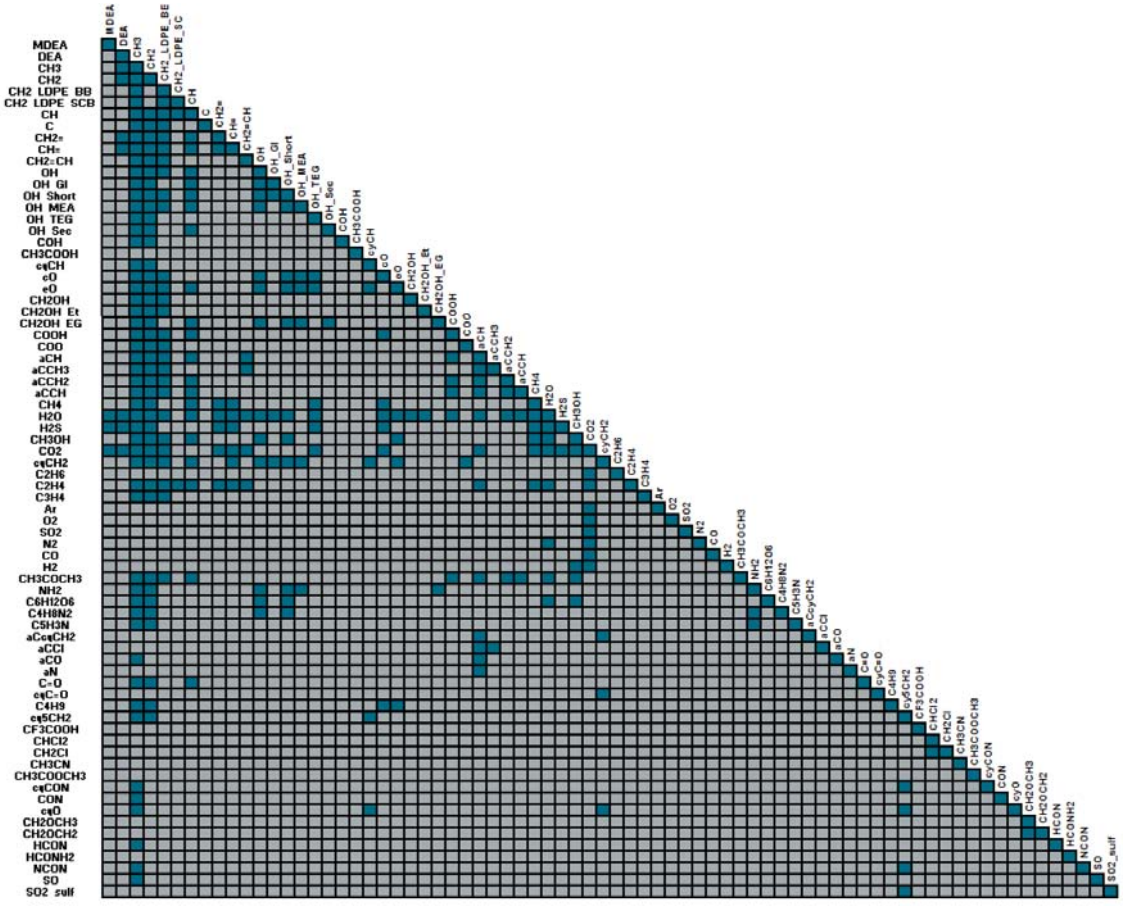

Figure 2.4: List of the functional groups present in the gSAFT-γ Mie databank, where the blue squares indicates the presence of the like-unlike parameters whereas the grey indicates where they are missed. Santos (2016).

2.3 Validation

In process simulation the first step is the selection of the more appropriate physical property model, followed by either its validation or the model parameters fitting against experimental data. The factors to consider, in order to choose the most appropriate method, are the nature of the system of interest and its composition, the conditions of pressure and temperature and the availability of the model parameters (Carlson, 1996).

As stated in the previous paragraph, the power of SAFT-γ Mie model is to be very general in such a way to be able to described widely the most complex chemical systems. For this reason SAFT-γ Mie model has been chosen to simulate the two absorption processes of natural gas sweetening and dehydration. This has been possible as all the required groups parameters (like and unlike) are present in the Mie databank (databank depicted in figure 2.4). In the following paragraph the validation carried out, in order to evaluate the goodness of the model parameters, will be illustrated.

The validation is, mainly, made by binary vapour-liquid equilibria (VLE) as the main feature to assess in absorption processes is the effective behaviour of the mixture where a mass exchange process takes place. Firstly, the interactions between the natural gas components have been explored, in particular focusing on the main alkanes present, from methane to propane (also butane and propane is some cases) and on the "undesired" components such as the acid gases (hydrogen sulphide and carbon dioxide) and water. After that, the interactions between the gas components and the absorbing solvent involved in those processes (diethanol amine (DEA) in the sweetening and triethylene glycol (TEG) in the dehyration) has been studied and validated.

The experimental data, used in the validation, have been chosen as close as possible to the processes conditions, except few cases where this has not been possible for physical-chemical and practical reasons. Before introducing the validation, it is also important to underline that, for such systems, often, it has not been easy to find reliable experimental data in the open literature. Therefore, all the validation (and parameters estimation) described could eventually be extended to new experimental data.

2.3.1 Natural gas

The first step in the validation of the SAFT-γ Mie thermodynamic model is, as already mentioned, the study of the interaction between the components present in the natural gas mixture. For the purposes of this work, the most important features to verify are the interactions between the "undesired" components and the main alkanes, rather than, for instance, the study of single components properties. In particular this has been possible comparing experimental and calculated vapour - liquid equilibria data.

In this firts subsection, the validation of the interactions between the acid gases and the main alkanes present in the natural gas mixture is described.

Figure 2.5 shows a comparison between the experimental and the predicted VLE data for the system H_2S - Methane. It is important to underline that both the species are modelled as a whole group, where in the hydrogen sulfide molecule bonding sites

are present either, as previously shown in figure 2.1.

At "low" temperature (277.6 K) the VLE is correctly calculated, matching the experimental data, whereas, at higher temperatures the prediction are poorer. This means that "high" temperature data were not included in the original parameter fitting, therefore, a better prediction, over a wider range of temperatures, would be possible simply by extending the experimental data through which the parameters are fitted. In this work the original parameters has been considered suitable to the thesis objectives, as the prediction becomes poor for pressures higher than 10 MPa, and, as will be illustrated in §3, those pressure are never reached in the sweetening process.

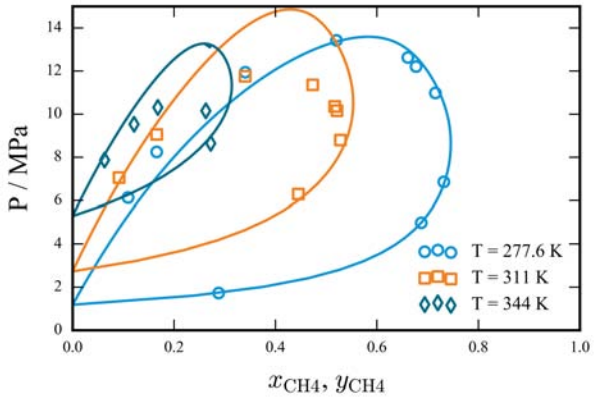

Figure 2.5: Isothermal VLE of the system H_2S - Methane. The symbols correspond to the experimental data from Reamer and Lacey (1951), and the curves to the SAFT-γ Mie calculation.

Figure 2.6 reports the 4 VLE systems: H_2S - Ethane, H_2S - Propane, H_2S - n-Butane, H_2S - n-Pentane where the experimental and the calculated data are compared. Before starting the discussion though, it is important to remind that, from SAFT-γ Mie point of view, n-Alknanes (except methane), such as the ones just mentioned, are seen as an ensamble of methanedyl $-CH_2-$ and methyl $-CH_3$ groups. The only difference between one molecule and another is simply the number of groups of each type. As one may notice, the plots present both dashed and solid curves. The dashed curves represent the SAFT-γ Mie calculation before the parameter fitting, which has been necessary as the original prediction for the systems H_2S - Ethane and H_2S - Propane was quite poor. Moreover, it is interesting to notice that, altough the prediction for those systems was not acceptable, in the other two systems considered, H_2S - n-Butane, H_2S - n-Pentane, the prediction could already be accepted. This fact suggests that the fitting procedure should focus on the interaction between H_2S and $-CH_3$ rather than on H_2S - $-CH_2-$. In fact, in the Ethane molecule only $-CH_3$ is present and in Propane the weight of the $-CH_3$ group is "higher" than the $-CH_2-$ one; instead, for higher alkanes the weight of $-CH_3$ is lower as the number of carbon atoms increases. Furthermore, the new unlike dispersion energy ϵ_{H_2S,CH_3}, after the fitting, is expected to be lower than the original one. In figure 2.6a., for example, the dashed lines (the original calculation) are always above the experimental data, represented by the simbols. Therefore, considering for instance a molar fraction of H_2S equal to 0.2, it is possible to notice that the original calculation predicted a boiling temperature higher than the experimental, therefore the energy was higher, allowing the mixture to stay in

the liquid phase for an higher range of temperature. Thus, the solid curves confirms what has been predicted in advance. During the fitting, the value of the ϵ_{H_2S,CH_3} slightly decreas in such a way that now the the experimental data for the systems H_2S - Ethane and H_2S - Propane are perfectly matched. ϵ_{H_2S,CH_2} has not been varied, in fact the H_2S - n-Butane and H_2S - Pentane predictions still remain acceptable, presenting a little improvement as well.

Altough the fitting should comprehend all the possible data present in literature, for the purposes of this work, just the data depicted in the plots have been considered since they well conver the conditions of pressure and temperature present in the processes considered. In conclusion, it is important to highlight that, the values at the bounds of the plots, representing the pure component conditions, are always perfectly matched.

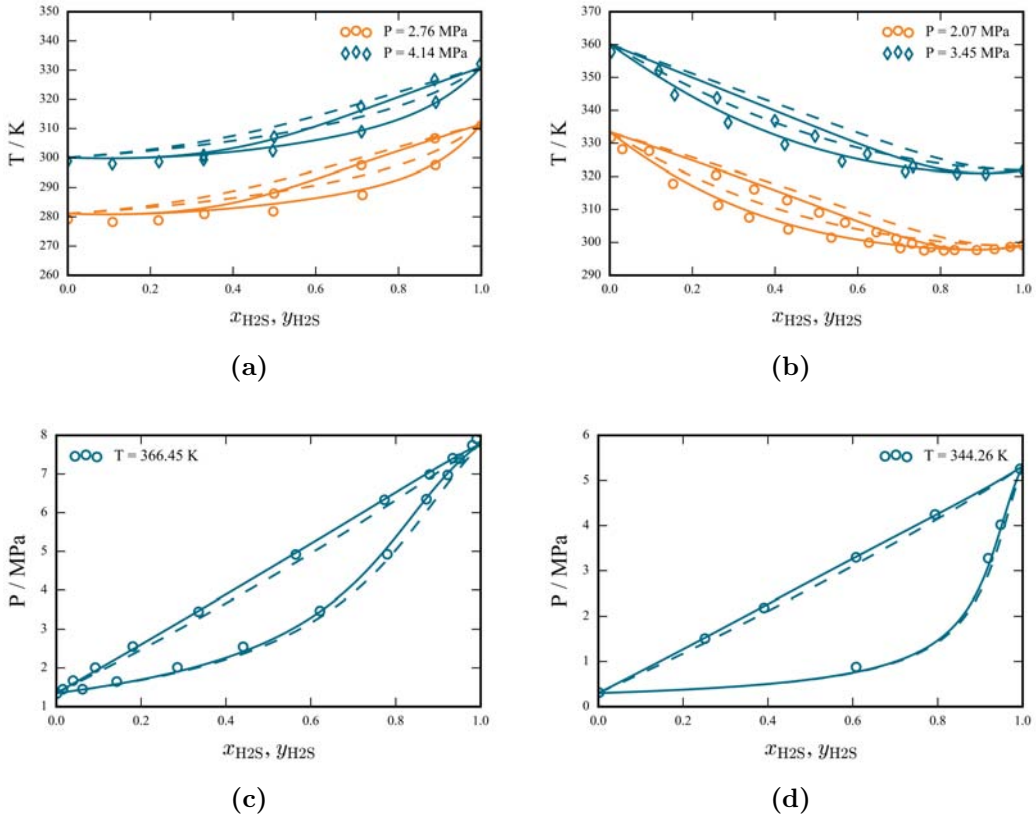

Figure 2.6: Isobaric and isothermal VLE of H_2S - n-Alkanes systems. a) H_2S - Ethane, experimental data from Kay and Brice (1953), b) H_2S - Propane, experimental data from Kay and Rambosek (1953), c) H_2S - n-Butane, experimental data from Leu and Robinson (1989), d) H_2S - n-Pentane, experimental data from Reamer, Sage, Lacey, 1953. The symbols correspond to the experimental data and the curves to the SAFT-γ Mie calculation. In particular, the dash curves represent the calculation before the parameter estimation whereas the solid ones represent the calculation after the estimation.

After the discussion for the H_2S, following the same rationale, the next part will discuss the other acid gas typically present in natural gas mixture: CO_2.

Figure 2.7 shows the VLE for the system Methane - CO_2. The good match between experimental and predicted data allows to confirm the goodness of the

original parameters present in the databank, for such interaction.

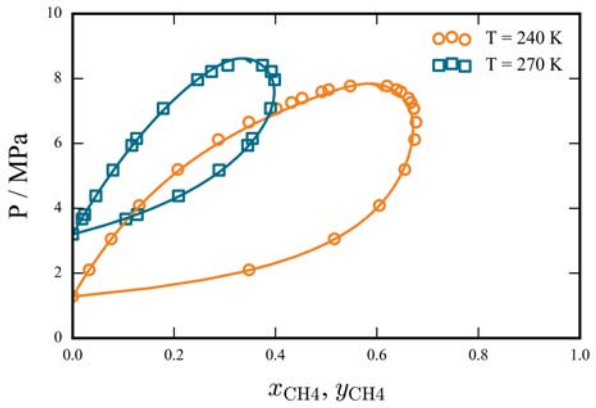

Figure 2.7: Isothermal VLE of the system Methane - CO_2. The symbols correspond to the experimental data from Al-Sahhaf, Kidnay, Sloan (1983), and the curves to the SAFT-γ Mie calculation.

Figure 2.8 illustrates the thermodynamic validation for the 4 systems: CO_2 - Ethane, CO_2 - Propane, CO_2 - n-Butane, CO_2 - n-Pentane where the experimental and the calculated data are compared. The original interaction parameters well predict the experimental data, even though a fitting has been carried out in order to better match the experimental data of the system CO_2 - Ethane (figure 2.8 a)) at a temperature of 230 K (at 210 K the prediction is already acceptable). In this case, clearly, only the unlike dispersion energy between $-CH_3$ and CO_2, ϵ_{CO_2,CH_3}, has been considered. In particular, differently from what stated previously for the system H_2S - Ethane, here the energy need to be increased, which is then confirmed by the fitting result. In fact, for example looking at the point of azeotrope, the original parameter predicts an higher pressure in order to condensate the mixture from gas to liquid phase. The new parameter does not affect the other 3 systems considered, even though slight changes may be noticed. Therefore the system CO_2 - Alkanes is validated.

So far the interactions between alkanes and the acid gases have been validated. The last step, in this first part of the validation, will be the study of the interactions between the alkanes and the other undesired element originally present in the natural gas mixture: water. In this case, for sake of simplicity, only the three main alkanes have been considered such as methane, ethane and propane, in particular by studying the solubiliy of water in the alkane liquid phase through flash calculations. In figure 2.9 these calculated solubilities are compared against the experimental data.

The plots show the good predictions against experimental data for each case considered and one may also notice that the conditions of temperature and pressure are consistent with the one of the processes.

However, the predictions lose quality for the higher temperature considered, at around 323 K, in the case of methane and ethane (figure 2.9 a) b)); where the model predicts a lower concentration of water in the alkane gas phase. This means that probably at higher temperatures this problem still remain or even become worse and the only solution is to fit the unlike interaction parameters (since water is present

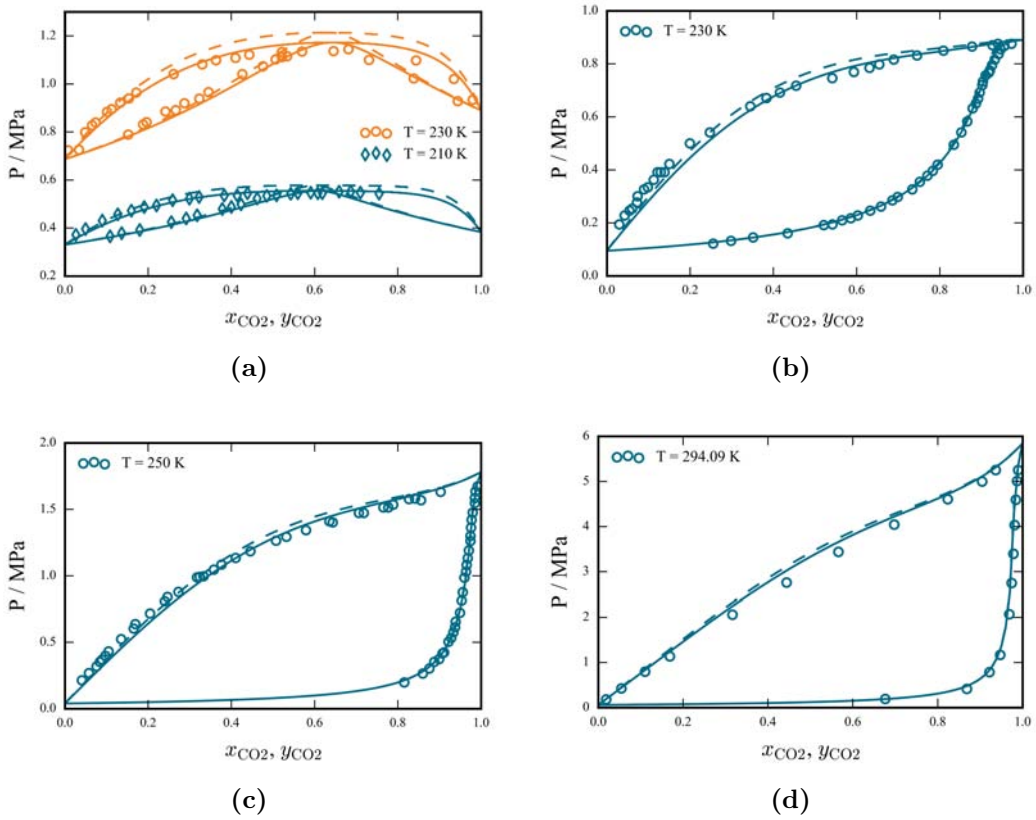

Figure 2.8: Isothermal VLE of CO_2 - n-Alkanes systems. a) CO_2- Ethane, b) CO_2 - Propane, c) CO_2 - n-Butane, d) CO_2 - n-Pentane. The symbols correspond to the experimental data from Vitu *et. al.* (2008) and the curves to the SAFT-γ Mie calculation. In particular, the dash curves represent the calculation before the parameter estimation whereas the solid ones represent the calculation after the estimation.

also the energy and range of the association sites might be included) against "higher" temperature data.

Altough a parameters fitting would be recommended, in the processes considered, such high temperatures are reached only in the regeneration section, where the natural gas is not present (or minimally) as discusses in §3 and §4. For this reason the model prediction is considered acceptable for the purposes of this work.

After the study of the interactions between the alkanes and the "undesired" elements (acid gases and water) present in the natural gas mixture, in this last step, it will be shown the SAFT-γ Mie model ability to correctly predict the interactions betweent these "undesidered" molecules. Before showing the results it may be useful to remind that H_2S, CO_2 and H_2O are built as a single group, provided with association sites (see figure 2.1).

First of all, the interactions between the two acid gases have been validated, as shown in figure 2.10. In the VLE equilibria depicted, it is possible to confirm the goodness of the model predictions as it perfectly matches the experimental data.

After that, the interactions between water and the acid gases has been studied through solubility calculations. Figure 2.11 respectively show a) the solubility of CO_2 in the water liquid phase and b) the solubility of water in the CO_2 gas phase.

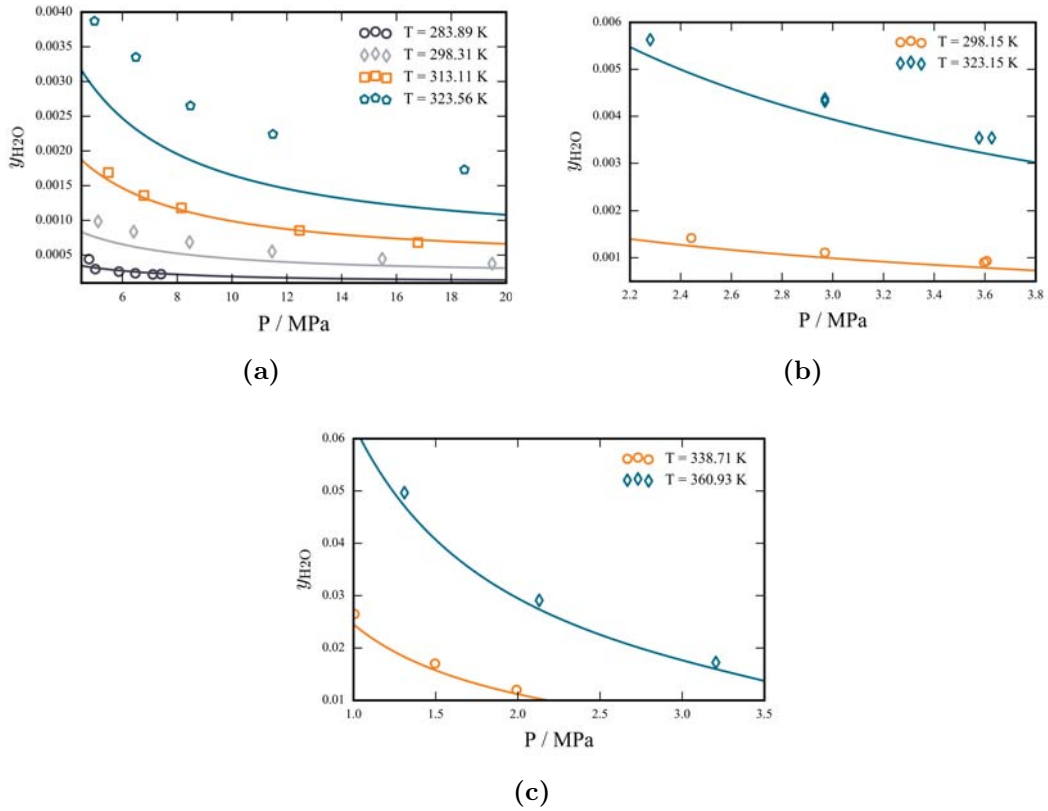

Figure 2.9: Isothermal solubility of water in different alkanes gas phase. a) Solubility in Methane gas phase, experimental data from Frost *et al.* (2014), b) Solubility in Ethane gas phase, experimental data from Mohammadi *et al.* (2004), c) Solubility in Propane gas phase, experimental data from Chapoy *et al.* (2004). The symbols correspond to the experimental data and the curves to the SAFT-γ Mie calculation.

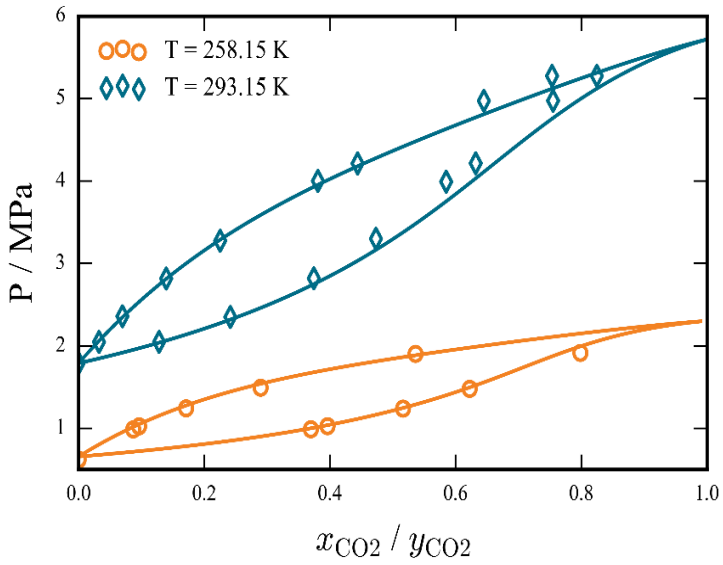

Figure 2.10: Isothermal VLE equilibria for the system CO_2 – H_2S. The symbols correspond to the experimental data from Chapoy *et. al.* (2013), and the curves to the SAFT-γ Mie calculation

The figures show that the experimental data are well predicted by the thermodynamic model even though in the case of CO_2 solubility in water liquid phase the prediction can be improved. For the purposes of this work, the predictions are considered acceptable; in fact, it is difficult to imagine that the sweetening process can be affected by such a small gap between experimental and predicted data for such small values of solubility.

In the end, figure 2.12 shows the VLE for the system H_2S - H_2O. Where it is possible to see the perfect match between the experimental and the predicted data.

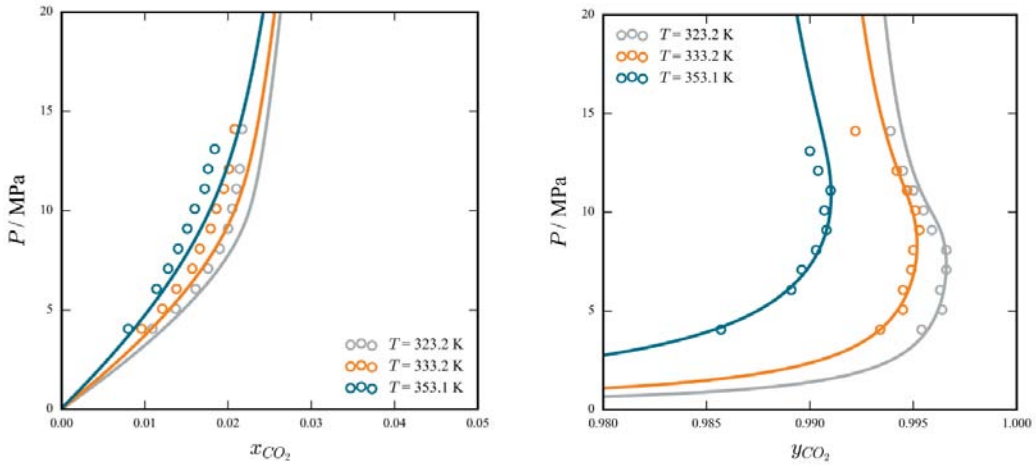

(a) **(b)**

Figure 2.11: a) Isothermal solubility of CO_2 in water liquid phase and b) isothermal solubility of water in CO_2 gas phase. The symbols correspond to the experimental data from Bamberger *et. al.* (2000), and the curves to the SAFT-γ Mie calculation.

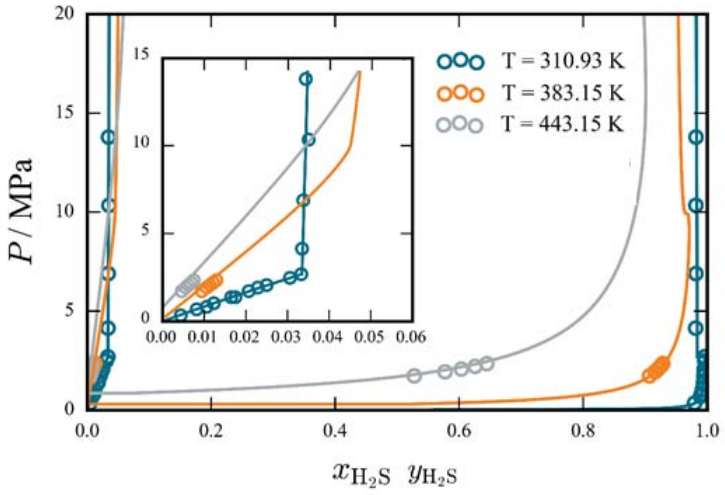

Figure 2.12: Isothermal VLE equilibria for the system H_2S – water. The symbols correspond to the experimental data from Sellek *et. al.* (1952), Gillispie and Wilson (1982), and Burgess *et. al.* (1969), and the curves to the SAFT-γ Mie calculation.

2.3.2 DEA

In this section, it will be evaluated the predictive ability of the thermodynamic model with respect to the solvent involved in the sweetening process of this work: the Diethanolamine (DEA).

Since in the sweetening process the DEA is involved as aqueous solution, the first step, in order to validate this solvent, has been the study of the interaction between DEA and water. Figure 2.13 shows respectively an a) isobaric and b) isothermal VLE. In these plots, it is possible to confim the goodness of the SAFT-γ Mie parameters for such system which are able to perfectly match the experimental data.

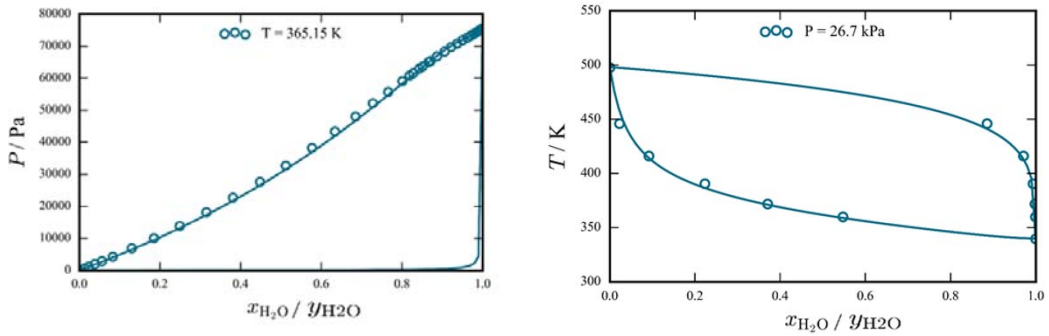

(a) (b)

Figure 2.13: Isothermal and isobaric VLE for the system water - DEA. The symbols correspond to the experimental data from Horstmann *et al.* (2002), and the curves to the SAFT-γ Mie calculation.

Next, the validation procedure involved the study of, probably, the most important property in the sweetening process, that is the interaction between the amine solution and the acid gases. It is, in fact, a key property that must be predicted as good as possible in order to get feasible results in the removal of acid gases from the natural gas stream, once the process will be simulated. This is done by evaluating the property of loading, which is the solubility of the acid gas in the amine aqueous solution (at fixed composition) against the acid gas partial pressure. Figures 2.14 respectively show a) the H_2S and b) the CO_2 loading for a fixed value of DEA aqueous solution concentration, expressed as weight fraction.

In the case of H_2S (2.14 a)) the model does not perfectly predict the experimental data. In particular, within the central region of loading, from 0.6 to 1.1 (roughly), the predicted values are lower than the experimental data, for all the temperatures considered. This fact may actually affect the results of the contactor column in the process, where the calculated removal efficiency might be lower than what it really is.

The CO_2 loading seems to be, generally speaking, better predicted. As one may see, the experimental data are perfectly matched for "low" temperatures, whereas as the temperature increases the predictions starts becoming poorer; the loading predicted is, in fact, lower than the experimental. One possible reason for this is that high temperature data were not included in the original parameters fitting. This fact, may affect the solvent purification section of the sweetening plant, where these "high" temperatures are reached. For a given partial pressure, an higher loading

may affect the correctness of CO_2 concentration in the lean solvent coming out from the stripper column, calculated in the sweetening simulation.

Possible solutions to obtain better predictions are either extending the experimental data through which the model parameters are fit, or modifying the model parameters themselves. It is important to remind, though, that those system are actually quite complex because they invoved molecules (more specifically groups), with different reaction sites (that are used to model the amine - acid gas reactions), and they are chosen by a trial and error approach (see §2.1). However, the model predictions have been considered accepted for the purposes of this work.

Another interesting feature regarding the study of the interactions between the acid gases and the amine are the quaternary loading plot, where both acid gases are present in the sperimentation procedure. This is done in order to study how they affect each other in the absorption capacity of the amine solution. Unfortunately, it has been impossible to replicate the literature data for lack of informations regarding the experimental procedure followed.

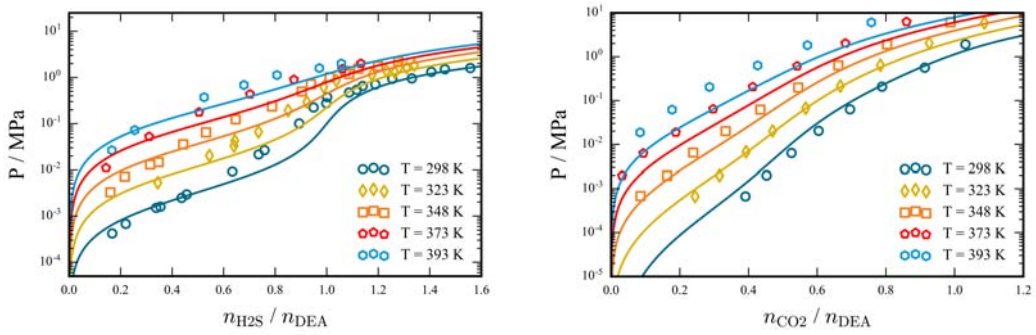

Figure 2.14: a) Partial pressure of H_2S as a function of the H_2S loading along the vapour - liquid equilibrium of the ternary mixture DEA + H_2O + H_2S, with a concentration of DEA in the liquid phase of 20%. b) Partial pressure of CO_2 as a function of the CO_2 loading along the vapour - liquid equilibrium of the ternary mixture DEA + H_2O + CO_2, with a concentration of DEA in the liquid phase of 35.4%. The symbols correspond to the experimental data, respectively from Lee *et al.* (1973) and Rodriguez *et al.* (2012) , and the curves form the SAFT-γ Mie calculation.

The last property to evaluate in the study of the interaction amine - acid gas is the heat of absorption. As already mentioned in the literature section, the reactive absorption of an acid gas is, actually, an hexotermic reaction which, therefore, realeses heat and increases the system temperature. In figure 2.15 it is represented the calculated heat of absorption against experimental data, at fixed amine concentration, for both the acid gases.

The heat released after the H_2S absorption is over-estimated of, roughly, 10 $kJmol^{-1}$, therefore with a maximum relative error of 30%. In the case of CO_2, instead, the heat of absorption is under-estimated of roughly the same amount of 10 $kJmol^{-1}$, so that to generate a maximum relative error of 15%.

This may affect the contactor temperature during the process simulation. In particular, the temperature of the rich solvent exiting the contactor colum might be higher/lower than expected, therefore, directly affecting the heat that has to be supplied in the downstream heat exchangers in order to have the rich solvent ready for the regeneration section. This aspect will be discussed in the sweetening results

section (see §3.2).

The main purpose of this work has been the study of the separation process of sweetening (and dehydration) from a mass exchange and phase equilibrium point of view. Therefore, the discrepancy detected in the heat of absorption prediction has not been considered worth to be adjusted at this level. The simulation results could be refined in the future work by including this property during the parameters fitting.

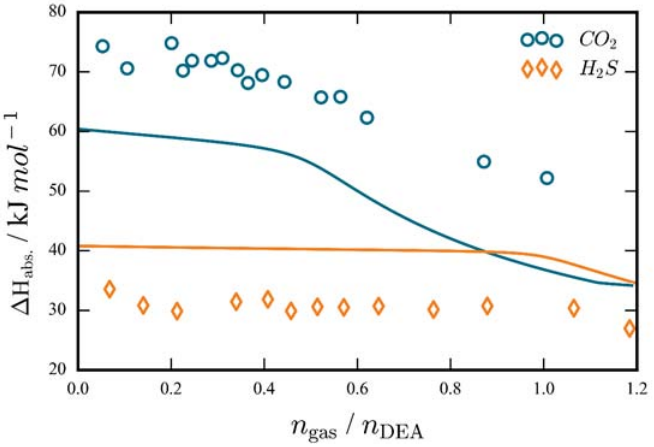

Figure 2.15: Heat of absorption of CO_2 in an aqueous solution of DEA at 20.6 wt% and heat of absorption of H_2S in an aqueous solution of DEA at 35.4 wt % at 300 K and 11 atm. The symbols correspond to the experimental data from Bullin *et al.* (-), and the curves to the SAFT-γ Mie calculation.

2.3.3 TEG

In this last section it is described the thermodynamic validation with respect to the solvent involved in dehydration (via absorption) process: the triethylene glycol (TEG).

Firstly, it has been study the interaction between TEG and water via VLE calculations. The a) isothermal and b) isobaric vapour - liquid calculations depicted in figure 2.16 confirm the goodness of the model parameters as the exprimental data are perfectly matched.

Lastly, it has been study the interaction between the TEG solvent and the most common alkane present in the natural gas mixture: methane. Figure 2.17 a) shows the goodness of thermodynamic model parameters in the estimation of methane solubility in TEG liquid phase. Instead, figure 2.17 b) shows that the opposite, that is the solubility of liquid TEG in methane gas phase is, actually, not well predicted by the thermodynamic model. Altough the model prediction clearly undestimate the concentration of TEG in methane gas phase, the values involved have a relly low order of magnitude 1E-06, 1E-07; therefore this can only minimally affect the dehydration process simulation results.

The TEG concentration in the dry gas exiting the glycol contactor column may, then, be lower than expected, leading to a possible underestimation of the glycol losses which has a direct impact of the glycol make up.

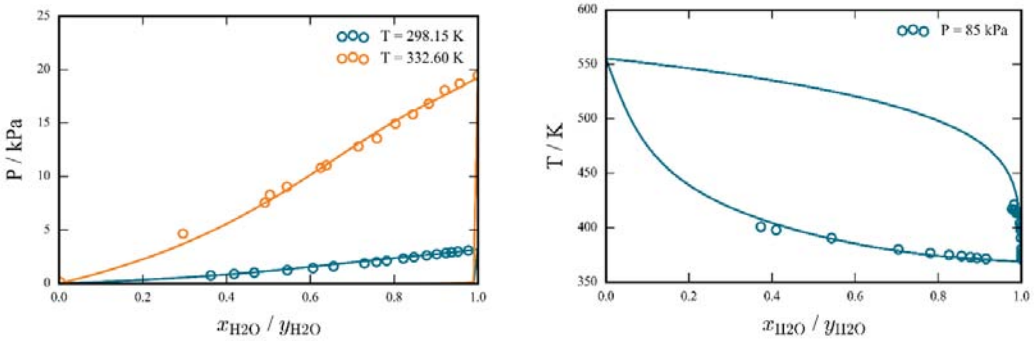

(a) **(b)**

Figure 2.16: Isothermal and isobaric VLE for the system water - TEG. The symbols correspond to the experimental data from a) Tsuji, Hiaki, Hongo (1998) and Derawi *et al.* (2003), b) Mostafazadeh *et al.* (2009), and the curves to the SAFT-γ Mie calculation

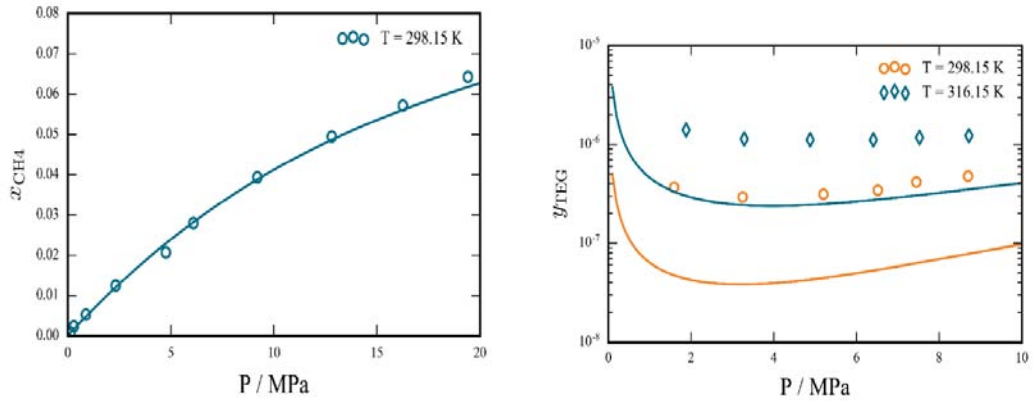

(a) **(b)**

Figure 2.17: a) Solubility of methane in TEG liquid phase as a function of pressure, b) Solubility of TEG in methane gas phase as a function of pressure. The symbols correspond to the experimental data from Jerinic *et al.* (2008), and the curves to the SAFT-γ Mie calculation

2.4 Multiflash^{TM}

Multiflash^{TM} is a thermodynamic package developed by Infochem Computers Services Ltd. which can be implemented within gPROMS®products. It contains a wide range of the most commonly used thermodynamics models, from equations of state to activity coefficient. In this work Multiflash^{TM} has been used as thermodynamic package in the simulation of the adsorption process (§6.1) involving the Peng - Robinson equation of state (PR EoS). Since the natural gas mixture considered in the simulation of the adsorption process is simply made of 4 components (CH_4, H_2O, CO_2 and N_2), involving a more complex thermodynamic model such as SAFT-γ Mie would not have been justify. The PR EoS is known to be appropriate to predict the behaviour of mixtures containing those components and, also, all the binary interaction parameters, for the mixture involved, were already present in the Multiflash databank as well. Therefore, neither parameters fitting nor thermodynamic validation has been necessary.

Chapter 3

Sweetening

This chapter illustrates the study carried out on the natural gas sweetening process model, where SAFT-γ Mie has been used as thermodynamic model for the simulation. In the first section the base case simulation is introduced, with the flowsheet implemented in gPROMS® ProcessBuilder enviroment; here the main process variables as well as the feed gas features are described. After the introductory section, the base case simulation results are analyzed, highlighting the critical points, which led to a sensitivity analysis on the columns tray efficiency, shown in the last section of the chapter.

3.1 Flowsheet assembling

The process flowsheet implemented in this work is a reproduction of the study of Abdulrahman *et al.*(2013), where the Khurmala sweetening plant has been simulated in Aspen HYSYS® V.7.3 and the Amine fluid package (Kent Eisenberg) has been used as thermodynamic model.

The flowsheet will be described following figure 3.1. Starting from the natural gas feed, the description will follow the path of the gas and the amine solution throughout the process, describing the main process units encoutered (the unit name is reported in italic, between brackets during the description).

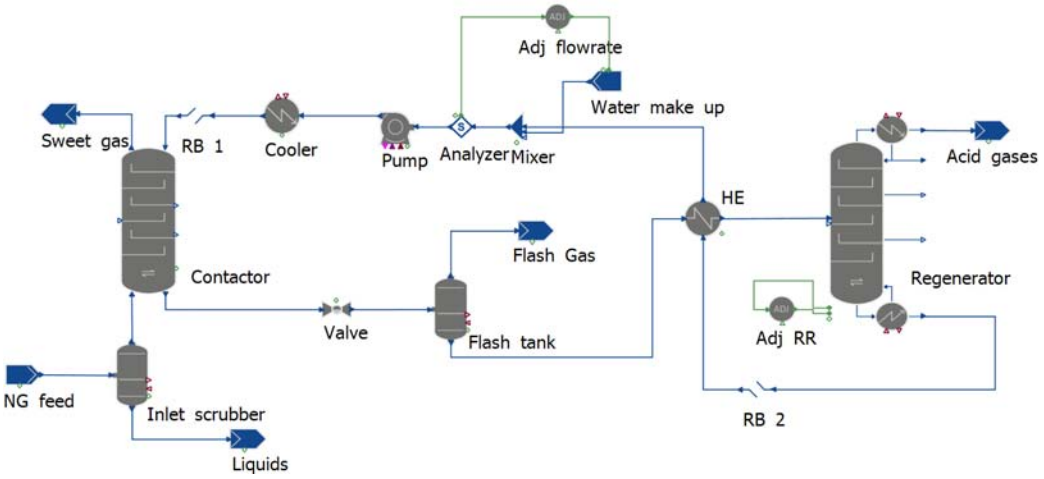

Figure 3.1: Sweetening flowsheet implemented in gPROMS® ProcessBuilder.

The 120 000 std $m^3\,h^{-1}$ (37.68 $kg\,s^{-1}$, 5 353.8 $kmol\,h^{-1}$) of acid natural gas are fed to the process (*NG feed*) at a pressure of 35.5 bar and at a temperature of 311.15 K (38°C), whereas the molar composition considered is specified in table 3.1.

Table 3.1: Initial composition of the acid natural gas feed, indicated in figure 3.1 as *NG Feed*.

Component	**Mass composition** [%]	**Molar composition** [%]
H_2S	7.22	5.37
CO_2	7.77	4.47
N_2	0.12	0.11
H_2O	0.09	0.13
CH_4	40.06	63.27
C_2H_6	16.48	13.88
C_3H_8	10.48	6.02
i - C_4H_{10}	3.12	1.36
n - C_4H_{10}	5.6	2.44
i - C_5H_{12}	2.93	1.03
n - C_5H_{12}	2.08	0.73
n - C_6H_{14}	4.05	1.19

Before entering the separation unit, the gas goes through a separator (*Inlet scrubber*), which is basically a model that allows to calculate the vapor liquid equilibria of the feed in order to separate the liquid phase (discharged from the bottom) from the vapour phase, which exits the drum from the top. Therefore, this unit allows to separate any free liquids present in the mixture such as water and high hydrocarbons (if the mixture is not fed at the dew point conditions). The vapour, at the dew point conditions, is sent to the bottom of the column section (*Contactor*). Inside the column, the gas is in contact with the absorbing solution, which is fed at the top of the column so as to realize a counter - current mass exchange (this unit is also called "absorber").

The solvent involved in this work is an aqueous solution of diethanol Amine (DEA) at 35 %wt; 400 $m^3\,h^{-1}$ (111.7 $kg\,s^{-1}$) are fed at a pressure of 35.5 bar and at a temperature of 313.15 K (40°C). As already mentioned in the literature section (§..), it is very important to feed the amine solution at a temperature higher than the gas, in order to avoid hydrocarbons condensation, which would be solubilized in the amine solution, thus decreasing its absorption capacity as well as losing valuable product.

The *Contactor* column is a column section model whose 20 trays are modelled as equilibrium trays, so as to neglect the mass transfer resistances between the gas and the liquid phase. The pressure inside the column is assumed constant, equal to 35.5 bar. The sweetened natural gas is then released from the top of the column (*Sweet gas*), whereas the rich amine solution, leaving the bottom, is sent through a series of units, which make possible its regeneration, depurating it from the absorbed acid gases so as to recycle it back in the contactor column. Leaving the regeneration section, the rich amine solution is directed to another knock out drum model (*Flash tank*), before being depressurized (*Valve*) to 6.2 bar. The pressure decrease leads to release part of the gas present in the liquid solution, which is then vented from the top of the drum (*Flash gas*). The amine solution, exiting the bottom of the

flash tank, is then heated up to 368.15 K (95°C) by the lean amine solution in the amine-amine heat exchanger (*HE*). The pressure drop in the heat exchanger is equal to 0.7 bar. Now, the rich amine solution, which has been depressurized and heated up, is ready to be processed in the distillation column (*Regenerator*), whose features are presented in table 3.2.

Table 3.2: Distillation column specifications, indicated as *Regenerator* in the flowsheet.

Number of stages	23
Feed stage	4
Pressure [bar]	1.9
Boilup ratio [-]	0.13
Condenser temperature [K]	330

This distillation column, provided of a partial condenser and a reboiler, has been modelled considering its trays at equilibrium, and the pressure is kept constant to 1.9 bar. In particular, the value of the boilup ratio[1] has been chosen so as to obtain the desired DEA concentration, whereas the condenser temperature has been set to 330 in order to use ambient liquid water as cooling fluid. In particular, in the column model the condenser temperature is directly related to the reflux ratio[2], so that it has been necessary to include an adjuster model (*Adj RR*), which adjusts the reflux ratio in order to have the desired temperature [3]. Furthermore, the column condenser works at total reflux: the condensed liquid phase is totally sent back to the column, whereas the vapour phase is vented (*Acid gases*). The regenerated amine solution, which exits from the bottom of the regenerator column, after being cooled down in the amine-amine heat exchanger (*HE*), is mixed (*Mixer*) with an external flowrate of water (*Water make up*). The water is added to the solution in order to supply the water losses througout the process sinks, so as to obtain the nominal flowrate of 400 $m^3\,h^{-1}$ as well as the nominal concentration. This has been possible with an adjuster (*Adj Flowrate*), which monitors the flowrate in the mixer downstream (informations provided by the (*Analyzer* model [4]) and it adjusts the make up of water. It is important to highlight that, the make up is pure water because in the present work the amine degradation has not been modelled and just water is lost throughout the process sinks. Finally, the lean amine is brought back to its nominal conditions (described earlier), after pressurization (*Pump*) and cooling (*Cooler*).

he recycle breakers present in the flowsheet (*RB 1* and *RB 2*), are models used to facilitate the initialisation procedure of simulations that contains closed loop. The initialisation procedure helps to solve the system, i.e. find a solution for time t = 0 by defining the set of equations that are solved as a first calculation step at a time t = 0 indipendently in each model. During the IP all the models are solved sequentially using the initial guesses provided in the recycle breakers. In particular, in this case, it has been necessary to correctly guess the composition of the two

[1] $BR = \frac{V}{B}$; B = Bottom product, V = Amount of vapur recycled to the bottom of column

[2] $RR = \frac{R}{VT+D}$; D = Liquid top product (=0), R = Reflux, VT = Vapour top product

[3] The adjuster model allows the user to assign a variable with a target value that must be met by changing a second variable.

[4] The analyzer model, when connected to a stream, gives detailed informations about the stream conditions such as temperature, pressure, flowrate, molar and mass composition and so on.

streams other than their flowrate, pressure and temperature, in order to get the flowsheet convergence.

3.2 Base case results

In the next section, the main results from the base case simulation described above are collected and described. Table 3.3 presents the conditions of temperature, pressure, mass flowrate and composition of the liquid and gas streams exiting the initial separator (*Inlet scrubber*).

Table 3.3: Main features of the liquid and vapour streams exiting the *Inlet scrubber*.

	Liquid phase	**Vapour phase**
Temperature [K]	35	35
Pressure [bar]	35.5	35.5
Mass flowrate [kg s^{-1}]	1.85	35.83
	Mass composition [%]	
H_2S	2.74	7.46
CO_2	1.21	8.1
N_2	0	0.13
H_2O	0.01	0.1
CH_4	3.57	41.95
C_2H_6	5.94	17.02
C_3H_8	9,77	10.52
i - C_4H_{10}	5.59	2.99
n - C_4H_{10}	12.61	5.24
i - C_5H_{12}	11.92	2.45
n - C_5H_{12}	10.17	1.66
n - C_6H_{14}	36.47	2.38

The table shows that 4.9 % of the gas initially fed is actually liquid, therefore, the gas is fed to the process slightly below its dew point, in the region of cohexistency of both vapour and liquid. In this situation, there might be an effective loss of valuable product that could be avoided simply bringing the gas at its dew point either by decreasing the pressure or increasing the temperature. It is also interesting to notice that the gas composition, fundamentally, does not change with respect to the feed gas one, even though the concentration of acid gases slightly increases.

Table 3.4 shows the results from the contactor model.

Clearly, the most important stream of the process is the sweet gas one, as it says if the acid gases are being removed and the specifications are being met. In this case, the solvent is able to completely absorb the H_2S and CO_2, whose removal efficiencies are respectively 100 % and 99.98 %. Furthermore, in table 3.5 a comparison is made with respect to the results of Abdulrahman *et al.* (2013), between the predicted acid gases concentration in the sweet gas stream.

Aspen HYSYS®, the process simulator used in Abdulrahman's work, calculates a H_2S concentration that is very close to the typical specification of sweetening plants (4 ppm), whereas gPROMS® ProcessBuilder predicts a complete removal

Table 3.4: Results of the *Contactor* column. The sweet gas, lean DEA and rich DEA streams main features and composition are reported.

	Sweet gas	**Lean DEA**	**Rich DEA**
Temperature [K]	313,152	313,15	330,87
Pressure [bar]	35,5	35,5	35,5
Mass flowrate [$kg\,s^{-1}$]	30,14	111,7	117,39
	Mass composition [%]		
H_2S	0	0	2.23
CO_2	0.02	0.64	3.08
N_2	0.15	0	0
H_2O	0.15	64.36	61.23
CH_4	49.67	0	0.05
C_2H_6	20.13	0	0.03
C_3H_8	12.44	0	0.02
i - C_4H_{10}	3.55	0	0
n - C_4H_{10}	6.2	0	0
i - C_5H_{12}	2.93	0	0
n - C_5H_{12}	2	0	0
n - C_6H_{14}	2.81	0	0
DEA	0	35	33.3

Table 3.5: Comparison between the sweet gas composition from Abdulrahman *et al.* (2013) and this work.

	Abdulrahman *et al.*	**gPROMS®**
Molar fraction of H_2S	3.42E-06	0
Molar fraction of CO_2	3.74E-04	1.16E-05

(the exact value predicted is 1E-24). On the other side, the CO_2 concentrations are more similar, with one order of magnitude difference. The big gap between the two concentrations of H_2S can be linked to different aspects. First of all, the differences in the solving method (Aspen HYSYS® is a sequential modular simulator), in the numerical solver involved as well as in the solver tollerance should be taken into account. In fact, all these features must be considered to distingush whether the H_2S and CO_2 concentrations calculated are meaningful. On the other hand, in Abdulrahman *et al.* (2013) the method through which the two columns are modelled is not specified, neither if they used an equilibrium - base method (possibly with a tray efficiency approach) nor if they implemented a rate based one. Therefore, it is not possible to compare the results from the two simulations and fully understand the main differences. Moreover, it is fundamental to highlight that, neither the results from Abdulrahman nor the ones form this work have been compared and validated against plant data, so that it is impossible to state whether or not the results predicted have a physical meaning. Finally, it is also important to mention that, the gas leaves the sweetening process at water saturation conditions (at dew point conditions), therefore, it will need to be dehydrated in an downstream process

in order to be available for the market (as developed in chapter 4).

Regarding the lean amine coming from the recycle loop, it is interesting to notice the presence of CO_2, about 0.64 % in mass fraction, which, however, does not affect the concentration of amine since, as already discussed, the amine is not lost throughout the process sinks. The presence of CO_2 in the recycled solution is due to the fact, that in the reboiler has not been possible to completely strip it out, as will be discussed later in this section.

Finally, analyzing the rich solvent stream, it is possible to calculate the total loading, expressed as the ratio of the molar mass of acid gases divided by the molar mass of DEA. In this work, the loading calculated is 0.428 which is very close to the value predicted by Abdulrahman, 0.43. The typical range of loading for this kind of processes, as indicated by Kohl and Nielsen (1978), is 0.45 - 0.73, which suggests that probably it is possible to improve the process performances, for example by decreasing the amine flowrate making the most of its absorption capacity. The temperature is also compared to Aspen results from Abdulrahman *et al.* (2013), which predicts a rich amine temperature of 337.75 K (64.6°C), whereas gPROMS predicts a temperature of 330.87 K (57.72°C). It is important to remind, from the thermodynamic validation section, that the heat of absorption of CO_2 and H_2S is the most poorly predicted property (with a maximum relative error of - 15% for CO_2 and for +30% for the H_2S). Therefore, this aspect should be taken into account to evaluate the goodness of gPROMS results .

Finally, the results from the *Regenerator* are reported in table 3.6.

Table 3.6: Results of the *Regenerator* column. The acid gases and the lean DEA streams main features and composition are reported.

	Acid gases	**Lean DEA**
Temperature [K]	330	393.73
Pressure [bar]	1.9	1.9
Mass flowrate [$kg\,s^{-1}$]	5.56	111.42
	Mass composition [%]	
H_2S	45.5	0
CO_2	49.5	0.64
N_2	0	0
H_2O	5	64.27
CH_4	0	0
C_2H_6	0	0
C_3H_8	0	0
i - C_4H_{10}	0	0
n - C_4H_{10}	0	0
i - C_5H_{12}	0	0
n - C_5H_{12}	0	0
n - C_6H_{14}	0	0
DEA	0	35.09

At the top of the regenerator, the acid gases are removed from the amine solution as well as a small percentage of water. Instead, the regenerated amine solution (lean) leaves the bottom of the column. The H_2S concentration in the lean solvent is zero

(1 E-13),whereas it is not possible to completely remove the CO_2 using such stripper column, as a small percentage of CO_2 is present in the lean stream. The presence of CO_2 in the lean solvent is probably the reason why the concentration of CO_2 in the sweet gas is much higher than the one of H_2S. The DEA composition as well as the mass flowrate of the lean solvent stream are then adjusted by the water make up, through which 0.28 kgs^{-1} of water are fed, exactly the amount lost in the process sinks.

3.3 Tray efficiency analysis

The tray efficiency sensitivity analyses have been organized as follows. At first, the *Contactor* column trays efficiency has been studied changing the trays efficiency [expressed in % with respect to the equilibrium] in the dedicated tab in the model, holding the *Regenerator* column at equilibrium. Then, the way around has been applied, studying the *Regenerator* trays efficiency keeping the *Contactor* trays at equilibrium. All the column trays have been considered at the same % of efficiency.

The idea behing this study is exploring the sweet gas (and lean amine) composition at different column trays efficiency. In particular it has been searched the limiting value of efficiency which allows to stay withing the upper limit range of H_2S composition in the sweet gas (4 ppm).

Figures 3.2 and 3.3, respectively, show the H_2S and CO_2 concentration profile in the vapour phase for each tray of the column section (*Contactor*), for different trays efficiency.

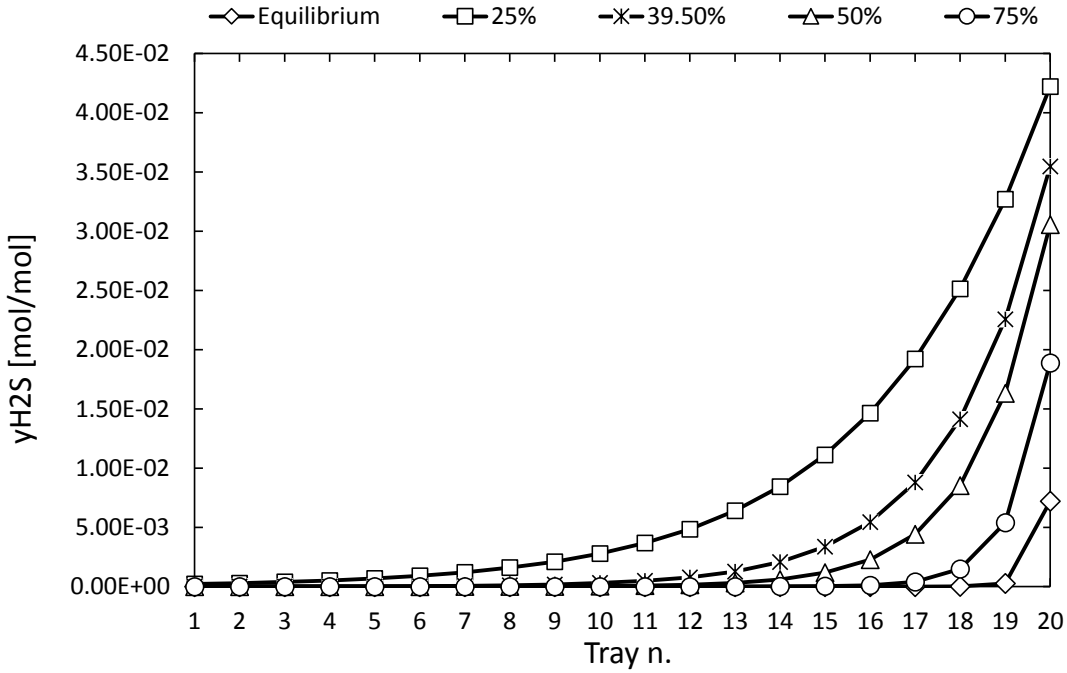

Figure 3.2: Profile of the molar fraction of H_2S in the vapour phase inside the contactor column for different tray efficiencies.

At equilibrium, the separation takes place just in the first two trays, whereas at lower efficiencies it is possible to see a sensible increase in the number of trays involved in the separation, up to 25% of efficiency, when all the column is effectively

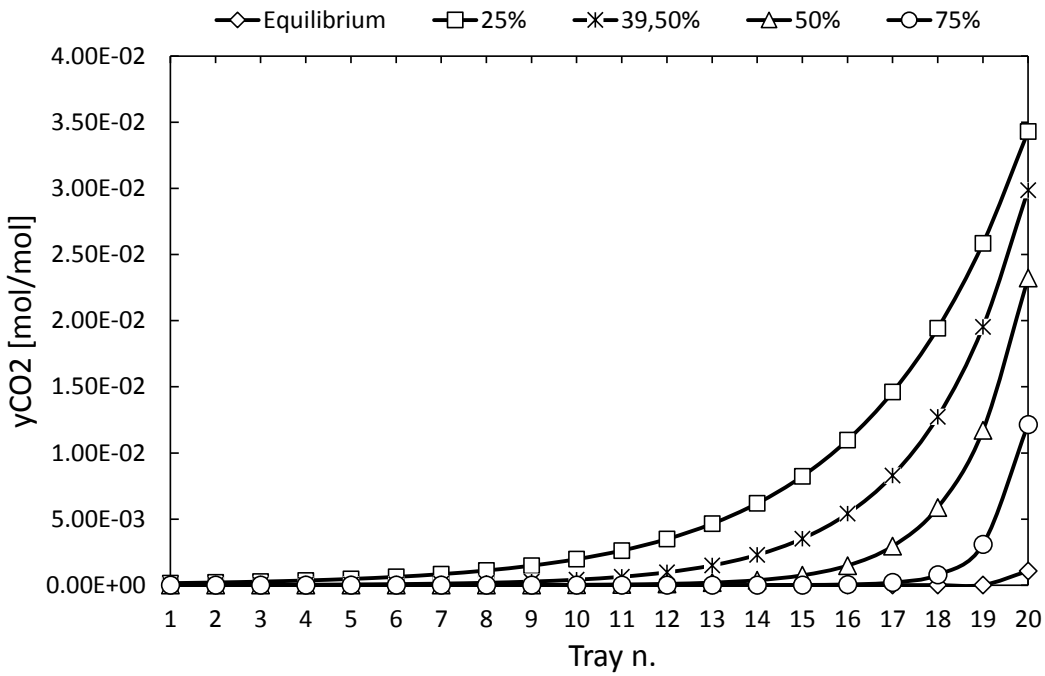

Figure 3.3: Profile of the molar fraction of CO_2 in the vapour phase inside the contactor column for different tray efficiencies.

working. Table 3.7 helps to visualize the concentration of each acid gas in the sweet gas leaving the top of the column (stage 1).

Table 3.7: Comparison of the molar fraction of H_2S and CO_2 in the sweet gas for different tray efficiencies.

	100 %	**75%**	**50 %**	**39,5 %**	**25 %**
Molar fraction H_2S	2E-24	3E-13	1E-07	3.7E-06	2.21E-04
Molar fraction CO_2	1.16E-5	1.16E-5	1.17E-05	1.37E-05	1.59E-04

Decreasing the efficiency down to 39.5 % leads to obtain a molar fraction of H_2S that corresponds to the specifications and matches Abdulrahman's result. Regarding the CO_2, instead, the concentration does not vary that much with the efficiency and this is probably due to the presence of CO_2 in the lean solvent coming from the regeneration section.

Figures 3.4 and 3.5 respectively show the H_2S and CO_2 concentration profile in the liquid phase for each tray of the regeneration colum (stripper), parametric to different trays efficiencies.

Both the profiles present a peak, corresponding to the feed tray, and then the concentrations decrease towards the last stage of the column (number 23). It is interesting to notice that, in both cases, tray efficiencies lower than 75% do not present any difference among them, therefore, 75% has been considered as reference (tray efficiencies within the range 75% - 100% have not been tested). In particular, in the case of H_2S, the equilibrium and the 75% curve present the same shape and, for both, the final concentration is zero (1E-13). The only difference is from tray 4 to tray 9 where, clearly, the 75 % curve is slightly above the equilibrium one. Also in the case of CO_2 profile, the 75% curve is slightly above the equilibrium one but

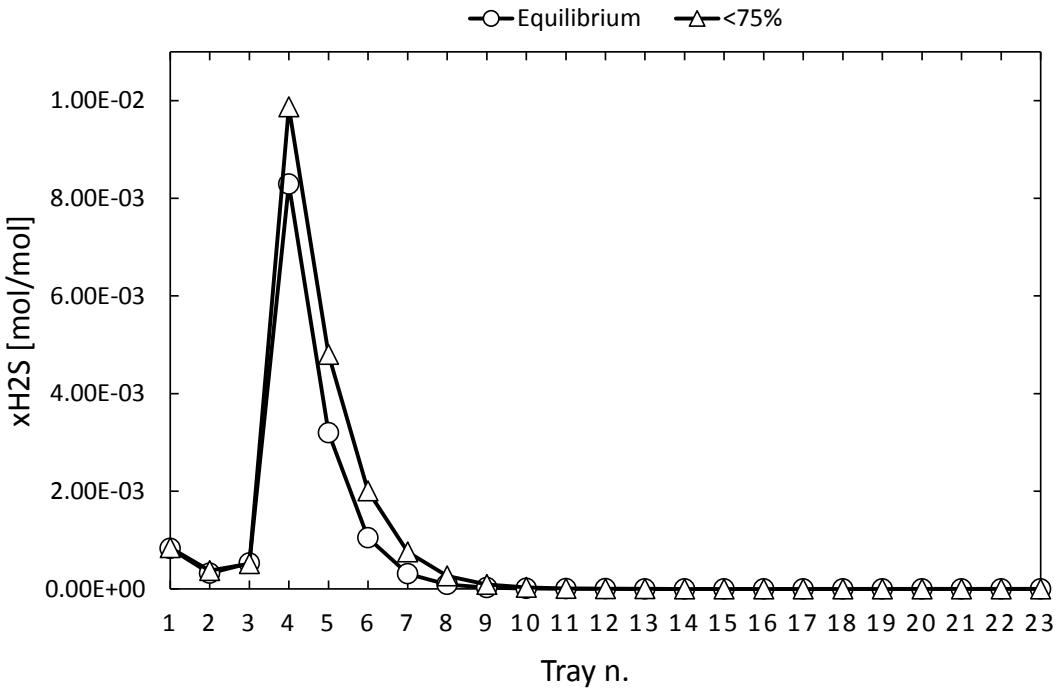

Figure 3.4: Profile of the molar fraction of H_2S in the liquid phase inside the regeneration column for different tray efficiencies.

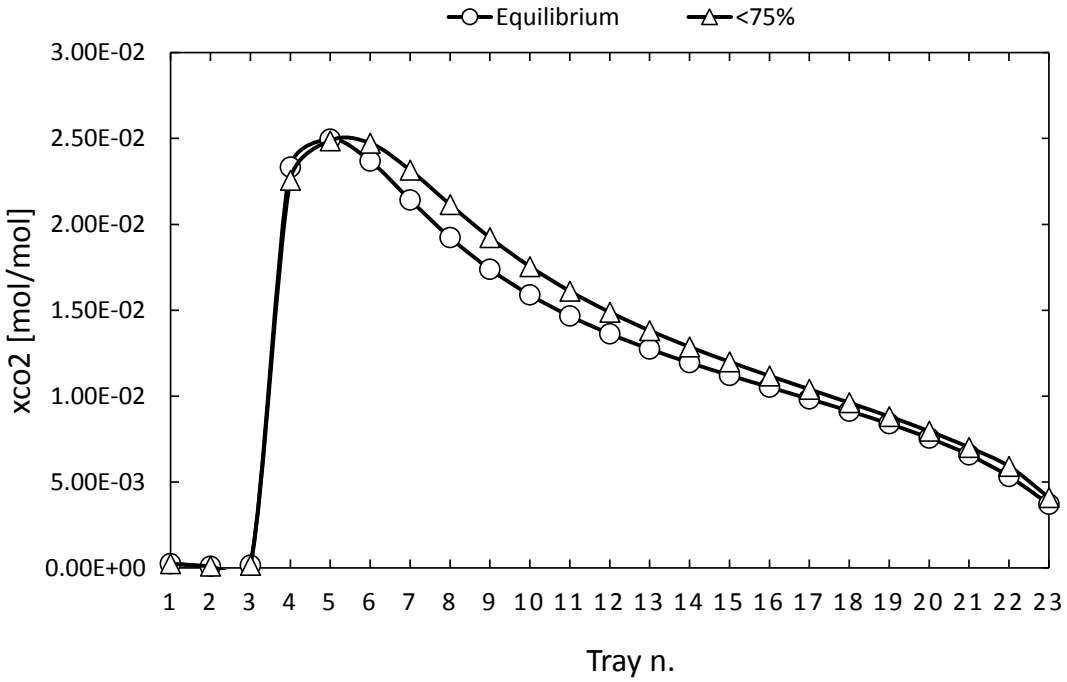

Figure 3.5: Profile of the molar fraction of CO_2 in the liquid phase inside the regeneration column for different tray efficiencies.

this happens from tray 4 up to the last tray, even though the final concentration in the lean solvent is equal to 0.64% for both cases.

The results from the tray efficiency analysis can be considered validated, as they match the results from the work of Aliabad and Mirzaei (2009). They compared ASPEN and HYSYS simulators, in particular, studying the behaviour of the H_2S and CO_2 concentrations in the absorber and in the stripper for different trays efficiencies testing DEA and MDEA (Methyldiethanol Amine) as solvents. The concentration of DEA is 34 %, close enough to the concentration used in this work, so that it has been possible possible to compare the results in a qualitative way. In the results from ASPEN, in fact, the profiles are very similar to the profiles obtained in this work, described above. Moreover, the concentration of H_2S in the sweet gas is quite low (1E-9), which suggests to retain valid the results from gPROMS simulations.

Chapter 4

Dehydration via absorption

This chapter illustrates the study carried out on the natural gas dehydration via absorption process model. Also in this case, the thermodynamic model SAFT-γ Mie has been used for the simulation. In the first section the contactor model validation is illustrated, which allows to verify the goodness of the model. In the second part the flowsheet assembling is introduced, where the main process units and specifications are described. In the end, the results are presented, showing the capability of the process model to produce meaningful data.

4.1 Contactor validation

The next section describes the validation of the absorber column involved in the modelling of the TEG dehydration simulation, demonstrating how the thermodynamic model SAFT-γ Mie combined with the column model present in gPROMS ProcessBuilder well replicate the literature data. For this purpose a simple contactor model has been implemented in ProcessBuilder as shown in figure 4.1.

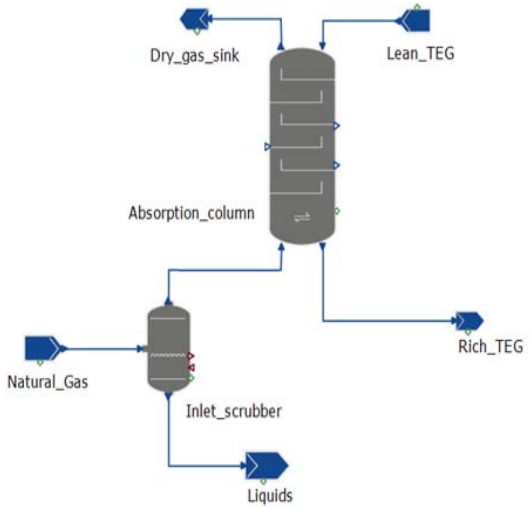

Figure 4.1: Simple contactor model implemented in gPROMS® ProcessBuilder.

In this simple flowsheet, natural gas is fed to an inlet knock out drum (*Inlet scrubber*) in order to remove any free liquids present in the initial gas mixture (in

particular water). Then, the gas is fed at the bottom of the column section model (*Absorption column*), modelled with equilibrium trays, where it finds in countercurrent the lean solvent TEG, which is fed at the top of the column. Clearly, the dry gas leaves the top of the column and the rich solvent exits from the bottom.

The first step, in the design of a TEG dehydration unit, is to establish the minimum TEG concentration for a given water dew point specification. The water dew point is a function of the glycol concentration as well as the contactor temperature, whereas it is relatively insensitive to pressure. Clearly, the outlet dewpoint depends on TEG flowrate and on the number of theoretical trays, but if the circulation of glycol (at fixed composition) is high enough there is no difference in the water dew point obtained. Figure 4.2 shows the water dew point against the contactor temperature, parametric to the glycol concentration.

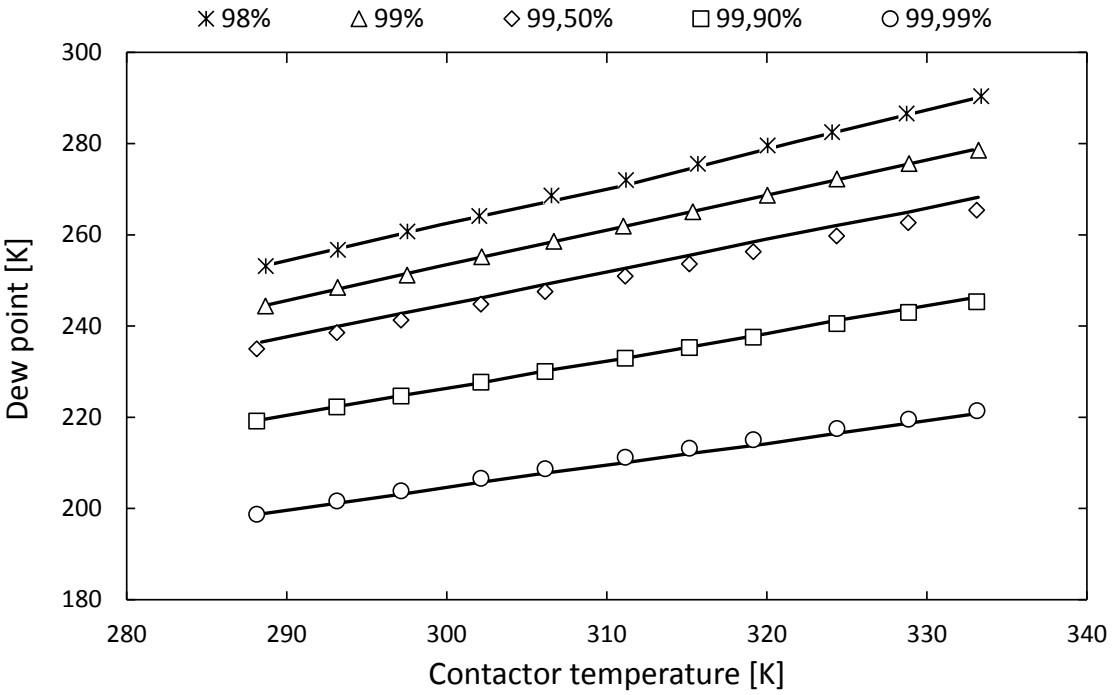

Figure 4.2: Dry gas dew temperature against contactor temperature for different TEG concentrations. The symbols correspond to the literature data from GPSA Data Book (2012) and the curves to gPROMS calculation.

The plot has been built, feeding the sweet gas from the sweetening process described in the previous chapter, at a fixed pressure of 1000 psia (the plot is valid up to 1500 psia). "Random" flowrates and composition of natural gas (at water saturation condition) can be chosen because what matters in this calculation is the water content in the gas, whereas different ratios between the other components do not affect the calculation. Even though a gas were fed a with an higher concentration of heavy hydrocarbons (e.g. n-nonane) the result would remain the same, since the dry gas dew point is calculated considering only the water, not the overall mixture. TEG is fed at a given composition, at a pressure of 1000 psia and with a flowrate high enough (relatively to the gas flowrate) in order to not see any difference in the calculated dew point. The value of the water dew point is a key process indicator on

the efficiency of water removal for TEG systems, and is calculated as shown below:

$$y_{H_2O}\phi^V_{H_2O}(T_{dew}, P, y_{H_2O}) = \phi^L_{H_2O}(T_{dew}, P) \tag{4.1}$$

where y_{H_2O} is the molar concentration of water in the dry gas and $\phi^V_{H_2O}$ and $\phi^L_{H_2O}$ are, respectively, the fugacity coefficient of water in the gas and in the liquid phase. The plot shows the good match between the calculated and the experimental data from GPSA Book (2012).

Once the glycol purity has been established, the next step is to determine the number of ideal trays required and the glycol flowrate. In order to do that, starting from the dew point required, it is necessary to calculated the water that must be removed for a given natural gas feed flowrate, so as to find the fraction of water to remove. Figure 4.3 shows, at fixed number of trays, which is the required Glycol Circulation Rate[1] (GCR), therefore the specific TEG flowrate (since it is known the mass of water absorbed), at a given composition, required to achieve the water dew point temperature.

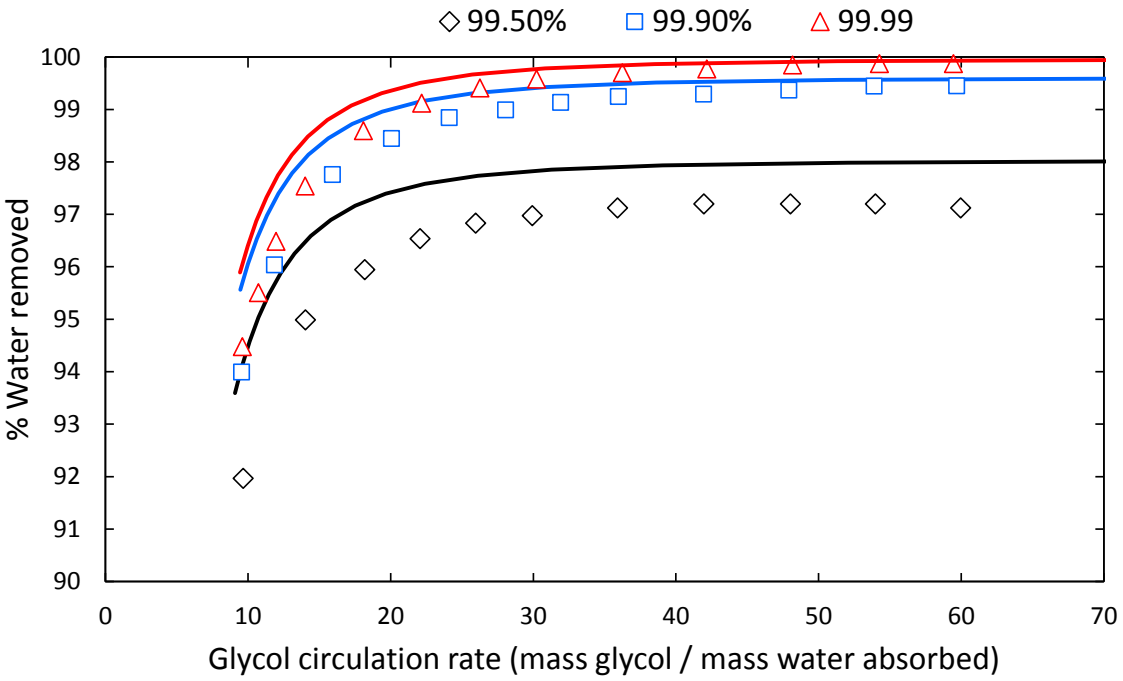

Figure 4.3: Glycol circulation rate (GCR) against the % of water removed for different TEG purities. The symbols correspond to the literature data from GPSA Data Book (2012) and the curves to gPROMS calculation.

The simulation has been done at a given temperature and pressure (104°F and 1000 psia, as specified in GPSA Book, 2012) even though it is important to highlight that the water removal fraction is not a strong function of temperature and pressure. The plot shows the good prediction of the contactor model against experimental data from the GPSA Data book (2012) and, in particular, at low GCR it is possible to observe a maximum relative error of 1%, whereas at high GCR the experimetal data are perfectly matched.

[1]Mass TEG/Mass of water absorbed

4.2 Flowsheet assembling

The process flowsheet implemented in this work is a reproduction of the study of Ghati (2013), where a TEG dehydration process has been designed using the Songo Songo natural gas composition, a gas field in Tanzania, as gas to process. In particular, the process has been simulated using Aspen HYSYS® process simulator with the Glycol package (Twu Sim Tasson equation of state) as thermodynamic model. Moreover, some process modifications are present based on Kohl and Kidnay (1997). Figure 4.4 shows the assembled flowsheet in gPROMS® ProcessBuilder.

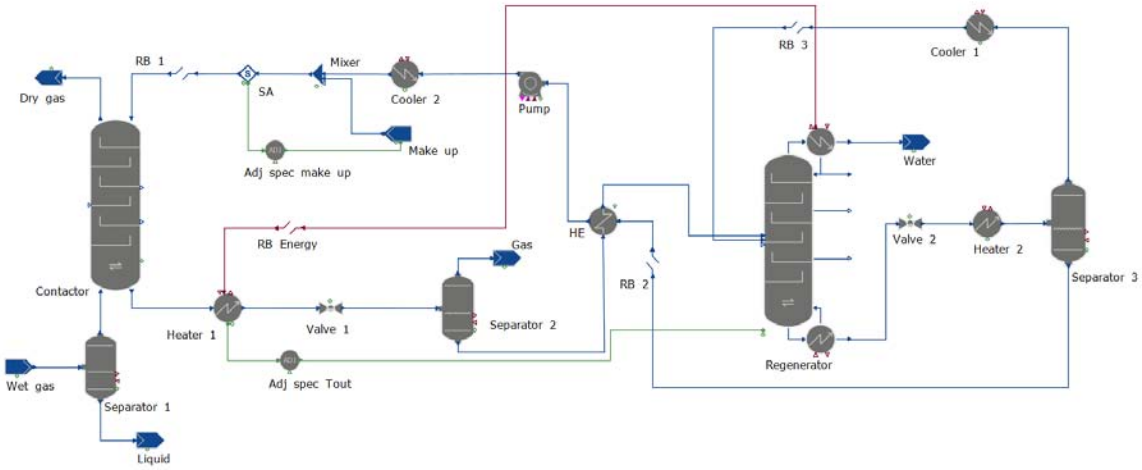

Figure 4.4: TEG dehydration flowsheet implemented in gPROMS® ProcessBuilder.

The 70 MMSCFD (16.23 $\mathrm{kg\,s^{-1}}$, 3486.5 $\mathrm{kmol\,h^{-1}}$) of natural gas to dehydrate (*Wet gas*) are fed to the process at a pressure of 81.7 bar and at a temperature of 303.15 K (30°C), whereas its composition is specified in table 4.1.

Table 4.1: Initial composition of the wet natural gas feed, indicated in figure 4.4 as *Wet gas*.

Component	**Mass composition** [%]	**Molar composition** [%]
H_2S	0	0
CO_2	0.97	0.37
N_2	1.2	0.72
H_2O	0.14	0.13
CH_4	92.83	97
C_2H_6	1.85	1.03
C_3H_8	0.82	0.31
i - C_4H_{10}	0.24	0.07
n - C_4H_{10}	0.31	0.09
i - C_5H_{12}	0.13	0.03
n - C_5H_{12}	0.13	0.03
n - C_6H_{14}	0.15	0.03
n - C_7H_{16}	0.66	0.11
n - C_8H_{18}	0.34	0.05
n - C_9H_{20}	0.23	0.03

The wet natural gas is fed to an inlet separator (*Separator 1*) in order to remove any trace of liquids, before entering the bottom of the column section (*Contactor*). The column has 3 equilibrium stages, operates at a pressure of 81.7 bar (the feed gas pressure) and, clearly, works in couter - current flow, as already described in the sweetening absorber. The solvent involved is an aqueous solution of TEG at 99 wt%; 0.3472 kg s^{-1} (9.016 kmol h^{-1}) are fed at the top of the column at a pressure of 81.7 bar and at a temperature of 308.15 K (35°C). The rich glycol, flowing from the bottom of the column, now needs to be heated up in order to be regenerated, and this can be done using the glycol as the cooling liquid of the regenerator condenser.

In order to do that, the rich glycol is fed to an heater model, which is connected to the condenser through an "energy stream", represented by the red line, which indicates that the duty of the heater is the same as the regenerator condenser [2]. The outlet temperature is fixed at 318.15 K (45°C), by changing the reflux ratio of the regenerator column thanks to an adjuster model (*Adj spec Tout*). The rich glycol is then depressurized down to 3.013 bar and flashed in a separator (*Separator 2*), where part of the gas and water are released as vapour. Before entering the regenerator, the liquid solution is finally heated up to 438.15 K (165°C) in the glycol - glycol heat hexchanger. Now, the rich glycol is fed to the third tray of the distillation column (*Regenerator*), which has 5 equilibrium stages and all the liquid from the top condeser is refluxed, so that to vent only vapour from the top. The stripper temperature is limited by the glycol degradation, therefore, the reboiler temperature is set to the maximum temperature allowed: 477.15 K (204°C). The lean glycol, once it exits the regenerator, it goes through a valve (*Valve 2*) where the pressure is reduced to subatmospheric conditions (0.8 bar) and it is reheated at 477.15 K (*Heater 2*) before being fed to a vacuum drum (*Separator 3*). The vapour released at the top of the vacuum drum is fed back to the regenerator column, where it acts as supplementary stripping gas (fed at stage number 4). The liquid at the bottom of the vacuum drum is the glycol at the desired concentration, it is cooled in the glycol - glycol heat exchanger and its pressure is increased up to 81.7 bar and cooled down at 308.15 K (35°C). Before being fed to the contactor column, it is necessary to add a make up of TEG solution, whose flowrate is regulated by an adjuster model (*Adj spec make up*). The solvent flowrate is set to the desidered value of 1250 kg h^{-1} (0.3472 kg s^{-1}) , and this is done in order to supply the solvent losses througout the plant sinks.

4.3 Base case results

In the next section the results from the base case flowsheet described above are presented. Table 4.2 shows the conditions of temperature, pressure, mass flowrate and composition of the liquid and gas streams exiting the inlet knock out drum. It it possible to see that, just a small amount of the inlet gas is separated as liquid (0.07%), mostly water. Altough the amount of water removed is quite small, it is sufficient to halve the water content in the gas phase, therefore reaching the dew point.

Next, table 4.3 presents the results from the contactor model. First of all, the dry gas stream, exiting the top of the column, presents a low concentration of

[2]Notice the presence of the recycle breaker (*RB Energy*), which helps the flowsheet convergence.

Table 4.2: Main features of the liquid and vapour streams exiting *Separator 1*.

	Liquid phase	**Vapour phase**
Temperature [K]	303.15	303.15
Pressure [bar]	81.7	81.7
Mass flowrate [$kg\,s^{-1}$]	0.012	16.223
	Mass composition [%]	
H_2S	0	0
CO_2	0.022	0.97
N_2	5.9E-04	1.204
H_2O	99.927	0.066
CH_4	0.046	92.897
C_2H_6	3.03E-03	1.849
C_3H_8	6.73E-04	0.816
i - C_4H_{10}	1.01E-04	0.243
n - C_4H_{10}	1.26E-04	0.312
i - C_5H_{12}	2.62E-05	0.129
n - C_5H_{12}	2.47E-05	0.129
n - C_6H_{14}	1.38E-05	0.154
n - C_7H_{16}	2.7E-05	0.658
n - C_8H_{18}	6.35E-06	0.349
n - C_9H_{20}	1.93E-06	0.224

water, which indicates that the process effectively removes water from the feed stream. Secondly, it is possible to see that the lean TEG, recirculated back after the regeneration, does not present any impurity, even though the concentration obtained is not exactly 99% as expected, because of the stripper regeneration capacity. It is worth to notice that, looking at Figure 4.3, even a small change in the glycol composition can affect the behaviour of the GCR with respect to the water removal fraction (to take into account for further analyses). Finally, the rich TEG stream, exiting the bottom of the column, is reported.

In table 4.4 a more accurate description of the dry gas stream is reported, which is helpful to evaluate the process performances. It is possible to notice that the water concentration, expressed in molar fraction, has the same order of magnitude of the one presented in Ghati's work (7.9E-05), even though the value predicted by gPROMS is slightly less conservative. On the other hand, a comparison between the water removal fraction and the GCR is not given for two reasons. Firstly, in the work of Ghati it is not specified whether the removal fraction is calculated with respect to feed gas or to the vapour phase coming from the knock out drum. Secondly, as already stated in §4.1, gPROMS, especially for the lower concentrations of glycol, predicts an higher value of water removal fraction for a fixed GCR, with respect to the experimental data. Conversely, it is unknown the behaviour of the Ghati model compared to the same experimental data. Futhermore, the dew point calculated, with respect to the contactor temperature as well as the GCR with respect to the water removal fraction are coherent to the validation presented in figure 4.2 and 4.3.

Finally, in table 4.5 the results from the stripper column are reported, where the

Table 4.3: Results of the *Contactor* column. The dry gas, the lean TEG and the rich TEG streams main features and composition are reported.

	Dry gas	**Lean TEG**	**Rich TEG**
Temperature [K]	303.80	308.7	303.66
Pressure [bar]	81.7	81.7	81.7
Mass flowrate [kg s^{-1}]	16.21	0.347	0.36
	Mass composition [%]		
H_2S	0	0	0
CO_2	0.971	0	0.066
N_2	1.205	0	5.09E-03
H_2O	2.845E-03	1.13	3.922
CH_4	92.961	0	0.357
C_2H_6	1.85	0	0.023
C_3H_8	0.816	0	0.016
i - C_4H_{10}	0.243	0	2.89E-03
n - C_4H_{10}	0.312	0	8.9E-03
i - C_5H_{12}	0.129	0	2.27E-03
n - C_5H_{12}	0.129	0	5.3E-03
n - C_6H_{14}	0.154	0	8.95E-03
n - C_7H_{16}	0.657	0	0.02
n - C_8H_{18}	0.34	0	0.038
n - C_9H_{20}	0.229	0	0.025
TEG	0	98.87	95.5

Table 4.4: Characterization of the water removal in the dry gas through different variables.

Variable	**Value**
H_2O molar fraction [-]	2.65-05
T_{dew} [K]	255.95
Water absorbed [kg s^{-1}]	0.01
Water removal fraction [%]	95.67
TEG Circulation ratio [-]	33.81

rich TEG solution is converted into lean TEG. The TEG stream is concentrated in the regenerator, where the glycol mass fraction goes from 95.5 wt% to 98.18 wt%. Altough the concentration obtained in the lean solvent stream is within the range expected in an atmospheric stripper, it is not enough for the required specification. That is why the vacumm drum is used, in order to further concentrate the lean TEG, even though it is not possible to reach exactly 99 wt%, but 98.87 has been the maximum possible. It is also interesting to notice that, the gas vented is mainly water with small fraction of methane present.

Table 4.5: Results of the *Regenerator* column. The vent gas and the lean TEG streams main features and composition are reported.

	Vent	**Lean TEG**
Temperature [K]	377.91	477.15
Pressure [bar]	1.2	1.2
Mass flowrate [$\mathrm{kg\,s^{-1}}$]	0.011	0.352
	Mass composition [%]	
H_2S	0	0
CO_2	0.87	0
N_2	6.54E-03	0
H_2O	94.35	1.817
CH_4	0.49	0
C_2H_6	0.117	0
C_3H_8	0.132	0
i - C_4H_{10}	0.02	0
n - C_4H_{10}	0.114	0
i - C_5H_{12}	0.025	0
n - C_5H_{12}	0.095	0
n - C_6H_{14}	0.2	0
n - C_7H_{16}	1.4	0
n - C_8H_{18}	1.1	0
n - C_9H_{20}	1.08	0
TEG	0	98.183

Chapter 5

Optimization

In this chapter it is introduced the process of assembling the two flowsheets of sweetening and dehydration, described in the previous chapters, in a unique flowsheet, where SAFT-γ Mie has been used as thermodynamic model. Starting with the description of the assembled flowsheet, underlining the differences with respect to the two flowsheets taken separately, the base case results is presented. After that, the process energy analysis is described, which allowed to formulate the optimization problem. Lastly, the optimization problem as well as the optimization results are analyzed.

5.1 Merged flowsheets

Figure 5.1 shows the entire flowsheet, where the sweetening and the dehydration via absorption processes are merged together. The natural gas fed to the process has the same features in terms of temperature, pressure, flowrate and composition of the gas involved in the sweetening study (§3.1). Whereas, the processes conditions have been kept equal to the conditions used during the study of the two processes took separately. The only differences appear in the stream connecting the two processes where a compressor and a cooler appear. In particular, the compressor (*Intermediate Compressor*) is used to increase the pressure of the sweet gas up to 81.7 bar, which is the nominal pressure involved in the glycol contactor. Then, after the compressor, a cooler (*Intermediate Cooler*) is necessary in order to cool down the gas temperature to the nominal glycol contactor temperature: 303.15 K (30°C).

In table 5.1 the main variables of interest resulting from the base case of the whole flowsheet are collected. The sweetening section does not present any difference with respect to the single flowsheet, in particular the H_2S is completely removed and also the molar fraction of CO_2 remains the same (in fact, the process conditions as well as the gas features have not been changed). Instead, the glycol section presents small differences with respect to the single flowsheet, such as the water fraction in the dry gas, water absorbed, T_{dew}, water removal fraction and GCR (see table 4.4). This is, clearly, due to the difference on the ratio between gas and solvent flowrates; the gas flowrate, here, is almost twice as much as the gas involved in the single glycol process. This aspect will be analyzed more in detail in the next section.

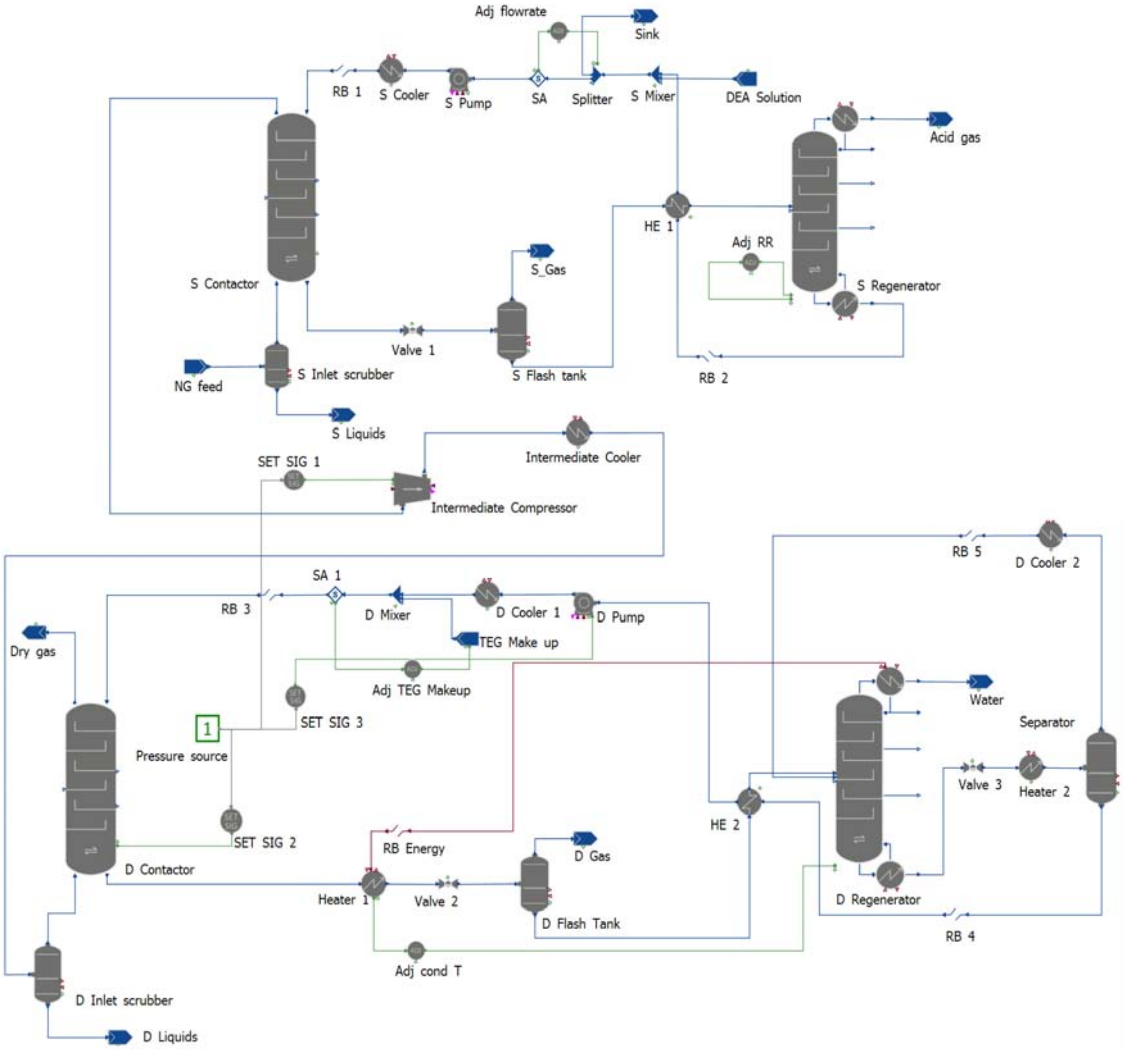

Figure 5.1: Flowsheet implemented in gPROMS® ProcessBuilder where where the sweetening and dehydration via glycol absorption processes are merged.

Table 5.1: Results from the merged flowsheets base case. Focus on the *Dry gas* stream.

Variable	Value
Time [min]	31.5
H_2S molar fraction [-]	0
CO_2molar fraction [-]	1.32E-05
H_2Omass fraction [kg/kg]	1.96E-05
T_{dew} [K]	257.64
Water absorbed [kg/s]	0.0117
Water removal fraction [%]	95.7
GCR[-]	29.23

5.2 Preliminar energy analysis

Table 5.2 shows the energy consumption of each unit present in the complete flowsheet. The three main sources of energy consumption, which summed up are responsible of 99.74 % of the overall consumption are: the sweetening pump, the sweetening reboiler and the intermediate compressor. In particular, the contribution of the sweeetening reboiler is responsible of 87.9 % of the overall energy consumption. The glycol units, such as the glycol pump and the glycol reboiler, affect only for the 0.26 %.

Table 5.2: Energy consumption expresses in kW and in percentage of the main unit present in the whole flowsheet

Flowsheet unit	**Energy consumption** [kW]	**Percentage** [%]
Sweetening pump	374.251	1.46
Sweetening reboiler	22 604.5	87.9
Intermediate compressor	2 668.77	10.38
Glycol pump	2.611	0.01
Glycol reboiler	64.67	0.25
Total	25 714.8	100

As anticipated in the previous section, this is due to the big difference of the ratio between the flowrate of solvent and the flowrate of gas processed; in the case of sweetening this ratio is equal to 2.96 whereas for the dehydration is equal to 0.012. The circulating amount of amine is 320 times higher than the glycol one, that is why the sweetening unit weights much more on the overall energy consumption. In fact, all the contributions considered are presented as extensive variables, therefore, they are directly dependent on the flowrate of solvent. Thus, in order to formulate an optimization problem, these units should be taken into account to minimize the overall energy consumption of the process.

Clearly, one may argue that the energy consumption contributions, considered in table 5.2, have different characteristics; in fact, the energy of pumps and compressors is purely electrical, whereas the reboilers energy is thermal. For the purposes of this work, they have been placed on the same level in the formulation of the optimization problem. This has been done mainly to demonstrate the ability of the software to deal with an optimization problem (on a "complex" flowsheet) involving multiple variables to optimize.

5.3 Formulation of the optimization problem

The first step of the optimization problem is the definition of the optimization function. (5.3) shows the objective function considered in this work, where the three main energy contributions described in the previous section are summed up.

$$f_{obj} = E_{SweetPump} + E_{SweetReb} + E_{IntermCompr}$$

Then, the next step has been the definition of the variables to adjust as well as the process constraints, so as to achieve the minimum of the objective function re-

specting the process specifications. Table 5.3 collects both the manipulated variables and the constraints.

Table 5.3: Manipulated variables and constaints of the optimization problem.

Manipulated variables	**Initial value**	**Admitted range**
Amine flowrate [kg/s]	111.7	50 - 150
Glycol contactor pressure [bar]	81.7	50 - 100
Constrained variables	**Lower bound**	**Upper bound**
Sweet gas H_2S molar fraction [-]	0	4 ppm
Dry gas H_2O mass fraction [-]	0	2E-05

The possible variables to adjust, considered in this case, are: the amine flowrate, as it has been shown before this variable is the most influent on the sweetening reboiler energy consumption and, the glycol contactor pressure, which is directly connected to the intermediate compressor. The admitted range for both variables has been chosen to be consistent to the typical values involved in these processes. In order to allow the optimizer to act on these variables, it has been necessary to modify the initial flowsheet. In the single sweetening flowsheet, there is an adjuster which adjusts the flowrate of amine at the desired value, regulating the water make up, which is basically a way to reintegrate the water losses throughout the plant sinks. Since the optimizer cannot act directly to the adjuster model to vary the amine flowrate, in this case the water make up has been substituted with an amine make up at fixed nominal composition of 35 wt% DEA (the same composition of the lean solvent stream coming from the stripper), as shown in figure 5.2.

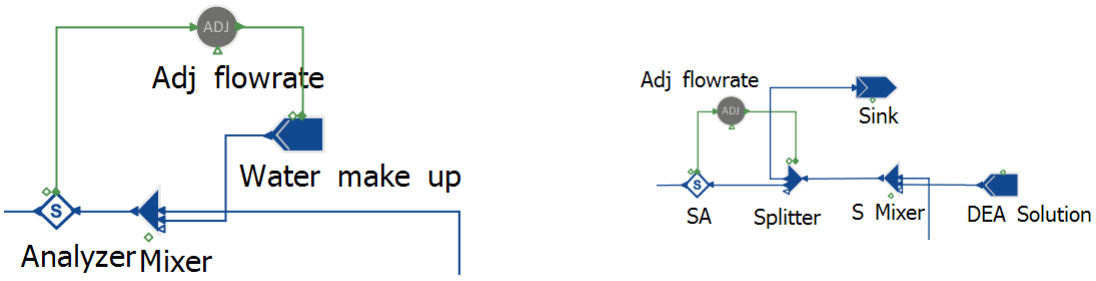

Figure 5.2: Modification of the make up in the sweetening flowsheet. To the left the base case configuration and to the right the modified one present in the "whole" flowsheet.

Then, a sink and a splitter have been introduced connnecting the adjuster to the splitter. The adjuster is introduced to act on the split ratio of the mixer, in order to vary and find the optimal flowrate of amine solution. The excess flowrate is, therefore, discharged in the sink. The make up of amine has to be fixed at a certain value depending on the upper bound of the flowrate admitted.

The other modification, with respect to the initial flowsheet, has been the introduction of the pressure source model in the glycol section of the process as shown in figure 5.3.

This model leads to simultaneously vary, not only the pressure in the contactor column, but at the same time, the outlet pressure of the intermediate compressor and of the glycol pump, which are, then, kept equal.

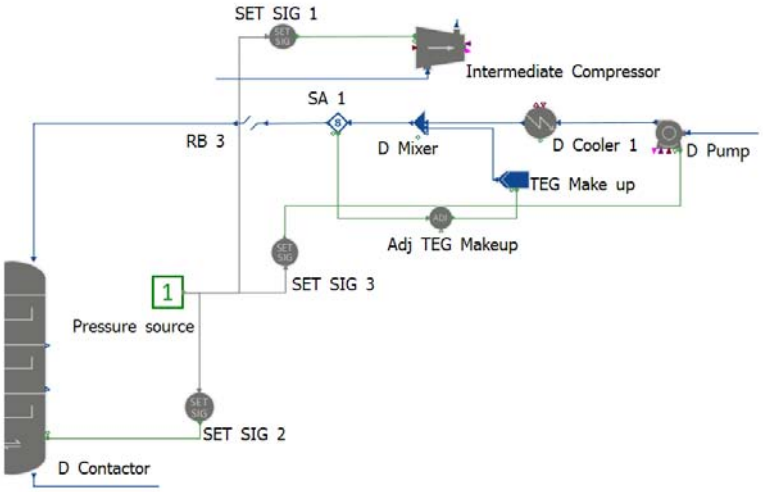

Figure 5.3: Particular of the *Pressure Source* model in the glycol section of the "whole" flowsheet, which is able to simulaneously adjust the pressure in the intermediate compressor, in the column and in the pump.

1

The optimization constraints are then defined as the process specifications. In this case the H_2S molar concentration and the H_2O in the dry gas have been considered. The lower bounds are equal to 0 and the upper bounds correspond to the typical specifications present in these processes.

5.3.1 Results

In this last section, the results of the optimization problem are reported, highlighting the main outcomes in terms of energy consumption reduction as well as the main consenquences to the process. Table 5.4 lists the variables adjusted by the optimizer that allowed for a reduction in the energy consumption. Although the glycol contactor pressure (intermediate compressor, contactor column, glycol pump) has been reduced by 1.6% with respect to the base case, the main result has been achieved regarding the amine flowrate in the sweetening process. In fact, the new value of amine flowrate is 26% lower than the value considered in the base case. Table 5.4 lists also the values of the constrained variables. The H_2S molar concentration in the sweet gas remains zero, therefore, the reduction of amine did not affect on the solvent absorption efficiency (at least regarding the H_2S). The other constrained variable, the water molar concentration in the dry gas, has been set to its upper bound, increasing by 2% with respect to the base case result.

The simultaneous reduction of both the amine flowrate and the glycol contactor pressure have led to an important reduction of the overall energy consumption of the process, which is presented in table 5.5. The reduction of the amine flowrate has a direct effect on the sweetening reboiler and sweetening pump consumption; as already underlined, in fact, all the energy contribution are expressed in extensive terms. Therefore, the reduction of energy consumption is directly linked to the the reduction of amine flowrate, even though they are slightly different (-25.9% vs. -25.1% and -26%). This suggests that the law linking the two variables is not perfectly

Table 5.4: Optimization results in terms of manipulated and constrained variables. The variations of the manipulated variables with respect to the base case is also provided.

Manipulated variabels		**Difference**
Amine flowrate [kg/s]	82.8	-25.9%
Glycol contactor pressure [bar]	80.34	-1,6 %
Constrained variables [-]		
Sweet gas H_2S molar concentration [-]		0
Dry gas H_2O mass concentration [-]		2E-05

linear, and other factor should be taken into account in other to minimize the energy consumption also from an intensive point of view, for instance considering the DEA concentration. Also the intermediate compressor energy consumption decreases by, roughly, the same amount of the pressure in the glycol contactor section. Considering all the energy contributions of the whole process, therefore, the optimization results show an overall energy consumption reduction of 23%.

Table 5.5: Energy consumption reduction.

Energy consumption [kW]		**Reduction**
Sweetening reboiler	16 934	25.1%
Sweetening pump	276.98	26%
Intermediate compressor	2 617.9	2%
Total	19 828.88	23%

Moreover, the optimization results can be seen also from other prospectives. For example, the direct effect of the reduction of amine flowrate has been the increase of the amine loading, one of the key variables to asset the sweetening performances. Altough the molar concentration of CO_2 in the sweet gas is, slightly, higher that the base case (1.65E-05), an important increase in the amine loading is present. The loading, in fact, moves from 0.428 in the base case to 0.58 in the optimized process. As already mentioned in §3.2, the former value was too low with respect to the typical values of loading reported in literature (0.45-0.73), whereas in the otpimized process this value is well within this range. This means that the amine solution works correctly following the standards guide lines present in literature. Differently, the dry gas stream, coming from the glycol section, does not present differences compared to the base case, with respect to the variables listed in table 5.1. Therefore, the dry gas stream has not been affected by the optimization. Lastly, 15 hours have been necessary to complete the optimization problem [1]. Therefore, it is important to consider that the computational time may increase by 1-2 orders of magnitude with respect to the base case, even though the optimization problem is relatively "simple".

[1]All the simulations have been carried out on Lenovo® ThinkCentre Edge 72 (Windows® 7 as operating system, third generation Intel® Core™ i7 as processor, 8 GB of RAM).

Chapter 6

Dehydration via adsorption

In this last chapter, it is described the work carried out on modelling the process of natural gas dehydration via adsorption. The chapter starts with an introduction of the main equations involved in the adsorption modelling, from the mass balance to the equilibrium isotherm, introducing the nominal conditions of the "base case" simulation and the technical features of the adsorption bed.

Then, the results of the base case are presented, followed by three sensitivity analyses, which explores the response of the system under different conditions of dispersion coefficient, mass transfer coefficient and number of discretization points.

In the end, it is presented the implementation of the pressure-temperature swing adsorption (PTSA) process with two beds working in parallel, which allow to obtain a continuous process despite the regeneration step needed to reactivate the beds.

6.1 Mathematical modelling

The aim, of this final section of work, has been the implementation of a pressure - temperature swing adsorption process, in order to obtain a continuous adsorption process able to completely remove water from a natural gas stream and achieve extremely low dew temperatures. In order to do that, the first step has been the modelling of a single adsorption bed to test its capacity to remove water from a natural gas stream and to provide sensible results. In particular, the work of Gholami *et. al.* (2010) has been chosen as a reference, mostly regarding the conditions of the natural gas mixture and the physical features of the adsorption bed.

The natural gas considered in this work is a simple mixture of 4 components: water, carbon dioxide, methane and nitrogen at a composition specified in table 6.1. The gas molar flowrate is constant at F = 23 929 kmol h^{-1}, it is fed as superheated vapour at P = 64.1 bar and T = 319.7 K (2 K the degree of superheating), to avoid water condensation due to pressure drops.

Table 6.1: Initial molar composition of the natural gas fed to the adsorption bed. This feed composition is maintained constant throughout all the work on the adsorption process.

	H_2O	CO_2	CH_4	N_2
Molar composition [–]	0.00184	0.00998	0.953	0.03518

The solid adsorbent considered in this work is zeolite 5A, in form of spherical pellets.

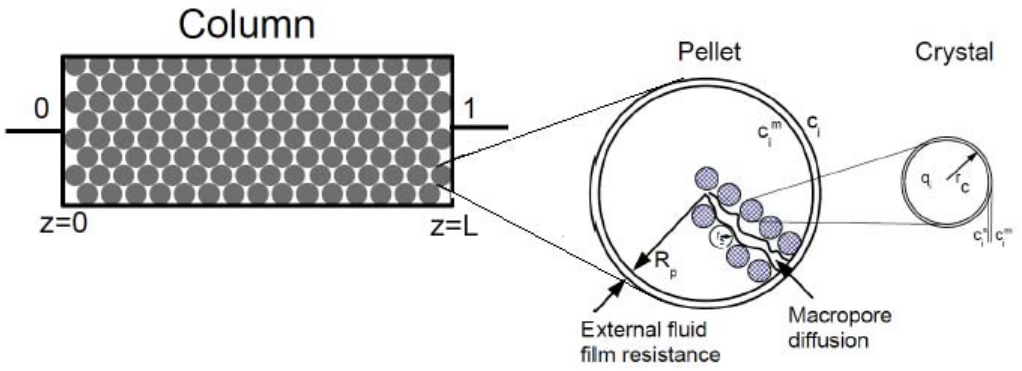

Figure 6.1: Scheme of the adsorption column showing the adsorbent pellets: the inset shows a schematic of an idealised adsorbent pellet including the spherical crystallities.

The physical properties of the solid adsorbent as well as the cylindrical bed geometry features are shown in table 6.2.

Table 6.2: Geometric features of the cylindrical adsorption bed and physical properties of the adsorbent pellets (Zeolite 5A) with whom the bed is filled. The symbols used in the equations are also reported.

Pellet characteristics		
Porosity [-]	ε_p	0.36
Density [kg m^{-3}]	ρ_p	1 812.5
Radius [m]	r_p	0.026
Heat capacity [J kg^{-1} K^{-1}]	$c_{p,ads}$	1 000
Thermal conductivity [Wm^{-2}K^{-2}]	λ_{ads}	0.5
Crystal radius [m]	r_c	1E-06
Bed characteristics		
Radius [m]	r_{bed}	3.5
Length [m]	L	5.5
Porosity [-]	ε	0.34

In the following subsections it will be described the mathematical framework of equations considered in modelling the adsorption bed, from mass balance to the adsorption equilibrium law, passing through energy and momentum balances. All the equations are described in a rigorous way, underlying, when needed, the simplifications/assumptions made. To notice, that the equations are expressed in a general way, following the work by Luberti (2015). To have a look at how the equations are effectively coded in ProcessBuilder refer to the work of Franco (2014).

6.1.1 Mass balance

The differential mass balance for the single component i in the gas phase is described by the axial dispersed plug flow model (6.1). It includes the accumulation

in the fluid phase, the convection flow term, the axial dispersion term and the "source" term caused by the adsorption process on the adsorbent particles.

$$\frac{\partial c_i}{\partial t} = -\frac{\partial (c_i v)}{\partial z} + \frac{\partial}{\partial z}\left(D_z c_T \frac{\partial y_i}{\partial z}\right) - \frac{(1-\varepsilon)}{\varepsilon}\frac{\partial \bar{Q}_i}{\partial t} \tag{6.1}$$

$$\bar{Q}_i = \varepsilon_p c_i^m + \rho_p \bar{q}_i \tag{6.2}$$

Here c_i is the gas phase concentration of component i, c_i^m is the macropore concentration of component i, c_T is the gas phase total concentration and y_i is the molar fraction of component i in the gas phase. Furthermore, $\bar{Q}_i$ is the average concentration of component i over the adsorbent pellet[1] calculated as shown in 6.2, where $\bar{q}_i$ is the sorbate average concentration of component i over the micropore[2], ε is the bed void fraction excluding the macropores (bed porosity) and ε_p is the pellet void fraction (pellet porosity), ρ_p is the pellet density and v is the superficial velocity. D_z is the mass axial dispersion coefficient calculated as:

$$D_z = \gamma_1 D_{i,m} + \gamma_2 d_p v_{int} \tag{6.3}$$

where $D_{i,m}$ is the molecular diffusivity of component i in the mixture, whose calculation is provided in Apendix A. v_{int} is the gas interstitial velocity[3], d_p is the particle diameter and γ_1 and γ_2 are constants usually equal, respectively to 0.7 and 0.5 as described in Ruthven (1984).

The concentration c_i^m in the macropores and the adsorbed concentration q_i in the micropores, presented in (6.2), are respectively described by the two diffusion equations:

$$\varepsilon \frac{\partial c_i^m}{\partial t} + \rho \frac{\partial q_i}{\partial t} + \frac{1}{r^2}\frac{\partial}{\partial r}\left(-D_{p,i} r^2 \frac{\partial c_i^m}{\partial r}\right) = 0 \tag{6.4}$$

$$\frac{\partial q_i}{\partial t} + \frac{1}{r^2}\frac{\partial}{\partial r}\left(-D_{\mu,i} r^2 \frac{\partial q_i}{\partial r}\right) = 0 \tag{6.5}$$

where $D_{p,i}$ and $D_{\mu,i}$ are, respectively, the effective diffusion coefficient for macropore and micropore, whose calculation is provided in Appendix A as well.

The equations just showed compose the rigorous approach to describe the mass balance in the adsorption processes. However, in many cases, the behaviour of these systems can be adequately described by a simpler model, the so called Linear Driving Force (LDF) where the variables of interest will change only with respect to time.

In the case of macropores this change will be proportional (through $k_{LDF,macro}$) to the difference between the current values of concentration and the associated

[1] $\bar{Q}_i = \frac{3}{r_p^3}\int_0^{r_p} Q_i r^2\, dr$ where r_p is the pellet radius

[2] $\bar{q}_i = \frac{3}{r_c^3}\int_0^{r_c} q_i r^2\, dr$ where r_c is the crystal radius

[3] $v_{int} = v/\varepsilon$

values for the closest external gas phase, so that the parabolic PDE (6.4) trasforms into the ODE:

$$\varepsilon \frac{dc_i^m}{dt} + \rho_p \frac{dq_i}{dt} = k_{LDF,macro}(c_i - c_i^m) \tag{6.6}$$

whereas in the micropores, the temporal evolution of concentration in the adsorbed phase is proportional (through $k_{LDF,micro}$) to the difference between the one at equilibrium q_i^* (predicted by the equilibrium isotherm law, §6.1.4) and the current value of concentration of the adsorbed phase, so that (6.5) becomes:

$$\frac{dq_i}{dt} = k_{LDF,micro}(q_i^* - q_i). \tag{6.7}$$

The k_{LDF}, for spherical particles, can be obtained based on the correlation published by Nakao and Suzuki (1983) in the case of macropore and based on Gholami *et al.* (2010) for the micropore.

$$k_{LDF,macro} = \frac{15\varepsilon_p D_{p,i}}{r_p^2} \tag{6.8}$$

$$k_{LDF,micro} = \frac{15\varepsilon_{cry} D_{\mu,i}}{r_c^2} \tag{6.9}$$

Here $D_{p,i}$ is the macropore diffusivity and $D_{\mu,i}$ is the micropore diffusivity (their rigorous calculation are provided in Appendix A). ε_{cry} is the crystal void fraction, assumed equal to the pellet void fraction ε_p. r_p and r_c are, respectively, the pellet and the crystal radius.

Once the k_{LDF} have been calculated, it is possible to compare them in order to find the controlling mechanism, which might lead to a semplification of the problem from a numerical point of view:

$$\frac{k_{LDF,macro}}{k_{LDF,micro}} = \frac{D_{p,i}}{D_{\mu,i}} \left(\frac{r_c}{r_p}\right)^2 \tag{6.10}$$

In particular, for the system analyzed, it results that $k_{LDF,macro}/k_{LDF,micro} = 2.24E-05$, showing that the macropore LDF is 5 orders of magnitude lower that the micropore one. This result allows to state that the diffusion in the macropores is, actually, the controlling mechanism.

In the adsorption bed model present in ProcessBuilder® neither the rigorous macropore mass balance (6.4), nor the macropore LDF (6.6) are present, but only the micropore LDF is coded (6.9), assuming that there is not mass transfer resistance in the macropore, so that $c_i = c_i^m$ (reasonable assumption in most of the adsorption processes). A possible way to overtake the problem is to see the $k_{LDF,macro}$ as it was a "fake" $k_{LDF,micro}$ and substitute it in the micropore LDF balance. Concluding, the equations used in this work have been (6.1) coupled with (6.9), using a $k_{LDF,"micro"} = k_{LDF,macro} = 0.017\ s^{-1}$.

6.1.2 Energy balance

Assuming the fluid and the bed at the same temperature, no heat losses through the wall and neglecting the internal energy in the macropore, the energy balance is expressed by:

$$\varepsilon\frac{\partial U_f}{\partial t}+(1-\varepsilon)\frac{\partial U_p}{\partial t}+\varepsilon\frac{\partial(H_f v_{int})}{\partial z}+\frac{\partial}{\partial z}\left(-\lambda_z\varepsilon\frac{\partial T_f}{\partial z}\right)+\sum_{i=1}^{n}\frac{\partial}{\partial z}\left(-D_z c_T\frac{\partial y_i}{\partial z}\tilde{H}_i\right)=0 \tag{6.11}$$

where U_f, H_f and $\tilde{H}_i$ are respectively the internal energy of the fluid phase per unit of volume, the enthalpy in the fluid phase per unit of volume and the partial molar enthalpy in the gas phase of component i, T_f is the gas phase temperature.

U_p is the internal energy in the pellet and takes into account the contribution of the macropore, the solid phase and the contribution of the adsorbed phase:

$$U_p=\varepsilon_p U_{p,f}+(1-\varepsilon_p)U_{p,s} \tag{6.12}$$

where $U_{p,f}$ is the internal energy in the macropore per unit of volume and $U_{p,s}$ is the internal energy in the solid and sorbate phase per unit of volume. In particular, the contribution of the adsorbed phase is calculated as:

$$U_{ads}=H_{ads}=H_{ads,ref}+\int_{T_{ref}}^{T_f}q_T c_{p,ads}dT-(-\Delta H_{ads}) \tag{6.13}$$

where q_T is the total adsorbed concentration in the solid, $c_{p,ads}$ is the specific heat capacity at constant pressure in the solid phase (value reported in table 6.2) and $-\Delta H_{ads}$ is the total heat of adsorption calculated from the components heat of adsorption ((6.19) in §6.1.4) as $-\Delta H_{ads}=\sum_{i=1}^{N_c}\int_0^{q_i}-\Delta H_i dq$.

λ_z is the thermal axial dispersion, calculated with the Specchia correlation (6.14) from the thermal conductivity in the fluid mixture (λ) and the thermal conductivity of the solid adsorbent (λ_{ads}, value reported in table 6.2).

$$\lambda_z=\varepsilon\lambda+(1-\varepsilon)\frac{1}{\frac{0.22\varepsilon^2}{\lambda}+\frac{2}{3}\lambda_{ads}} \tag{6.14}$$

6.1.3 Momentum balance

The pressure drop along the column is estimated with the Ergun equation:

$$-\frac{dP}{dz}=\frac{150\mu(1-\varepsilon)^2}{d_p^2\varepsilon^2}v+\frac{1.75\rho_g(1-\varepsilon)}{d_p\varepsilon}v^2 \tag{6.15}$$

Where the particles size, the fluid velocity, the bed dimensions and the fluid viscosity (μ) are taken into account.

6.1.4 Adsorption equilibrium

In order to calculate the concentration in the adsorbed phase at equilibrium q_i^*, presented in (6.9), the extended dual-site Langmuir model has been chosen:

$$q_i^* = q_{s,1}\frac{b_{i,1}Py_i}{1+\sum_{j=1}^{n} b_{i,1}Py_i} + q_{s,2}\frac{b_{i,2}Py_i}{1+\sum_{j=1}^{n} b_{i,2}Py_i} \tag{6.16}$$

where $q_{s,1}$ and $q_{s,2}$ are the saturation concentrations of the solid phase[4] respectively of site 1 and 2, and they depend on temperature following (6.17) through the fitting parametes $A_{i,n,1}$ and $A_{i,n,2}$.

$$q_{s,n} = \frac{A_{i,n,1}}{T} + A_{i,n,2} \tag{6.17}$$

$b_{i,1}$ and $b_{i,2}$ are the affinity parameters of component i respectively of site 1 and 2, and they esponentially depend on temperature (6.18) through the fitting parameters $b_{i,0,1}$ and $b_{i,0,2}$.

$$b_{i,n} = b_{i,0,n}\exp(\frac{-\Delta H_{i,n}}{RT}) \tag{6.18}$$

The heat of adsorption term for component i in (6.16) is then calculated as an "averaged sum" of the fitted heats of adsorption for the two sites 1 and 2.

$$\Delta H_{i,ads} = -\left(\frac{\Delta H_{i,1}q_{s,1}b_{i,1}(1+b_{i,2}P)^2 + \Delta H_{i,2}q_{s,2}b_{i,2}(1+b_{i,1}P)^2}{q_{s,1}b_{i,1}(1+b_{i,2}P)^2 + q_{s,2}b_{i,2}(1+b_{i,1}P)^2}\right) \tag{6.19}$$

All the equilibrium parameters have been fitted from experimental equilibrium data in the work of Gholami *et al.* (2010) and are collected in table 6.3.

Table 6.3: Adsorption equilibrium parameters of water, methane, carbon dioxide and nitrogen in zeolite 5A, fitted by Gholami *et al.* (2010).

	$\mathbf{H_2O}$	$\mathbf{CO_2}$	$\mathbf{CH_4}$	$\mathbf{N_2}$
$\boldsymbol{A_{i,1,1}}$ [mol K kg^{-1}]	-3 799.94	516.743	348.971	605.423
$\boldsymbol{A_{i,1,2}}$ [mol K kg^{-1}]	18.711	-0.794	0.542	-0.582
$\boldsymbol{A_{i,2,1}}$ [mol kg^{-1}]	3 684.491	-932.131	348.971	605.423
$\boldsymbol{A_{i,2,2}}$ [mol kg^{-1}]	-4.45	6.083	0.542	-0.582
$\boldsymbol{b_{i,0,1}}$ [kPa^{-1}]	3.58E-07	3.32E-07	6.77E-06	3.73E-05
$\boldsymbol{b_{i,0,2}}$ [kPa^{-1}]	1.62E-05	6.43E-07	6.13E-07	3.18E-05
$\boldsymbol{\Delta H_{i,1}}$[J mol^{-1}]	-44 140.04	-41 077.1	-13 672.21	-7 528.091
$\boldsymbol{\Delta H_{i,1}}$[J mol^{-1}]	-45 199.99	-29 812.29	-20 307.22	-7 941.248

[4] $\lim_{P\to\infty} q^* = q_{s,1} + q_{s,2}$

Equation (6.16) reflects the competitive adsorption of different adsorbates on the adsorption sites. It is in fact clear, that the adsorbed amount of a component will be lower than one single component system at the same conditions. Figure 6.2 shows the equilibrium concentration in the solid phase for the 4 components considered in this work at "low" and "high" temperature (these two temperatures have been chosen as they are the temperatures involved during the adsorption and desorption process in the PTSA process modelling). In both cases water is, by far, the most strongly adsorbed component, but at "low" temperature its concentration at equilibrium (8.5 mol kg^{-1}) is, basically, not a function of pressure, whereas at "high" temperature the dependece on pressure is stronger and the maximum value reached is much lower than at low temperature, as expected. Regarding the other components, at low temperature carbon dioxide is the most strongly adsorbed and its maximum concentration is 0.38 mol kg^{-1}, whereas the maximum methane concentration is 0.14 mol kg^{-1} and nitrogen is basically not adsorbed. At high temperature methane becomes the most adsorbed component and its concentration in the solid phase reaches a maximum value of 0.9 mol kg^{-1}, whereas carbon dioxide and nitrogen are, basically, not adsorbed within the entire range of pressure.

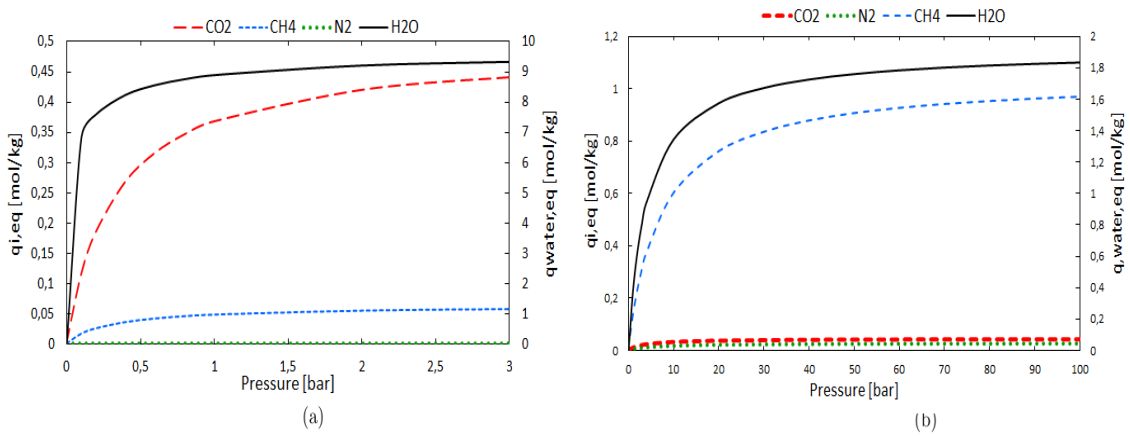

Figure 6.2: Difference in the equilibrium solid concentration loading q^* predicted by the dual site Langmuir isotherm for the 4 components of the mixture considered in table 6.1 at two different temperatures: T = 319.7 K (a) and T = 596 K (b). The left y axes refers to CO_2, CH_4 and N_2 whereas the right y axes refers to H_2O

6.2 One bed model

The first step of the work has been the implementation of a single bed flowsheet, in order to monitor the response of the model with respect to the main variables of interest such as pressure, temperature, molar concentration in the gas phase and molar concentration in the solid phase. Starting from the base case (whose features are described in the above section), the model behaviour has been studied through a series of sensitivity analyses. The flowsheet scheme in presented in figure 6.3, showing the source *Wet gas*, through which the gas is fed to the bed, the *Adsorption bed* and the *Dry gas*, where the dehydrated gas is discharged.

The initial conditions of the feed gas phase as well as the adsorption bed features are respecively described in §6.1. The flow is in "pressure driven" mode (the flow

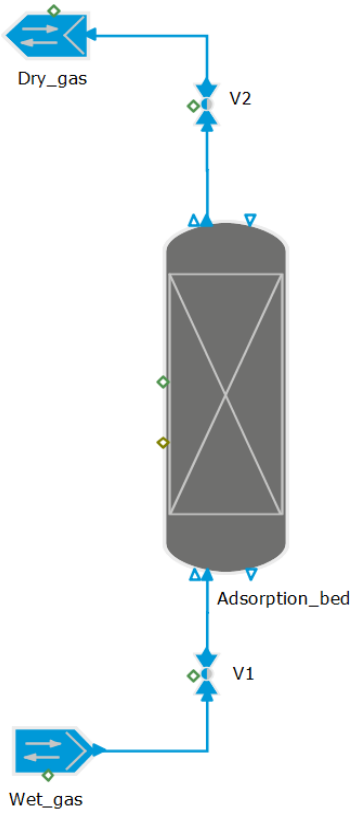

Figure 6.3: Flowsheet representing the single bed adsorption model, implemented in gPROMS® ProcessBuilder.

direction and intensity is governed by the difference in pressure between the source and the sink) and the pressure at the sink is fixed at 63.8 bar (in the source the pressure is 64.1 bar). The two valves V1 and V2, present in figure 6.3, which allow to control the inlet and outlet stream, are modelled as:

$$F = C_v x_{sp} \Delta P \tag{6.20}$$

where F is the molar flowrate, x_{sp} is the stem position (at $x_{sp} = 0$ the valve is fully closed, at $x_{sp} = 1$ the valve is fully open) and C_v is the flow coefficient equal to $1E6$ kmolh^{-1}bar^{-1}. In particular, the molar flowrate is specified in V1 (23 929 kmolh^{-1}), whereas valve V2 is, simply, considered fully open ($x_{sp} = 1$). This rationale has been followed in order to meet the specification of wet gas flowrate to treat as well as to build a complete PTSA process, where numerous valves have to be controlled in order to obtain a continuous operation (this aspect will be clear in §6.3). An important aspect worth to notice is that the flow coefficients have been chosen by a trial and error approach, in order to find the right combination able to guarantee a continuous operation and to meet the process specifications, without wondering whether or not the values found correspond to real valves. In fact, at this level of the work it is important to verify the response of the model with respect to the adsorption process itself, and the verification/optimization of the process stream units, such as valves, could be clarified in a future study, maybe trying to replicate an existing plant. This approach has been followed also during the PTSA process modelling.

Then, the initial composition of the gas phase, inside the bed, have been specified, as shown in table 6.4, which is exactly equal to the initial composition of the feed gas 6.1 minus the water amount. Also the number of discretization points (50) and the finite volume as numerical method, are specified at this level.

Table 6.4: Initial molar composition of the gas phase inside the bed at the beginning of the simulation.

		H_2O	CO_2	CH_4	N_2
Molar composition	[-]	0	0.009998	0.954757	0.035245

6.2.1 Base case results

In figure 6.4 the water concentration profile at the end of the bed ($x = L$) is plotted, along the simulation time (which has beed fixed at 60 000 seconds). This plot is commonly used in the analysis of adsorption processes because it provides the so called breakthrough time. Despite different definitions present in literature, it is generally defined as the time to reach the complete saturation of the adsorption bed. The bed is, in fact, able to completely remove water from the gas stream until $\sim$ 49 000 seconds, where the water concentration at the end of the bed starts rising, showing that the bed is saturated and it is not more able to remove it from the gas stream. After a transition time of $\sim$ 2 000 seconds, the concentration turns into a flat profile, constantly equal to the water molar concentration in the feed gas (0.00184). Therefore, it is possible to conclude that the bed can work for about 49 000 seconds ($\sim$ 13.6 hours, a typical value for this kind of process), before needing the regeneration step to strip out the adsorbed water and regenerate the solid adsorbent.

Figure 6.5 reports the concentration of each component in the solid phase, the so called *"bed loading"*, at the end of the bed along the simulation time. The plot confirms that water is the most strongly adsorbed component (§6.1.4). At the breakthrough time, water adsorption causes a complete displacement of methane and a partial displacement of carbon dioxide present in the solid phase. After the transition zone, in fact, the water concentration reaches a constant value equal to the equilibrium loading, as already showed in figure 6.2, equal to 9.5 mol/kg.

Figure 6.6 shows the gas temperature profile along the bed length at different times. At the beginning of the simulation (after 60 seconds) the first piece of bed starts adsorbing water. The heat of adsorption, liberated inside the particles, is transferred to the gas stream in the active adsorption zone, leading to an increase of the gas temperature by $\sim$ 2C°. On leaving this zone, however, the gas encouters downstream cold gas, so that after an initial peak, the temperature moves back to its initial value. But, as the high temperature wave progresses in advance through the bed length, with respect to the concentration wave the exit gas temperature starts to rise well before the concentration breakthrough. In fact, after 480 seconds all the bed has almost reached the "hot" temperature. It is also interesting to notice that at 2 100 seconds (35 minutes), in the first piece of bed, which has reached the saturation (and no more heat of adsorption is released), the temperature starts decreasing because of the fresh cold gas that is being fed.

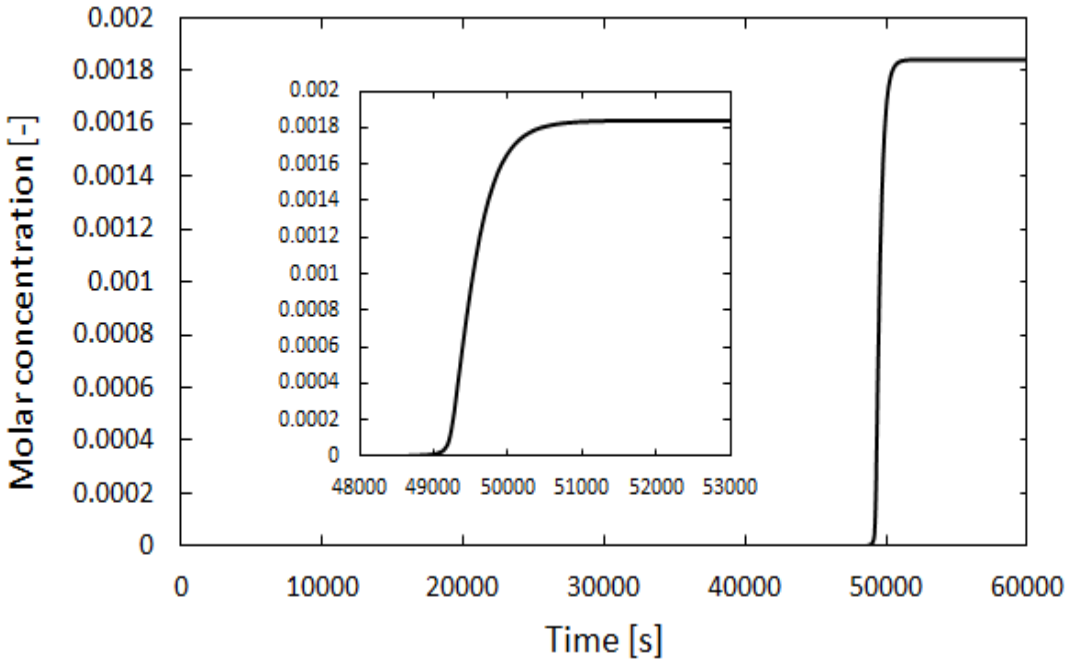

Figure 6.4: Water molar concentration at the end of the bed (water breakthrough) in the base case simulation. The zoom plot helps to visualize the exact time where the concentration of water in the sink starts rising (meaning a complete saturation of the bed).

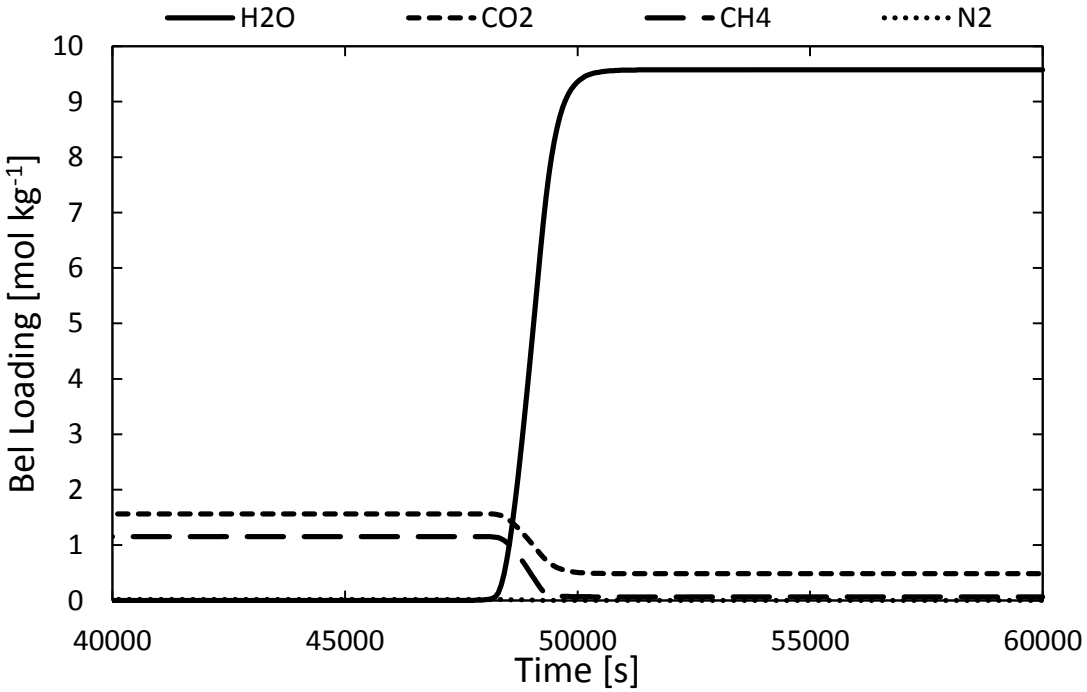

Figure 6.5: Solid loading of each component present in the mixture.

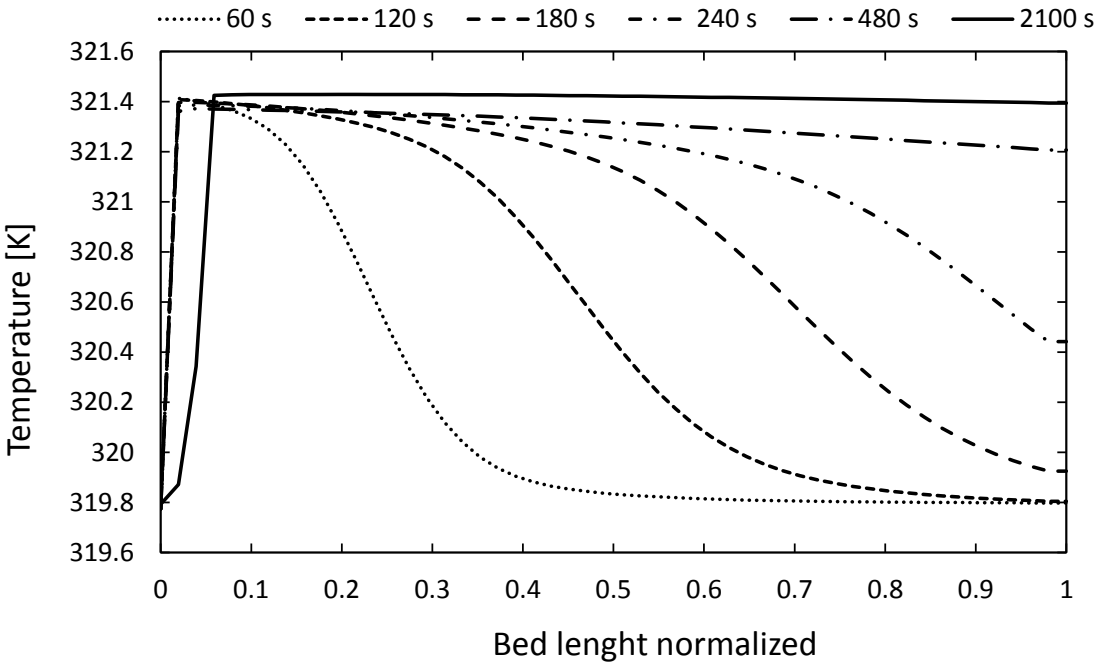

Figure 6.6: Base case temperature profile along the bed length (normalized) at different times: 60 seconds (1 minute), 120 seconds (2 minutes), 180 seconds (3 minutes), 240 seconds (4 minutes), 480 seconds (8 minutes) and 2100 seconds (35 minutes).

The velocity of temperature wave helps also to give an explanation for the time necessary to heat up the whole bed. Figure 6.7 shows the gas temperature profile at $x = L$ along the simulation time, and in particular, shows the initial time necessary to the temperature wave to propagate and heat up the whole bed. In this plot, it is also possible to recognize the breakthrough time, corresponding to which the gas temperature drops down to its initial value, in this case we speak about *breakthrough of temperature*. After the bed saturation occurs, no more heat of adsorption is released so that the bed temperature drops down to the feed cold gas temperature. It is still not clear the phenomenon behind the oscillations, even though they might arise from numerical issues.

Furthermore, a simulation considering the bed at isothermal conditions (at a temperature equal to the feed gas temperature) has showed no difference neither in the predicted breakthrough time nor in the profile shape of concentration. This result is due to the small increase of temperature, which is linked to the low initial concentration of water in the feed gas. In fact, an higher increase in temperature would lead to a lower solid equilibrium concentration of water with respect to the isothermal case, with the direct consequence of a smaller breakthrough time.

Concluding, the momentum balance equation (6.15) coupled to the pressure at the sink and the valve models, predicts a pressure drop along the bed equal to 0.2 kPa and a superficial velocity of 0.26 $\mathrm{m\,s^{-1}}$, which is within the typical range of industrial packed beds velocity.

6.2.2 Breakthrough case studies

The water breakthrough curve, previously showed in figure 6.4, is the key variable for this kind of process, since it gives informations regarding the degree of purity

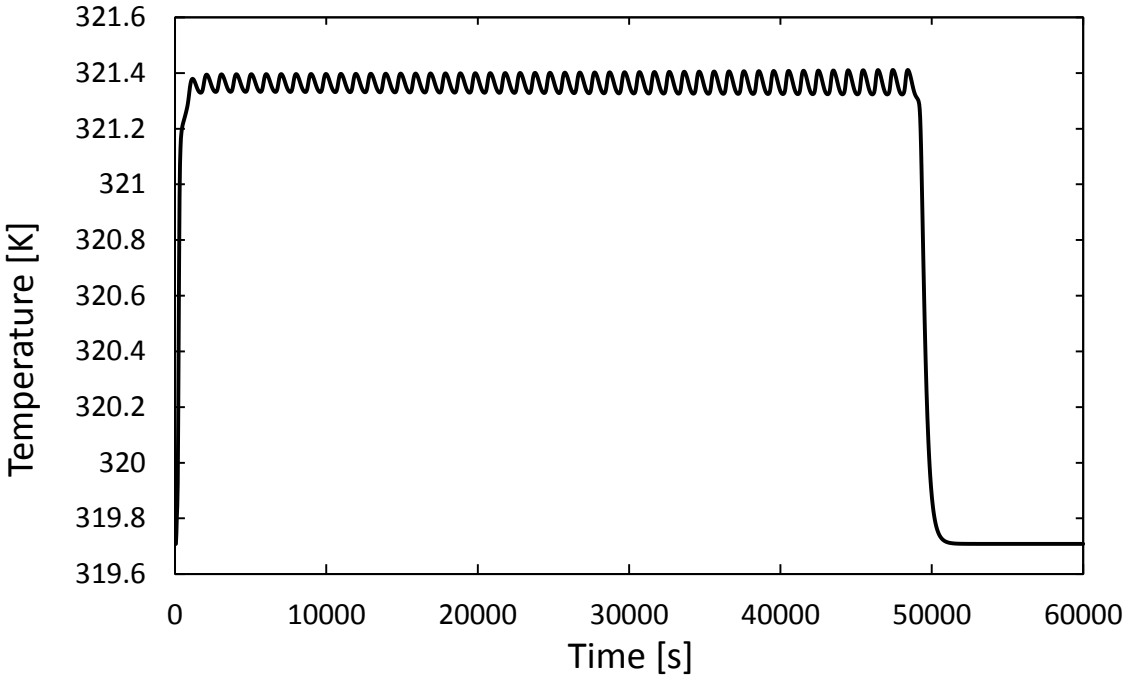

Figure 6.7: Base case temperature profile at x = L (temperature breakthrough) along simulation time.

reached in the outlet gas as well as the bed life time. Ideally, the shape of the breaktrough would be a pure shock (a rectangular curve) but this is clearly not possible for three main effects, which have been studied trough specific sensitivity analyses:

- the axial dispersion,
- the mass transfer resistance,
- the numerical dispersion.

Figure 6.8 shows the effect of axial dispersion coefficient D_z (present in the mass balance equation (6.1) and calculated as showed in equation (6.3)) on the water breakthrough curve. The axial dispersion, resulting from the base case, is 1E-02 m^2s^{-1} (quite "high" because of the big size of the bed pellets) and in the plot it has been compared to an axial dispersion coefficient with a lower (1E-03 m^2s^{-1}) and a higher (1E-01 m^2s^{-1}) order of magnitude. The plots shows, no fundamental differences in the breakthrough time between the base case and 1E-03 m^2s^{-1}, whereas with a value of 1E-01 m^2s^{-1} the curve stretches, leading to a breakthrough time of $\sim$ 48 500 seconds, which is 500 seconds lower than the base case.

Figure 6.9 shows the effect on the water breakthrough of different mass transfer coefficients with respect to the base case, which value is 0.02 s^{-1}. Other than the base case value, a mass transfer coefficient of 1E-03 s^{-1} and 5E-04 s^{-1} have been plotted, that respectively lead to a breakthrough time of 48 000 and 46 500 seconds. In particular 5E-04 s^{-1}, that is close to the value used in the study of (Hyungwoong and Chang-Ha, 2003), leads to a difference in the breakthrough time -5% lower with respect to the base case. It has been also plotted the breakthrough curve

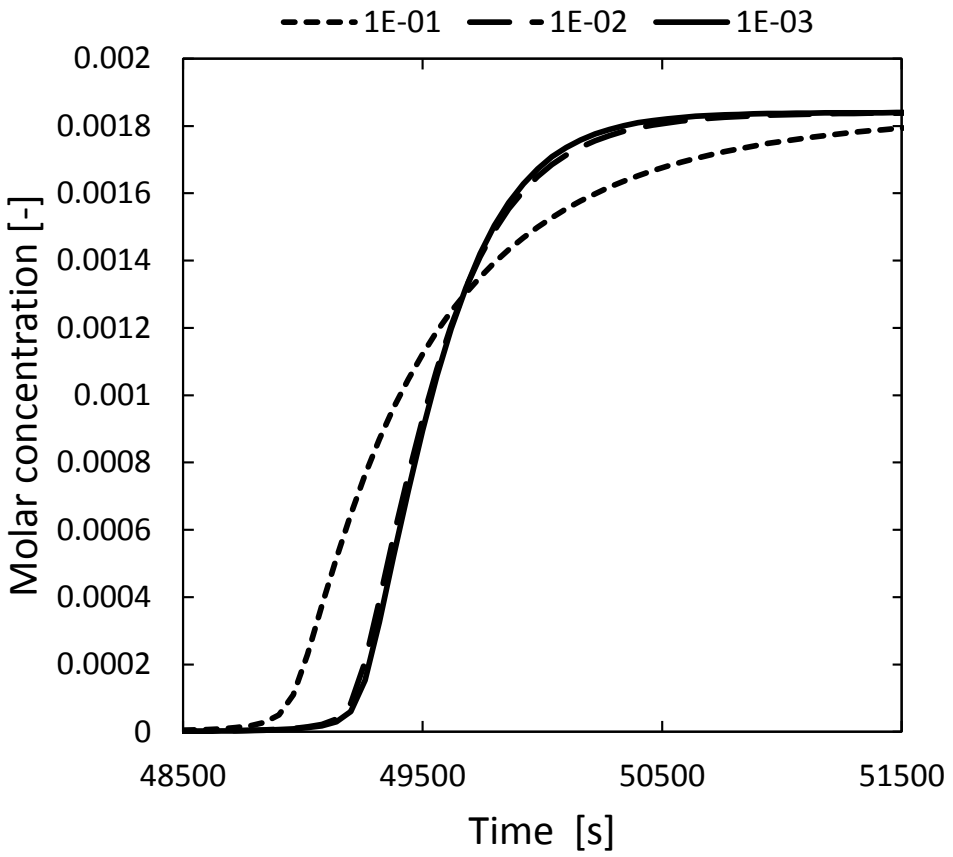

Figure 6.8: Water breakthrough for different values of D_z involved in the sensitivity analysis on the axial dispersion.

considering a mass transfer coeffficient of 2 160 s^{-1} which comes from the micropore LDF calculation(6.9), and does not show any difference compared to the base case neither in shape nor in time.

In the end it has beed studied the so called numerical dispersion effect. The numerical dispersion depends on the number of the domain discretization points that must be specified in the numerical solver section, during the flowsheet setting. In particular, this study has been done in order to find the best number of discretization points after which no meaningful differences, neither in shape nor in breakthrough time are visible and for which the simulation takes a feasible time to converge. Figure 6.10 shows the water breakthrough for 10, 25, 50, 100 and 150 points.

It is interesting to notice how, lowering the number of points, leads to progressively streach the curve, so that to decrease the breaktrough time, which in the worst case (10 pt) becomes 47 000, 4% lower with respect to the base case (50 pt). The plot allows then to establish the "best" number of points, also considering table 6.5, where the computational time has been reported for each value of the grid points. Therefore, it is possible to state that for this process the best number of grid points is around 100, which leads to a good balance between accuracy (the shape and time is not much different oompared to the simulation where 150 points has been used) and computational time (26 minutes).

Concluding, it is possible to state that, although there might be slight differences in the predicted breakthrough time, considering different values of axial dispersion coefficient, mass transfer coefficient and number of grid points, meaningful differ-

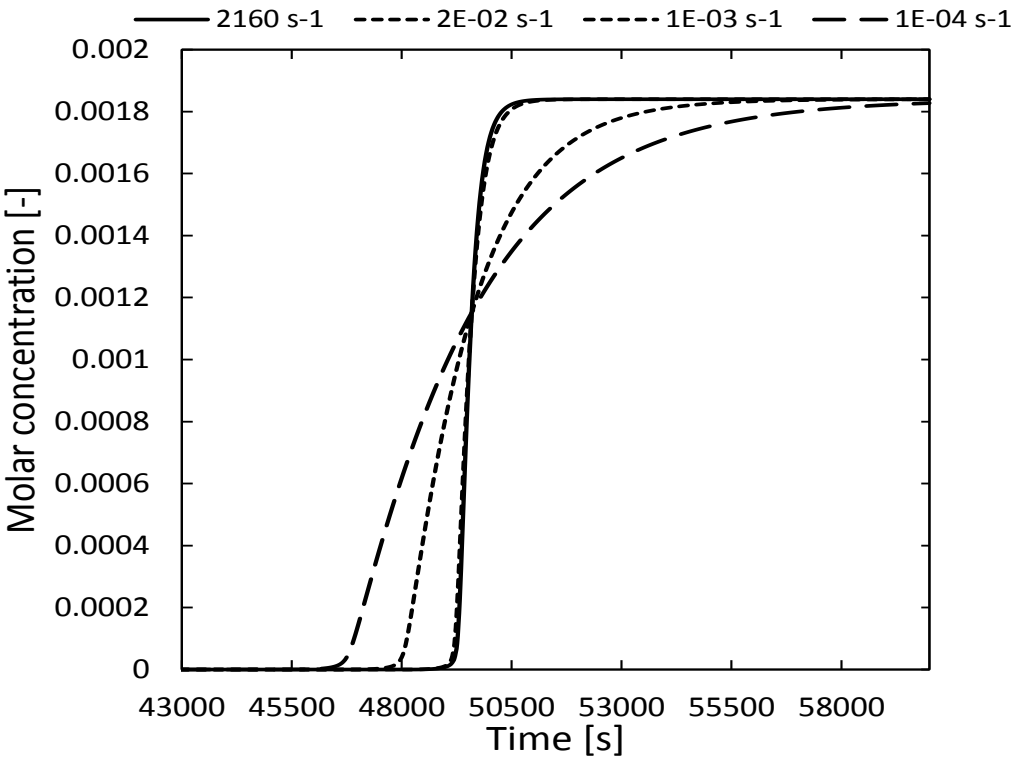

Figure 6.9: Water breakthrough for different values of K_{LDF} involved in the sensitivity analysis with respect to the mass transfer resistance.

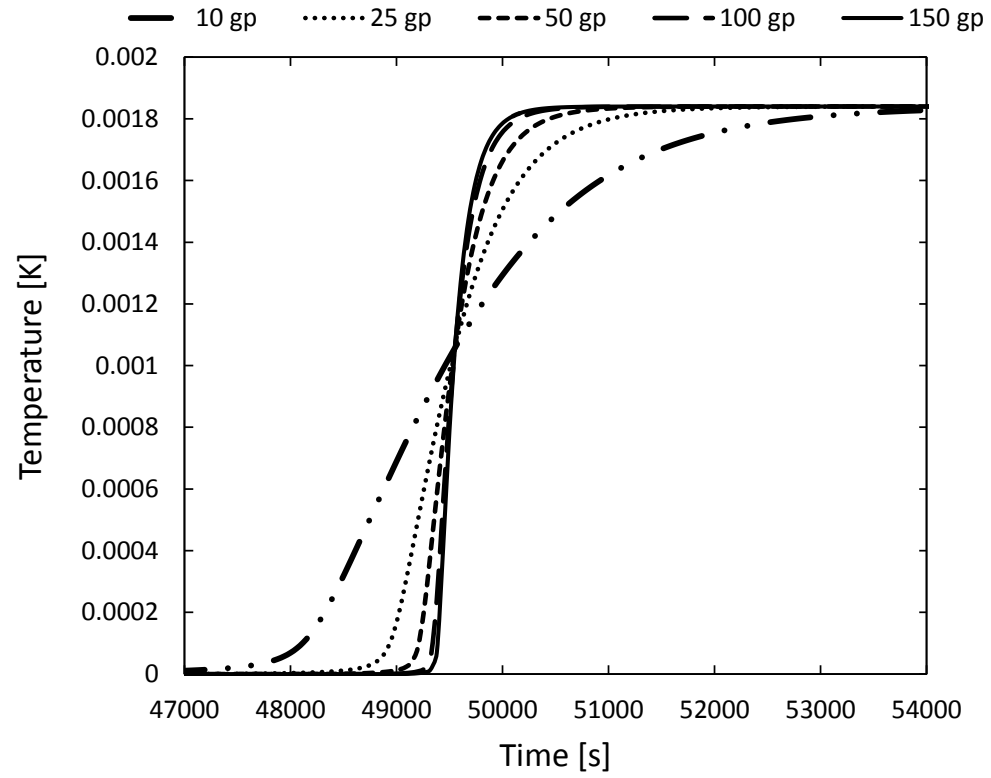

Figure 6.10: Water breakthrough for different numbers of grid points, which shows the phenomenon of numerical dispersion.

Table 6.5: Computational time against the number of grid points involved in the numerical dispersion sensitivity analysis.

Grid points	**Computational time** [min]
10	1
25	3
50	7
100	26
150	56

ences with respect to the base case have not been detected (in the worst case the difference is -5%). In fact, in real processes of gas dehydration via adsorption, where there are two or more beds working in parallel, the bed regeneration step usually starts when the bed is half, or 3/4 saturated, which means for this work, values of around (25 000 - 30 000 seconds). Therefore, it is clearly reasonable that a difference of 2 000 seconds does not affect at all the simulation, in optic to build a complete process where also the regeneration step is involved.

6.3 Pressure-temperature swing adsorption

In this last section, it is described the pressure-temperature swing (PTSA) adsorption flowsheet, implemented in ProcessBuilder®. The PTSA process is made by two parallel adsorption beds, following as reference, the literature process scheme depicted in (fig.in par). The two beds have been designed following the same technical features involved in the single bed model, described in table 6.2. The basic concept, behind the implementation of the PTSA process, has been to exploit the behaviour of the water equilibrium concentration at high temperatures and low pressures as shown in fig. 6.11, in order to reactivate the saturated solid adsorbent. The plot shows, that at low temperature and high pressure, for example in the conditions applied in adsorption study described in the previous paragraph, the equilibrium concentration of water in the zeolite is "high" (around 10 mol kg_{bed}^{-1}), whereas progressively moving toward the region of high temperature and low pressure, the equilibrium concentration in the solid decreases, down to zero for the lowest pressures and highest temperatures.

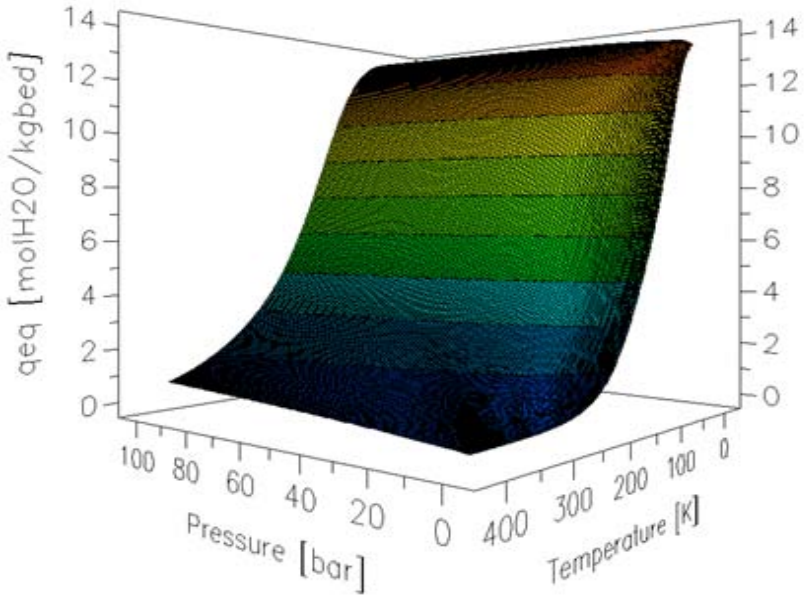

Figure 6.11: Water molar concentration in the solid phase as a function of temperature and pressure.

6.3.1 Flowsheet assembling

The PTSA flowsheet implemented in the ProcessBuilder® enviroment is showed in fig. 6.12.

The wet natural gas to dehydrate, fed from the two sources *Wet gas Feed*, has the same features of temperature, pressure, composition and flowrate (controlled by valves V1) of the gas considered in the single bed model, described above. The technical characteristics of the two parallel beds A and B are also equal to the single bed model as well as the solid physical properties. There are two different sinks for each bed, the *Dry Gas* sink and the *Waste gas* one. The dry gas sink collects the dehydrated gas (the process product) and it is connected to the bed

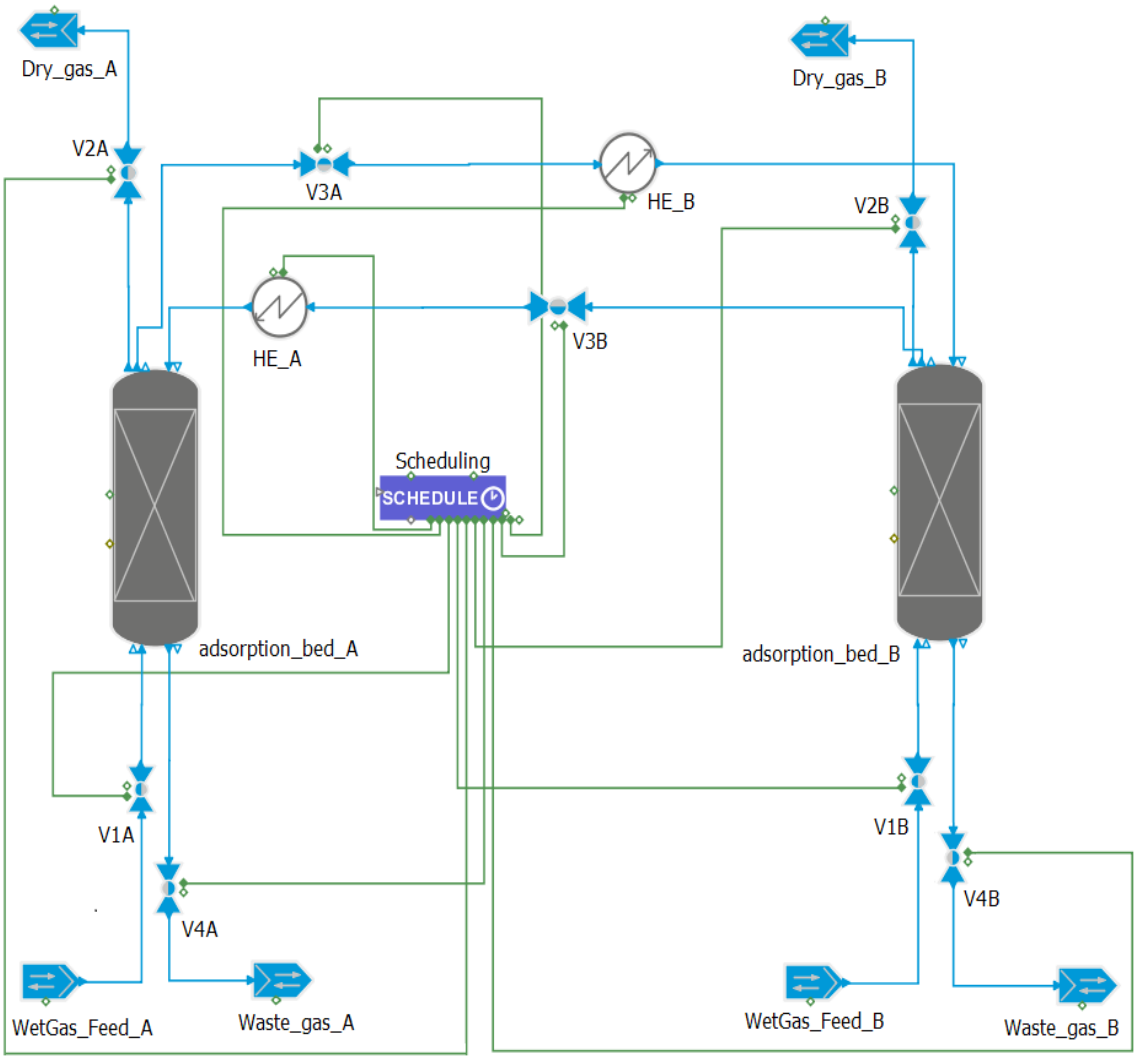

Figure 6.12: Flowsheet representing the pressure-temperature swing adsorption process implemented in ProcessBuilder®.

through valve V2, whereas the waste gas sink, which collects the gas involved in the regeneration step of the bed, has to be either vented or recycled back (in the present work the recycle of this gas stream has not been considered); this stream is controlled through valve V4. The two beds interact because they are connected through two streams, which guarantee that part of the dry gas coming out from one bed during the adsorption step is directed to the other bed as "regeneration gas". The flowrate of the regeneration gas is controlled by valve V3 and its temperature by the heat exchanger HE; it has been decided to use 5 % of the dry gas as regeneration gas, heating up its temperature by 300 K during the hot regeneration step. It is also important to underline that the entire process works in pressure driven mode (as in the single bed flowsheet). This is what happens in reality, meaning that all the material fluxes are moved because of a pressure difference that exists from one point to another. In particular, these pressure differences are specified in the source and sink models and the values used in this work are presented in table 6.6.

Therefore, the desired flowrates are realized regulating the opening and closing of the valves (modelled following (6.20), using the same flow coefficient specified for the single bed model), specifying either the flowrate (in the case of valves V1 and

Table 6.6: Pressure of the sinks and sources present in the PTSA flowsheet depicted in figure 6.12.

	Feed	**Dry outlet**	**Waste outlet**
Pressure [bar]	64.1	63.8	1

V3) or the stem position (for valves V2 and V4).

The dynamic simulation of the PSTA process is, therefore, divided into 6 steps (actually 3 different steps but doubled as the number of beds), which determine one complete operational cycle, where each bed is adsorbing (half cycle) and being regenerated (half cycle). The 6 steps are defined in the schedule model, which acts to the flowsheet by opening/closing the valves and turning on/off the heat exchangers. In table 6.7 these steps are described by showing how the schedule model acts to the valves and the heat exchangers as well as their duration time.

Table 6.7: Specifications present in the schedule model which allows determine each step of the process. This is provided for both the beds. It is also showed the duration time of each step.

	Step	**V1** [kmolh^{-1}]	**V2** [-]	**V3** [kmolh^{-1}]	**V4** [-]	**HE** [K]	**Time** [s]
			Bed A				
1	Adsorption	23 929	1	0	0	0	40
2	Adsorption	23 929	1	1 196.45	0	300	20 000
3	Adsorption	23 929	1	1 196.45	0	0	10 000
4	Blowdown	0	0	0	1	0	40
5	Hot purge	0	0	0	1	0	20 000
6	Cold purge	0	0	0	1	0	10 000
			Bed B				
1	Blowdown	0	0	0	1	0	40
2	Hot purge	0	0	0	1	0	20 000
3	Cold purge	0	0	0	1	0	10 000
4	Adsorption	23 929	1	0	0	0	40
5	Adsorption	23 929	1	1 196.45	0	300	20 000
6	Adsorption	23 929	1	1 196.45	0	0	10 000

It is important to underline that the adsorption step has been chosen to be 30 040 s, which means, since the breakthrough time is 49 000 s, that the bed is 61% saturated along its length. In figure 6.13 half cycle is depicted, in particular the case when bed A is adsorbing and bed B is being regenerated. A detailed description and analysis will be described in the next section.

The flowsheet just described is a simplification of the complete PTSA depicted in §1.4.2. After the study of the single bed in the previous section, where the model has showed its goodness under adsorption conditions (showing a breakthrough time and a shape of the curves congruent to the literature studies), the goals of this study have been exploring the behaviour of the bed model with respect to the regeneration conditions (high temperature and low pressure) as well as the capacity to interact with another bed in a pressure driven framework so that to guarantee the adsorption process to be continuous.

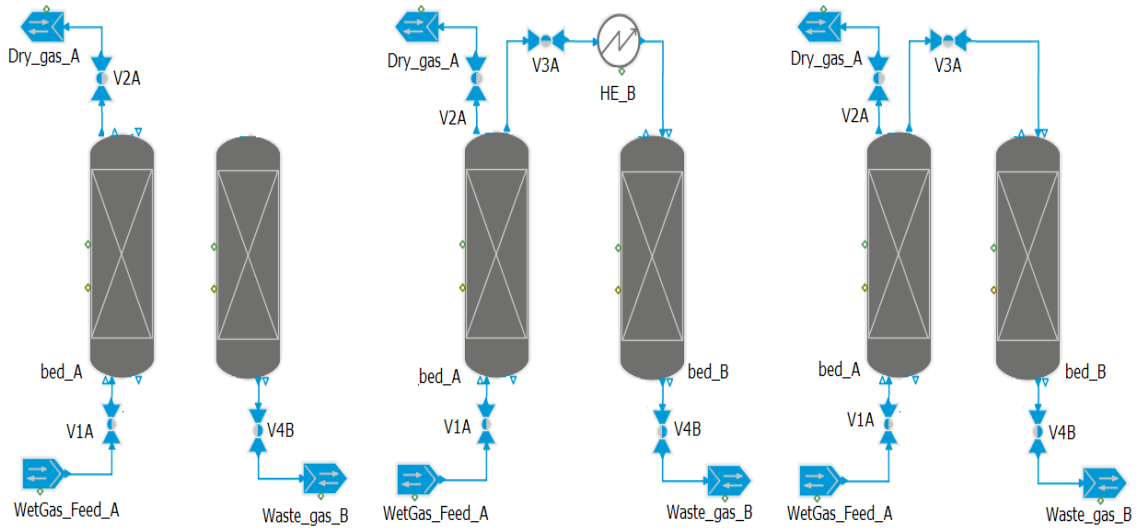

Figure 6.13: The three steps of half cycle, where the Bed A is in adsorption mode and Bed B is being regenerated.

6.3.2 Results

In this section the results from the PTSA model are presented. The third cycle (from 180 240 s to 240 320 s) has been chosen as the reference cycle for presenting the results, because after this cyle the simulation reaches the steady state. The time range has been re-scaled from 0 s to 60 080 s (duration of 1 cycle) to get an higher legibility of the results. The plots are also valid for the following cycles. In particular, the profiles have been plotted at the beginning of the beds, which is the most critical part in terms of regeneration (at 10% of bed length).

Figure 6.14 shows the pressure profiles of the two beds after half cycle (the results are the same along all the beds length). At 30 040 s the adsorption step ends for bed A, valves V1A and V2A are closed and the blowdown step begins by opening valve V4B. The gas inside the column is then discharged at atmosferic pressure in the waste gas sink and the pressure inside the column drops down to 12 bar. At the same time, the natural gas feed is switch from bed A to bed B, by opening valves V1B and V2B. Thus, the pressure in bed B increases, from the nominal regeneration value (7 bar) to the adsorption nominal pressure of (64 bar). Up to this point, it is important to underline that the momentum balance, from purge to adsorption, produce a pressure step (from 7 to 64 bar), that is why a pressurisation step has not been necessary (a pressurization step would have meant filling the bed after the regeneration step by opening the feed valve and keeping close the outlet one). Once the blowdown step ends for bed A, after 40 s (at 30 080 s), the hot purge step starts by opening valve V3A and turning on the heat exchanger HEB (which does not influence the pressure profile). Pressure further decreases down to a value of 7 bar, which is maintained constant throughout all the purge step (hot and cold).

Figure 6.15 shows the temperature profile of the two beds during the third cycle of simulation.

Analyzing, for instance, Bed A, during the first half of the cycle it is adsorbing, therefore the temperature profile is flat, equal to the feed gas temperature (319 K). Then, at 30 040 s the blowdown step begins followed by the hot purge, where the regeneration gas temperature is increased up to 596 K. The plot shows that the gas

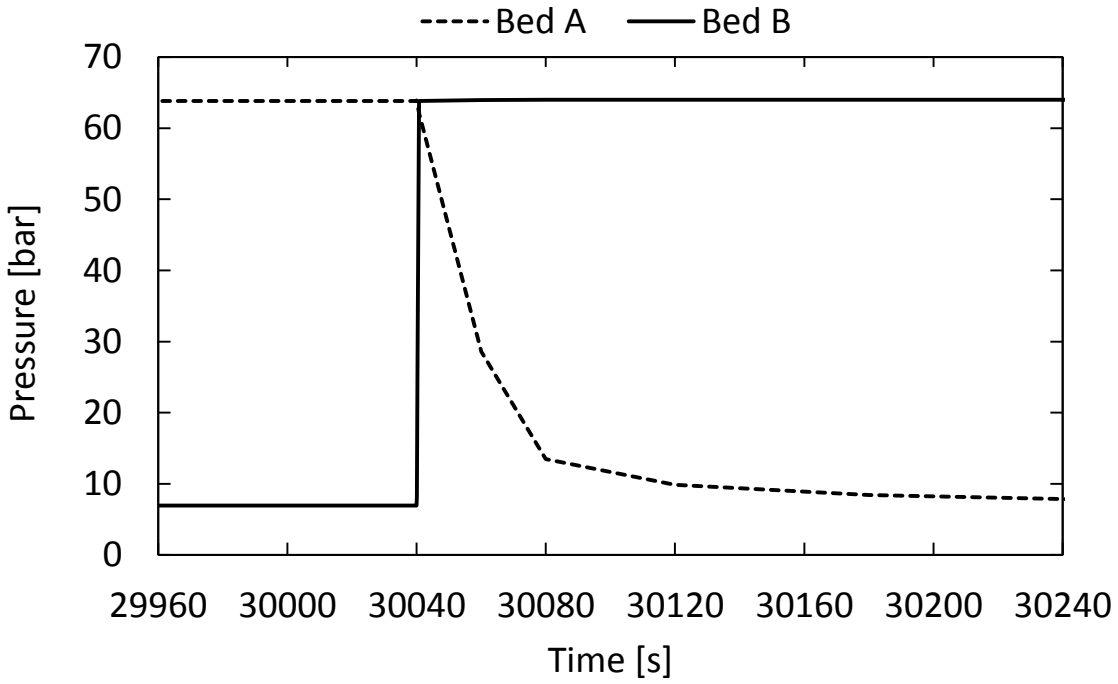

Figure 6.14: Pressure profile of Bed A and Bed B present in the PTSA flowsheet presented in figure 6.12. In particulat the plot shows the middle point of the third cycle of simulation, where Bed A starts the regeneration step and Bed B starts adsorbing.

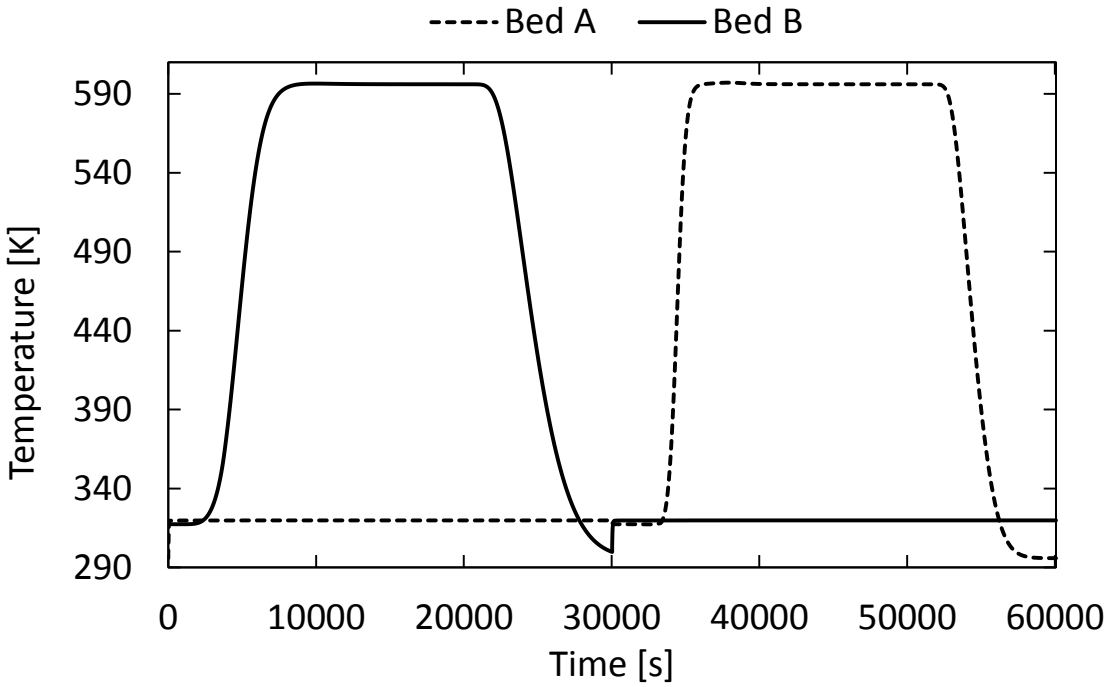

Figure 6.15: Temperature profile of Bed A and Bed B of the PTSA process presented in figure 6.12, during the third cycle of simulation.

takes about 1 000 seconds to reach the desired temperature for the all bed length (at least 90 % of the bed length). Thus, the hot purge lasts for 20 000 s until time 50 120 s when the heat exchanger is turned off and the regeneration gas is stopped being up. Therefore, the cold purge begins and the bed temperature decreases down to 300 K. This temperature is lower than the temperature that the regeneration gas has initially, probably because of the Joule-Thomson effect due to the pressure drops in valve V3.

A possible improvement of the process, could be the reduction of the cold purge time (now it is 10 000 s) since the bed temperature reaches the desired value of 319 K at 56 540 *s*, after just 6 420 *s* from the beginning of the step.

Figure 6.16 shows the concentration of the 4 components in the mixture during the third cycle for bed A, also in this case at the beginning of the bed.

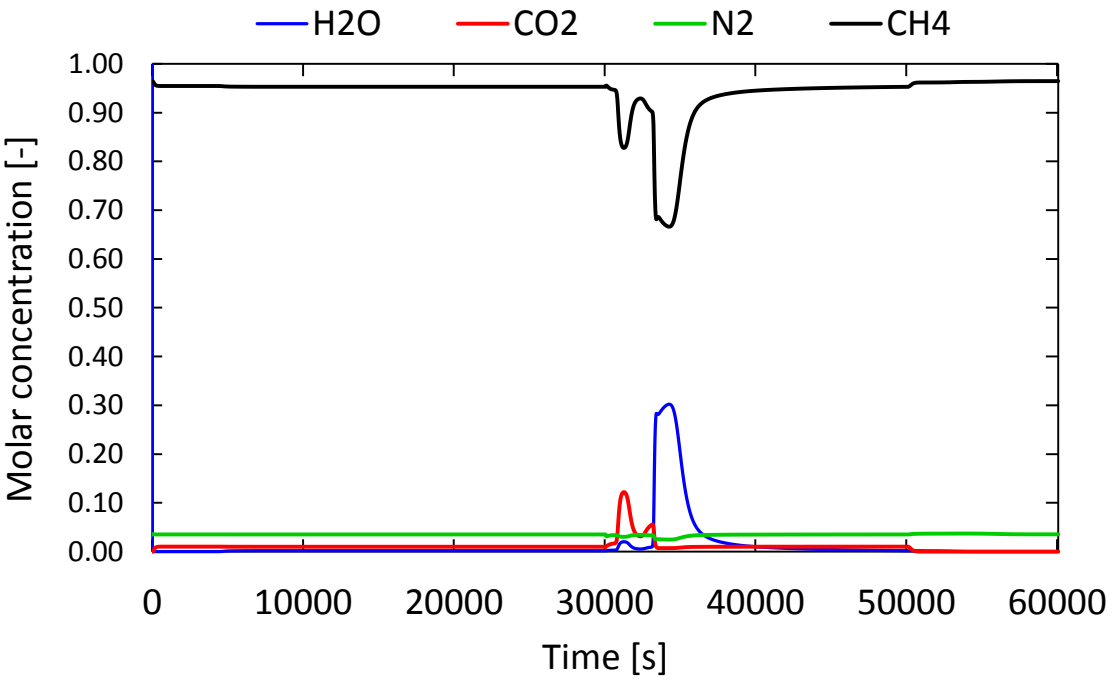

Figure 6.16: Gas phase molar concentration of all the components present in the mixture. The plot refers to the entire third cycle of simulation.

During the adsorption step (half cycle) water breakthrough takes place (with consequent displacement of methane and carbon dioxide) at 4 900 s (to remind that the plot shows the concentration at 10% of the bed length). This event cannot be seen in the plot as the variation in concentration due to the breakthough is too small if compared to the concentration "jump" during the regeneration. In fact, during the blowdown step a slight amount of water is released, with an increase in water concentration in the gas phase (first peak) and during the hot purge step the bed is completely regenerated by releasing all the water previously adsorbed (second peak). After the main peak, the concentration progressively decreases down to zero at the end of the cold purge, when the bed is completely regenerated as ready to start the next adsorption step.

Conclusions

The growing production of natural gas has jutified the interest of modelling the processes involved during its production. In particular, modelling these processes by using gPROMS® ProcessBuilder process simulator may bring great advantages in terms of predictivity and flexibility.

The first part of the work is based on modelling the two absorption processes of sweetening and dehydration by using gSAFT® as thermodynamic package. The thermodynamic validation against experimental data has highlighted the ability of SAFT® to correctly predict the experimental data, even without being specifically tailored for these particular applications. However, it has been necessary to adjust the interaction parameters between the groups $-CH_3$ and H_2S and between $-CH_3$ and CO_2, in order to obtain better predictions. The only limitation that the model has shown is the calculation of the heat of absorption of H_2S and CO_2 in the amine solution. In the case of H_2S the heat of absorption is over estimated by 10 kJ/mol whereas for CO_2 it is uder estimated by 10 kJ/mol. Altough this poor predictions is probably due to the lack of experimental data during the parameters fitting, it has not been considered worth to be adjusted at this level. The work on thermodynamic validation has also contribute to extend the experimetal data set available for parameters fitting.

Once the thermodynamic model has been validated, the flowsheets have been implemented following some literature case studies. All the simulation results have been simply compared to the literature ones, where Aspen HYSYS® has been used as process simulator.

In the case of sweetening the model predicts a concentration of acid gases in the sweet gas much lower than the literature source. This is probably due to the difference in the column modelling approach: equilibrium based vs. rate based (even though in the literature source the approach used is not specified). Another literature study has contribute to validate this hypothesis, showing very low concentration of CO_2 and H_2S in the sweet gas using the equilibrium approach with Aspen HYSYS®. At this point it is important to underline that modelling the two columns with the equilibrium based approach is an extreme simplification, since the reactions taking place in the liquid phase contribute to deviate the mixture far away from the equilibrium conditions. In fact, the rate based would be the best approach because it allows to model the actual rates of multicomponent mass and heat transfer, also taking into account the effect of the chemical reactions. But, clearly, this approach is way more complex and it requires a dedicated study that would have gone beyond the objetives of this work.

Fortunately, in the case of glycol some experimental data have allowed to validate the absorption column. The complete flowsheet response, instead, has been

compared with the literature source, showing a concentration of water in the dry gas slightly different with respect to the one predicted in Aspen HYSYS®, even though they have the same order of magnitude. This small difference is due to the different thermodynamic package used. In this case the equilibrium based is the correct approach to model the two columns.

Once the single flowsheets responses have been compared and "validated" with the literaure, the two absorption processes have been connected in series in the same flowsheet (exploiting the use of the same thermodynamic package). Then, a rigorous optimization has been possible contributing to demonstrate the high potential of having two different processes in the same flowsheet. In fact, it has been possible to reduce the overall energy consumption (-23%) by acting on variables in both the processes and constraining both the acid gases and water contents in the final product (thanks to the gPROMS® equation oriented approach).

The modelling of dehydration via adsorption has started modelling a single adsorption bed. The bed has been modelled following a mathematical framework present in literature, even though it has not been possible to perfectly reproduce it since the lack of the macropore diffusion equation. This issue have led to predict a different bed saturation time with respect to the literature case study. However, once the single bed saturation time has been found, the two beds PTSA has been modelled, following literature suggestion but without reproducing a specific work. The work on the adsorption model has contribute to show the flexibility of custom modelling, so as to easily adapt the intrisic adsorption mathematical framework to a specific case study. At the same time though, it has also been showed the limitation of the mass balance equations on modelling the macropore mass transfer resistance.

Future work

In the case of sweetening process a detailed study is recommended so as to model the two columns with a rate based approach, modelling the actual rates of multicomponent mass and heat transfer, avoiding the simplification of equilibrium trays. Furthermore, for both the absorption processes, it is suggested, exploiting the high flexibility and predibility of gSAFT®, to try different solvents that might lead to advantages in terms of profitability. Clearly, this can be done prior thermodynamic validation against equilibrium experimental data. A long view suggestion is also exploiting the opportunity of using the same thermodynamic package so as to include also the other steps involved in the gas chain (e.g. the mercury removal or the nitrogen rejection) into the "whole" flowsheet.

In the case of the adsorption model, it is suggested to add the macropore diffusion equation in the material balance, since the macropore resistance has an high contribution on the overall mass transfer in the solid phase. This would probably lead to match the saturation time predicted by the literature study.

However, for all the processes a comparison and a validation against real plant data is highly recommended.

Aknowledgments

I would like to express my deep gratitude to my supervisor Prof. F. Bezzo to have given me the possibility to experience this thesis project abroad, for the technical support and the precious suggestions.

My thankfulness goes also to Professor C. Pantelides, for the opportunity to work at PSE, giving me the possibility to learn a lot about gPROMS.

A special thanks goes to my supervisors at PSE, Dr. M. Patel and Dr. L. Domingues, for sharing with me their scientific knowledge and experience on process modelling, driving me throughout all the difficulties that I met during this project, being always available and extremely patient. It has been an honour working alongside such expert engineers like you.

I would also like to thank all the people at PSE always willing to help and support me. In particular I would like to thank Dr. M. Luberti, for the time spent on the adsorption model, helping me with his technical and moral support, grazie!

Bibliography

Abdulrahman R. K. and Sebastine I. M. (2013), Natural gas sweetening process simulation and optimization: A case study of Khurmala field in Iraqi Kurdistan region, *Journal of Natural Gas Science and Engineering*, **14**, 116-120.

Abdulrahman R. K. and Sebastine I. M. (2013), Natural gas dehydration process simulation and optimization: a case study of Khurmala field in Iraqi Kurdistan region, *Int. J. Chem. Mol. Nu. Mat. Met. Eng.*, **7**, 350-353.

Abedinzadegan Abdi M., Meisen A. (1999), A novel process for diethanolamine recovery from partially degraded solutions. 1. Process description and phase equilibria of the DEA – BHEP – THEED – Hexadecane system, *Ind. Eng. Chem. Res.*, **38**, 3096-3104.

Al-Lagtah N. M. A., Al-Habsi S. and Onaizi S. A. (2015), Optimization and performance improvement of Lekhwair natural gas sweetening plant using Aspen HYSYS, *J. Nat. Gas Sci. Eng.*, **26**, 367-381.

Al-Sahhaf T., Kidnay A.J., Sloan E.D. (1983), Liquid + Vapor equilibria in the N2 + CO2 + CH4 system, *Ind. Eng. Chem.*, **22**, 372-380.

Al Wahedi Y., Rabie A.H., Al Shaiba A., Geuzebroek F., Daoutidis P. (2016), Optimization of adsorption-based natural gas dryers, *Ind. Eng. Chem. Res.*, **55**, 4658-4667.

Aliabad Z.H. and Mirzaei S. (2009), Removal of CO2 and H2S using aqueous alkanolamine solutions, *Engineering and Technology*, **49**, 194-203.

Anyadiegwu C. I. C., Kerunwa A., Oviawele P. (2014), Natural gas dehydration using thiethylene glycol (TEG), *Petroleum and Coal*, **56**, 407-417.

Aspen Technology, Inc. (2006), Aspen HYSYS property package: Overview and best practices for optimum simulations, *Aspen process engineering webinar*.

Bamberger A., Sieder G., Maurer G. (2000), High-pressure (vapor + liquid) equilibrium in binary mixtures of (carbon dioxide + water or acetic acid) at temperatures from 313 to 353 K, *J. Supercrit. Fluids*, **17**, 97-110.

Berrouk A. and Ochieng R. (2014), Improved performance of the natural gas

sweetening Benfield - HiPure process using process simulation, *Fuel Process. Technol.*, **127**, 20-25.

Bird R.B., Stewart W. E., Lightfoot E.N. (2007), *Transport phenomena*, Wiley, Madison (Usa).

Bullin A.J., Polasek J.C., Fitz C.W., *The impact of acid gas loading on the heat of absorption and voc and btex solubility in amine sweetening units*, Bryan research and engineering, Inc., Bryan, TX (Usa).

Burgess M.P. and Germann R.P. (1969), Physical properties of hydrogen sulfide – water mixtures, *AIChe J.*, **15**, 272-275.

Carlson E.C. (1996), *Don't gamble with physical properties for simulation*, *Chemical Engineering Progress*, 35-46.

Chapoy A., Mokraoui S., Valtz A., Richon D., Mohammadi A.H., Tohidi B. (2004), Solubility measurement and modeling for the system propane-water from 277.62 to 368.16 K, *Fluid Phase Equilib.*, **226**, 213-220.

Chapoy A., Coquelet C., Liu H., Valtz A., Tohidi B. (2013), Vapour-liquid equilibrium data for the hydrogen sulphide (H2S) + carbon dioxide (CO2) system at temperatures from 258 to 313 K, *Fluid Phase Equilib.*, **356**, 223-228.

Dan Laudal C. (2009), *Thermodynamic simulation of the water/glycol mixture*, Master thesis, Aalborg University Esbjerg, Esbjerg (Denmark).

Demirbas A. (2010), *Methane gas hydrate*, Springer, Trabzon (Turkey).

Derawi S.O., Kontogeorgis G.M., Michelsen M.L., Stenby E.H. (2003), Extension of the cubic – plus – association equation of state to glycol – water cross – associating systems, *Ind. Eng. Chem. Res.*, **42**, 1470-1477.

Dufal S., Papaioannou V., Sadeqzadeh M., Pogiatzis T., Chremos A., Adjiman C.S., Jackson G., Galindo A. (2014), Prediction of thermodynamic properties and phase behaviour of fluids and mixtures with the SAFT-γ Mie group contribution equation of state, *J.Chem. Eng. Data*, **59**, 3272-3288.

El Mawgoud H. A., Elshiekh T. M. and Khalil S. A. (2015), Process simulation for revamping of a dehydration gas plant, *Egypt. J. Petr.*, **24**, 475-482.

Franco C. R. S. (2014), *Pressure swing adsorption for hydrogen purification*, Master Thesis, Department of Chemical Engineering, University of Porto (Portugal).

Frost M., Karakatsani E., Solms N., Richon D., Kontogeorgis G.M. (2014), Vapor – liquid equilibrium of methane with water and methanol. Measurements and modeling, *J. Chem. Eng. Data*, **59**, 961-967.

Ghati M. (2013), A study on selection and design of natural gas dehydration technology, *Specialization project*, Norwegian University of Science and Technology, Trondheim (Norway).

Gholami M., Talaie M.R., Roodpeyma S. (2010), Mathematical modeling of gas dehydration using adsorption process, *Chem. Eng. Sci.*, **65**, 5942-5949.

Gholami M., Talaie M. R. (2010), Investigation of simplifying assumptions in mathematical modeling of natural gas dehydration using adsorption process and introduction of a new accurate LDF model, *Ind. Eng. Chem. Res.*, **49**, 838-846.

Gillespie P.C. and Wilson G.M., *Tech.Rep.* (GPA Research Report RR-48), 1982.

GPSA Engineering Data Book (2004), 12th edition - FPS, Gas processor suppliers association, Tulsa (Usa).

GPSA Engineering Data Book (2012), 13th edition - FPS, Volume II, Gas processor suppliers association, Tulsa (Usa).

Haji – Sulaiman M.Z., Aroua M.K., Benamor A. (1998), Analysis of equilibrium data of CO2 in aqueous solutions of diethanolamine (DEA), methyldiethanolamine (MDEA) and their mixtures using the modified kent – eisenberg model, *Chem. Eng. Res. Des.*, **76**, 961-968.

Heinz-Wolfgang Haring (2008), *Industrial gases processing*, Wiley, Munchen (Germany).

Horstmann S., Mougin P., Lecomte F., Fischer K., Gmehling J. (2002), Phase equilibrium and excess enthalpy data for the system methanol + 2,2' –diethanolamine + water, *J. Chem. Eng. Data*, **47**, 1496-1501.

Hyungwoong A., Chang-Ha L. (2003), Adsorption dynamics of water in layered bed for air-drying TSA process, *AIChE J.*, **49**, 1601-1609.

Jerinic D., Schmidt J., Fischer K., Friedel L. (2008), Measurement of the triethylene glycol solubility in supercritical methane at pressures up to 9 MPa, *Fluid Phase Equilib.*, **264**, 253-258.

Kay W.B., Brice D.B. (1953), Liquid – Vapor equilibrium relations in ethane – hydrogen sulfide system, *Ind. Eng. Chem.*, **45**, 615-618.

Kay W.B., Rambosek G.M. (1953), Liquid – Vapor equilibrium relations in binary systems - Propane – Hydrogen sulfide system, *Ind. Eng. Chem.*, **45**, 221-226.

Kent R. L., Eisenberg B. (1976), Better data for amine treating, *Hydrocarbon process*, **55**, 87-90.

Kidnay A.J. Parrish W.R. (2006), *Fundamentals of natural gas processing*, Tay-

lor and Francis Group, Boca Raton (Usa).

Kohl A. and Nielsen R. (1997), *Gas purification*, Gulf Publishing Company, Houston (Usa).

Lee J., Otto F. D., Mather A. E. (1973), Solubility of hydrogen sulphide in aqueous diethanolamine solutions at high pressure, *J. Chem. Eng. Data*, **18**, 71-73.

Li Y. G., Mather A. (1996), Correlation and prediction of the solubility of CO_2 and H_2S in aqueous solutions of thiethanolamine, *Ind. Eng. Chem. Res.*, **35**, 4804-4809.

Leu A.D., Robinson D.B., (1989), Equilibrium phase properties of the n-Butane-Hydrogen sulfide and Isobutane-Hydrogen sulfide binary systems, *J. Chem. Eng. Data*, **34**, 315-319.

Lewis W.K. and Whitman W.G. (1924), Principles of gas absorption, *Ind. Eng. Chem. Res.*, **16**, 1215-1220.

Luberti M. (2015), *Design of a H2 Pressure Swing Adsorption process at an advanced IGCC plant for cogenerating hydrogen and power with CO2 capture*, Ph.D. Thesis, University of Endinburgh (UK).

Marques R. M. (2014), *Modelling the natural gas sweetening and dehydration prior to liquefaction*, Master thesis, Istituto Técnico, Lisbon (Portugal).

Mohammadi A.H., Chapoy A., Tohidi B., Richon D. (2004), Measurements and thermodynamic modeling of vapor – liquid equilibria in ethane-water systems from 274 to 343 K, *Ind. Eng. Chem. Res.*, **43**, 5418-5424.

Mostafazadeh A.K., Rahimpour M.R., Shariati A. (2009), Vapor – liquid equilibria of water + triethylene glycol (TEG) and water + TEG + Toluene at 85 kPa, *J. Chem. Eng. Data*, **54**, 876-881.

Muhammad A., GadelHak Y. (2014), Correlating the additional amine sweetening cost to acid gases load in natural gas using aspen hysys, *J. Nat. Gas Sci. Eng.*, **17**, 119-130.

Muhammad A., GadelHak Y. (2015), Simulation based improvement techniques for acid gas sweetening by chemical absorption: a review, *Int. J. Greenhouse Gas Control*, 37, 481-491.

Nazir A., Ismailpour A., Saleem F., Idrees M. U. and Zaidy S. A. H. (2010), *Natural gas sweetening and effect of declining pressure*, Norwegian University of science and technology, Trondheim (Norway).

Netusil M. and Ditl P. (2012), *Natural gas dehydration*, Intech, Prague (Czech Republic).

Papaioannou V. (2012), *A molecular based group contribution equation of state for the description of fluid phase behaviour and thermodynamic derivative properties of mixtures (SAFT-γ Mie)*, Ph.D. Thesis, Imperial College London (UK).

Papaioannou V., Lafitte T., Avendano C., Adjiman C.S., Jackson G., Muller E. A. and Galindo A. (2014), Group contribution methodology based on the statistial associating fluid theory for heteronuclear molecules formed from Mie segments, *J. Chem. Phys.*, **140**,-.

Papaioannou V., Calado F., Lafitte T., Dufal S., Sadeqzadeh M., Jackson G., Adjiman C. S. and Galindo A. (2016), Application of the SAFT-γ Mie group contribution equation of state to fluids of relevance to the oil and gas industry, *Fluid Phase Equilib.*, **416**, 104-119.

Pellegrini A.L., Moioli S., Picutti B., Vergani P. and Gamba S. (2011), *Design of an acidic natural gas purification plant by means of a process simulator*, Dipartimento di Chimica, Materiali e Ingegneria Chimica "G. Natta", Politecnico di Milano (Italy).

Pereira F.E., Jackson G., Galindo A. and Adjiman C. S.s (2010), A duality based optimization approach for the reliable solution of (p,T) phase equilibrium in volume-composition space, *Fluid Phase Equilib.*, **299**, 1-23.

Qeshta H. J., Abuyahya S., Pal P. and Banat F. (2015), Sweetening liquefied petroleum gas (LPG): Parametric sensitivity analysis using Aspen HYSYS, *J. Nat. Gas Sci. Eng.*, **26**, 1011-1017.

Reamer H.H., Sage B.H., Lacey W.N. (1951), Phase equilibria in hydrocarbon systems – volumetric and phase behaviour of the methane – hydrogen sulfide system, *Ind. Eng. Chem.*, **43**, 976-981.

Reamer H.H., Sage B.H., Lacey W.N. (1953), Phase equilibria in hydrocarbon systems – Volumetric and phase bahaviour of n-pentane – hydrogen sulfide system, *Ind. Eng. Chem.*, **45**, 1805-1809.

Ribeiro A. M., Sauer T. P., Grande C. A., Moreira R. F. P. M., Loureiro J. M. and Rodrigues A. E. (2008), Adsorption equilibrium kinetics of water vapour on different adsorbents, *Ind. Eng. Chem. Res.*, **47**, 7019 - 7026.

Rodriguez J., Mac Dowell N., Llovell F., Adjiman C.S., Galindo A. (2012), Modelling the fluid phase behaviour of aqueous mixtures of multifunctional alkanolamines and carbon dioxide using transferable parameters with the SAFT – VR approach, *Mol. Phys.*, **110**, 1325 – 1348.

Ruthven D.M. (1984), *Principles of adsorption and adsorption processes*, University of New Brunswick, Fredericton, (Usa).

Santos L. M. (2016), *Modelling the phase behaviour of polymer-solvent mixtures and surfactant systems with the SAFT-γ Mie EoS*, Master thesis, Istituto Técnico, Lisbon (Portugal).

Selleck F.T., Carmichael L.T., Sage B.H. (1952), Phase behaviour in the hydrogen sulfide-water system, *Ind. Eng. Chem.*, **44**, 2219-226.

Shafeeyan M.S., Wan Daud W.M.A., Shamiri A. (2013), A review of mathematical modeling of fixed-bed columns for carbon dioxide adsorption, *Chem. Eng. Res. Des.*, **92**, 961 - 988.

Tobin J., Shambaugh P. and Mastrangelo E. (2006), *Natural gas processing: the crucial link between natural gas production and its transportation to market*, Energy information administration, Office of Oil and Gas.

Tsuji T., Hiaki T., Hongo M. (1998), Vapor – Liquid equilibria of the three binary systems: Water + TEG, Ethanol + TEG, and 2-Propanol + TEG, *Ind. Eng. Chem. Res.*, **37**, 1685-1691.

Twu C. H., Tassone V., Sim W. D. and Watanasiri (2005), Advanced equation of state method for modeling TEG-water for glycol gas dehydration, *Fluid Phase Equilib.*, **228-229**, 213-221.

Vitu S., Privat R., Jauber J.N., Mutelet F. (2008), Predicting the phase equilibria of CO2 + hydrocarbon systems with the PPR78 model (PR EOS and kij calculated through a group contribution method), *J. Supercrit. Fluids*, **45**, 1-26.

Wang Yu, Douglas L. M. (2009), Adsorption equilibrium of carbon dioxide and water vapour on zeolites 5A and 13X and silica gel: pure components, *J. Chem. Eng. Data*, **54**, 2839-2844.

Xu Z., Cai J., Pan B. (2013), Mathematically modeling fixed-bed adsorption in aqueous systems, *J. Zhejiang Univ.-Sci A (Appl. Phys. and Eng.)*, **14**, 155-176.

Appendix A

Bulk or molecular diffusion becomes dominant where the pore diameter is larger than the mean free path of the molecules. An estimation for the diffusivity of an individual component in a gas mixture may be obtained from the approximate relationship:

$$\frac{D_{1,m}}{1-y_1} = \left(\sum_{j=2}^{n} \frac{y_j}{D_{1,j}} \right) \tag{A.1}$$

Thus, in a multi component mixture the molecular diffusivity becomes composition dependent. In (A.1), $D_{1,j}$ represents the molecular diffusivity of the binary gas mixture, which is essentially independent of composition. In order to calculate this value the Chapman – Eskog equation is used:

$$D_{1,2} = \frac{1.5810^{-7} T^{\frac{2}{3}} \sqrt{\left(\frac{1}{M_1} + \frac{1}{M_2}\right)}}{P \sigma_{1,2}^2 \Omega_{1,2}} \tag{A.2}$$

Where M_i is the molecular weight, T and P respectively temperature and pressure. $\sigma_{1,2}$ is the collision diameter from the Lennar - Jones potential, calculated as $\sigma_{1,2} = \frac{1}{2}(\sigma_1 + \sigma_2)$ and $\Omega_{1,2}$ is a function of Lennard - Jones force ϵ_{12}/kT, where $\epsilon_{12} = \sqrt{\epsilon_1 \epsilon_2}$. The values of the Lennard - Jones collision diameter and force are provided by Bird (2007).

The resulting values for the diffusivity of each component in the mixture, considered in the adsorption process, are listed in table A.1.

Table A.1: Molecular diffusivity constant of component i in the mixture, considered in the adsorption process §6.

	$\mathbf{H_2O}$	$\mathbf{CO_2}$	$\mathbf{CH_4}$	$\mathbf{N_2}$
$\boldsymbol{D_{i,m}}$ [m^2s^{-1}]	4.32E-07	2.66E-07	2.14E-07	2.79E-07

Another contribution to the diffusivity in the macropore is given by the Knudsen diffusivity, which becomes relevant at low pressure or in those adsorbents in which the pore diameters are lower than the molecular mean free path, in fact this mechanism is a consequence of the collision between the diffusing molecules and the pore

wall.

$$D_{k.i} = 97 r_p \sqrt{\frac{T}{M_i}} \tag{A.3}$$

In the transition region between these two mechanism the two contributions can be summed up as two resistances in parallel (A.4), where also the tortuosity factor is taken into account $\tau = \varepsilon + 1.5(1 - \varepsilon)$:

$$D_{p,i} = \frac{1}{\tau_p} \left(\frac{1}{D_{m,i}} + \frac{1}{D_{k,i}} \right)^{-1} \tag{A.4}$$

Micropore diffusion is an activation process, therefore in contrast to the molecular and Knudsen diffusivities, the temperature dependence is strong and follows the Arrhenius law:

$$D_{\mu,i} = D_{\infty} \exp(\frac{-E_i}{RT}) \tag{A.5}$$

where $D_{\infty,i}$ is the micropore diffusivity at infinite temperature and E_i is the adsorption activation energy for component i. The kinetic parameters for the micropore used in this work are the parameters fitted in the work of Gholami *et al.* (2010) and are listed in table A.2.

Table A.2: Fitting parameters for the calculation of the micrpore diffusivity of component i in the mixture, obtained from the work of Gholami (2010).

	H_2O	CO_2	CH_4	N_2
$\boldsymbol{D_{\infty,i}}$ [$m^2 s^{-1}$]	2.39E-08	5.9E-11	7.2E-12	5.2E-13
$\boldsymbol{E_i}$ [$Jmol^{-1}$]	17 288.47	26 334	12 551.94	6 275.97

The macropore and micropore resistances considered are depicted in figure A.1.

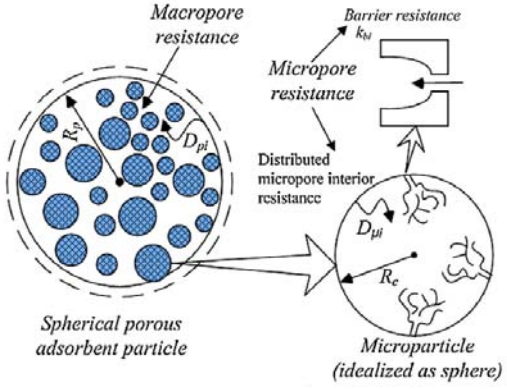

Figure A.1: Schematic diagram showing various resistances within the solid particle (Shafeeyan 2013).